Development of Phosphole- and Thiophene-Hybrid Molecules for Organic Functional Materials

Keiichi Ishida

2022

Development of Phosphole- and Thiophene-Hybrid Molecules for Organic Functional Materials

Keiichi Ishida

2022

Laboratory of Photoorganic Chemistry
Department of Molecular Engineering
Graduate School of Engineering
Kyoto University

Preface

The studies of this thesis were carried out under the guidance of Prof. Dr. Hiroshi Imahori at the Department of Molecular Engineering, Graduate School of Engineering, Kyoto University for five years since 2017.

This thesis focuses on the synthesis and properties of phosphole- and thiophene-fused π-conjugated molecules. The development of novel π-conjugated molecules has attracted much attention owing to their tremendous potential in various fields including energy conversion, organic electronics, fluorescence imaging, and nonlinear optics. Incorporation of main group elements, i.e., boron, silicon, phosphorus, and sulfur into π-conjugated systems is one of the effective strategies to modulate their electronic structures and to achieve desired physicochemical properties for practical applications. In line with this strategy, cyclopentadiene analogues with main group elements, i.e. heteroles, have been extensively studied. However, the π-systems with combination of different heteroles are still elusive, although they could realize diverse properties by integrating features of each heterole. From this viewpoint, the author attempted to realize the hybrid character of phosphole and thiophene by precise molecular design. The aim of this thesis is to create new class of phosphole- and thiophene-hybrid molecules and to understand their structural and physicochemical properties for organic functional materials.

Contents

General Introduction and Overview of This Thesis

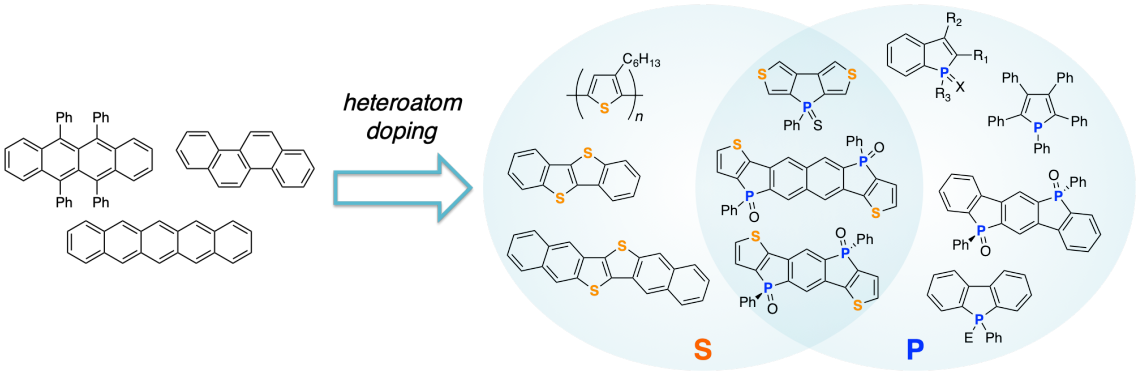

Contents

1-1. Polycyclic Aromatic Hydrocarbons

Polycyclic aromatic hydrocarbons (PAHs) are a class of organic molecules composed of solely sp^2 carbon atoms and hydrogen atoms, and containing two or more aromatic rings. They have attracted chemists over a century to their unique properties derived from rigid and planar structure, and delocalization of π-electrons. Pioneering works on their synthesis and physical properties were carried out by Roland Scholl and Eric Clar in the first half of the 20th century.[1] Clar also established the useful theory "Clar's aromatic π-sextet rule" to understand their stability and reactivity.[1b] Despite the active studies on PAHs, their potential utilities as functional materials had been overlooked because the most scientists believed that organic molecules were not able to utilize for (semi)conductors.

However, in 1977 Heeger, MacDiarmid, and Shirakawa reported the conductive organic polymer,[2] which won the award of the Chemistry Nobel Prize in 2000. This innovative report sparked interest in π-conjugated organic molecules all over the world. Furthermore, the subsequent isolation of fullerene (1985), carbon nanotubes (1991), and graphene (2004) increased the attention to π-conjugated systems.[3]

Among a number of PAHs, linearly benzene-fused molecules, "acenes" have been studied extensively so far.[4] Their structure can be regarded as well-defined zigzag-edge of graphene, and their physicochemical properties depend strongly on the number of benzene rings. The energy-gap between HOMO and LUMO effectively reduced (Figure 1b) and the reorganization energy becomes small as the number of benzene rings increases. On the other hand, the acenes become less stable with the increasing a number of benzene rings because the rise of HOMO levels leads to undesired oxidation and photodecomposition. Since anthracene, tetracene, and pentacene are relatively stable compared to higher analogues (n>6), they have been attracted interest in various fields.

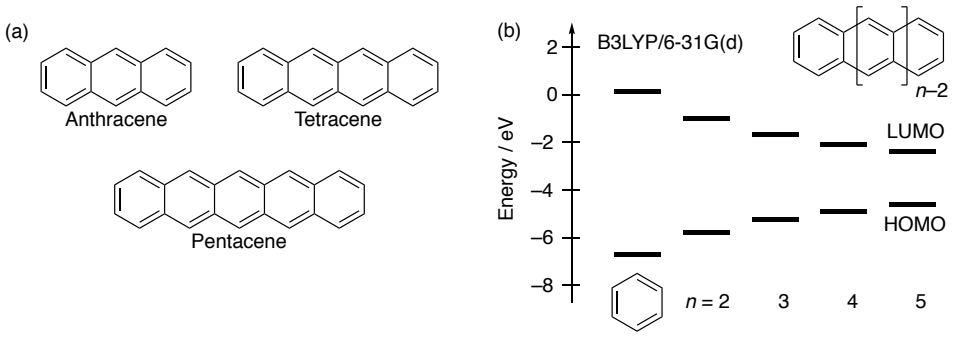

Figure 1. (a) Representative examples, and (b) HOMO/LUMO energy diagram of acenes.

One of the key physical properties of acenes is carrier transport ability.[4e,g] The electronic coupling between adjacent molecules in the solid state is very important for achieving high carrier transporting property. In general, acenes exhibit 2-dimensional herringbone structure, which is effective motif for carrier transporting materials. The two types of intermolecular alignment are observed in the herringbone packing; edge-to-edge and edge-to-face alignments. These intermolecular interactions in herringbone structure construct effective charge transporting pathway in the solid state. Tetracene, for example, demonstrated excellent hole mobilities as high as 1.3 $cm^2\ V^{-1}\ s^{-1}$ in single-crystal OFET device (Figure 2a, b).[5] In the case of tetraphenyl derivative of tetracene, i.e., rubrene, the molecular arrangement in the solid state shows both herringbone structure and π-stack alignment with large overlap of adjacent molecules (Figure 2c, d). As a result, rubrene single crystal-based devices achieved the hole mobilities more than 20 $cm^2\ V^{-1}\ s^{-1}$.[6] Pentacene is also one of the most frequently studied molecules and 5 $cm^2\ V^{-1}\ s^{-1}$ of hole mobility was reported even in thin-film device.[7] The excellent properties of acenes as p-type semiconductor also make them suitable for organic photovoltaics (OPVs). The OPVs based on acenes with C_{60} yielded power conversion efficiencies (PCE) as high as 2.3% for tetracene[8] and 2.7% for pentacene.[9]

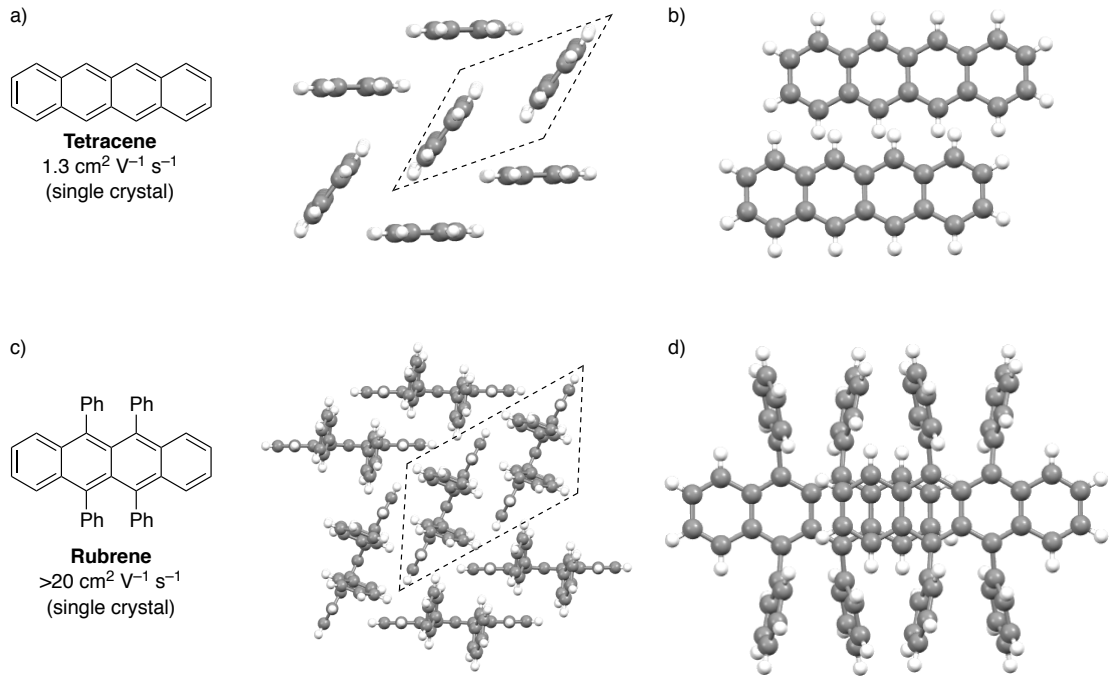

Figure 2. Packing structures and edge-to-edge pairs of (a,b) tetracene and (c,d) rubrene.

The optical properties of acenes are also worthy of consideration. The delayed fluorescence of anthracene crystal was investigated by Schneider in 1965,[10] and magnetic field dependence of the prompt fluorescence intensity in tetracene crystal was clarified by Groff in 1969,[11] which demonstrates the occurrence of singlet fission. Additionally, Pope and Herfrich demonstrated the first electroluminescence of anthracene single-crystal in 1960s using anthracene anion radical as a cathode and cation radical as an anode.[12] This is the beginning of organic light-emitting diodes (OLEDs).

1-2. Heteroatom-containing Aromatics

As mentioned above, PAHs are an attractive class as organic functional material. But considering the practical applications, there is room for improvement in terms of stability and performance. However, it is difficult to realize desired physical properties because of the limitation of molecular design. In other words, the compositions of PAHs are restricted to only sp^2-hybridized carbon atom and hydrogen atom, which cannot provide the structural and electronic diversity. On the other hand, main group elements exhibit dramatic diversity in terms of orbital interaction with π-system, coordination nature, and structural features. For example, a trivalent boron atom has a vacant p-orbital and incorporation of boron atom into π-systems stabilized LUMO level due to efficient p-π* interaction (Figure 3a). The vacant p-orbital of a boron atom also acts as a receptor of Lewis base and the coordination of Lewis base to the boron atom changes its planar conformation to tetra-coordinated tetrahedral conformation (Figure 3b). Therefore, incorporation of main group elements into PAHs is one of the most effective strategy for realizing desired physicochemical properties.[13–17] In fact, π-conjugated molecules containing heteroatoms have shown excellent performance in various fields, including energy conversion,[14] organic electronics,[15] fluorescence imaging[16] and nonlinear optics.[17]

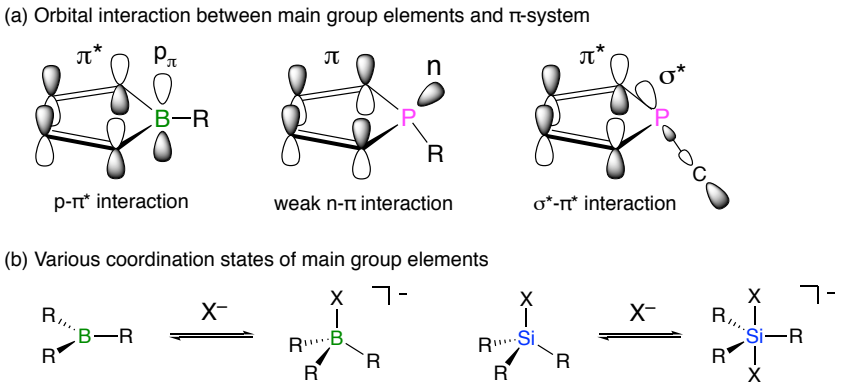

Figure 3. Representative characters of main group elements.

Among the heteroatom-containing π-systems, cyclopentadiene analogues, i.e., heteroles are received much attention because of their unique properties. For example, thiophene, which is one of the well-known heteroles, is a stable 6π-electron aromatic molecule and its facile functionality accelerates development of thiophene chemistry. Sulfur atom plays an important role in carrier transporting property owing to efficient intermolecular S–S contacts which increase the electronic coupling with neighboring molecules. Additionally, typical thiophene can act as an electron-donating component in π-conjugated molecules whereas the oxidized

thiophene, thiophene *S*,*S*-dioxide, can act as an electron-withdrawing component. Namely, the oxidation states of sulfur atom can also modulate the electronic properties of thiophene derivatives.

Phosphorus-containing heterole, i.e., phosphole exhibits different properties from thiophene because of their structural and electronic nature of the phosphorus atom. Because the phosphorus center adopts a trigonal pyramidal geometry, the lone pair of the phosphorus in the phosphole system is not efficiently interacted with the cyclopentadiene moiety and thus, the aromatic character of the phosphole is reduced. In addition, phospholes have high electron-accepting properties due to the effective hyperconjugation between the σ*-orbital of the P–C bonds and the π*-orbital of the butadiene moiety (Figure 3a). Furthermore, orbital energies of the π-system can be tuned by chemical modification of the phosphorus center.

1-3. Thiophene-based Polycyclic Aromatics

Thiophene has long been attracting much attention as a building block of functional material, and pioneering work on polythiophene-based OFET devices was reported by Ando and co-workers in 1986.[18] The field-effect mobility and stability were quite low, however, it was the first demonstration of organic semiconductor-based electronic device. Along with the development of materials, purification methods, and fabrication techniques, the mobility of polythiophene-based OFET devices reached to 0.1 cm^2 V^{-1} s^{-1} for solution processed OFETs[19] and 1.0 cm^2 V^{-1} s^{-1} for vapor-deposited OFETs only after 10 years.[20] Considering the development of PAHs in the field of organic semiconductors, the combination of PAHs and thiophene-based π-conjugated molecule are promising strategy for achieving superior carieer transporting ability.

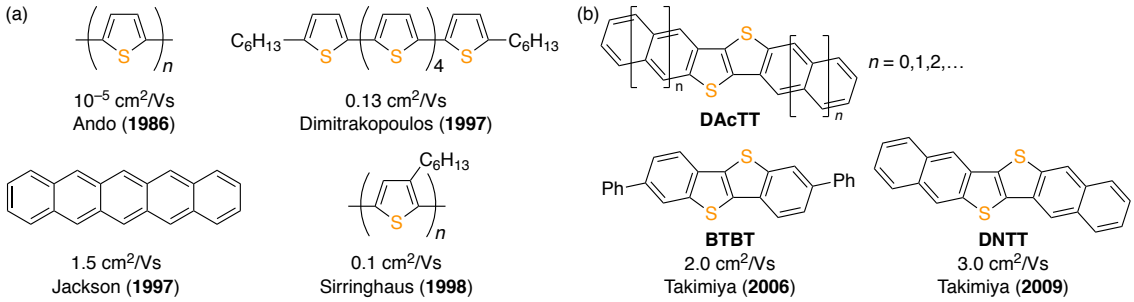

Figure 4. Representative examples of organic molecules as p-type semiconductors.

To date, a large number of thiophene-based polycyclic aromatics have been synthesized and elucidated their carrier transporting abilities.[15a] Among them, diacene-fused thienothiophenes (DAcTTs) are the most successful class in terms of stability, hole mobility, and accessibility (Figure 4b). [1]Benzothieno[3,2-*b*]benzothiophene (**BTBT**), which was reported by Horton in 1949,[21] is representative of DAcTT. Although its derivatives with alkyl substituents[22] and ester moieties with long alkyl chain[23] have been attracted attention as liquid crystalline materials, Takimiya and co-workers demonstrated that **BTBT** derivative achieved excellent OFETs performance in 2006 for the first time (Figure 4b).[24] Their devices showed excellent performance in ambient condition with 2.0 cm^2 V^{-1} s^{-1} is representative of mobility, 10^7 of on/off current ratio (I_{on}/I_{off}) and almost no degradation after 250 days. After their report, 2,7-alkyl-substitued **BTBT**s were also applied to OFET device.[25] The introduction of alkyl chain brings two advantages that make solution process possible due to high solubility in common organic solvent (ca. 90 g L^{-1} in $CHCl_3$) and increase intermolecular interaction owing to "fastener effect".[25d,26] As a result, mobilities were higher than 1 cm^2 V^{-1} s^{-1} and the highest

value 5 cm^2 V^{-1} s^{-1} was reported for solution-processed OFET device in 2009.[25c] The π-extended DAcTTs also exhibit excellent properties, for example, the mobility of naphthalene derivative (**DNTT**) based OFET was up to 3 cm^2 V^{-1} s^{-1} by vapor process.[27] Furthermore, its alkyl derivative showed 8 cm^2 V^{-1} s^{-1} for vapor deposition process[28] and 11 cm^2 V^{-1} s^{-1} for hot-solution processing technique that constructs crystalline thin film.[29]

The outstanding carrier transporting abilities of DAcTTs can be understood from their crystal structures and theoretical calculations for intermolecular HOMO overlaps (transfer integrals *t*). The packing structures of **1** and **2** exhibit herringbone structure, which are similar to the structure observed in tetracene and pentacene. Although the intermolecular interaction between edge-to-edge pairs of PAHs are relatively small because of less effective intermolecular contacts (Figure 2b), in the case of DAcTTs, S–S contacts and large HOMO coefficients on central sulfur atoms increase the intermolecular interaction and realize effective two-dimensional carrier transport pathway. In fact, calculated *t* values based on DAcTTs packing structures are quite large for all molecular pairs.

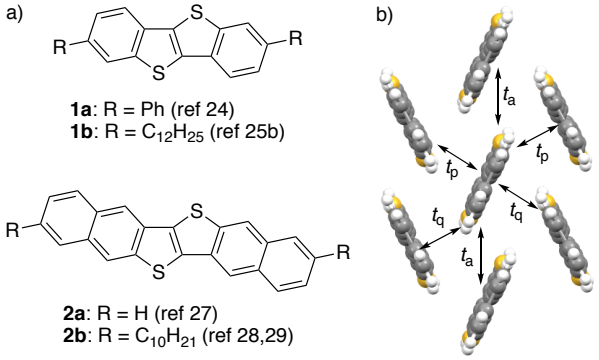

t / meV	**1a**	**1b**	**2a**
t_a	34	62	71
t_p	65	46	91
t_q	65	46	14
μ / cm^2 V^{-1} s^{-1}	2.0	3.9	3.0

Figure 5. (a) Structures of BTBTs and DNTTs, and (b) packing structure of **2a** and calculated *t* values in the herringbone packing of DAcTT semiconductors.[15a]

1-4. Phosphole-based Polycyclic Aromatics

Phosphole chemistry is late blooming field compared with the other heteroles. Pyrrole, thiophene, and furan have been known for over 130 years, whereas the first report on the synthesis of 1,2,3,4,5-pentaphenyphosphole (**3**) were independently published from Hübel and Johnson in 1959.[30] The first C-unsubstituted phosphole **4** was synthesized in 1967[31] and the phosphole without any substituents (1*H*-phosphole **5**) was characterized at low temperature in 1983.[31] Although phosphole chemistry have been well developed in terms of their structure and reactivity in 20th century,[33] phosphole-based functional molecules have not been actively studied. Réau and co-workers reported 2,5-diarylphospholes **6** and demonstrated fine-tuning the optical and electrochemical properties by modification of 2- and 5-substituents and of nature on phosphorus atom.[34] Furthermore, Baumgartner and co-workers described the potential utility of dithieno[3,2-*b*:2',3'-*d*]phospholes (**7**) as functional materials.[35]

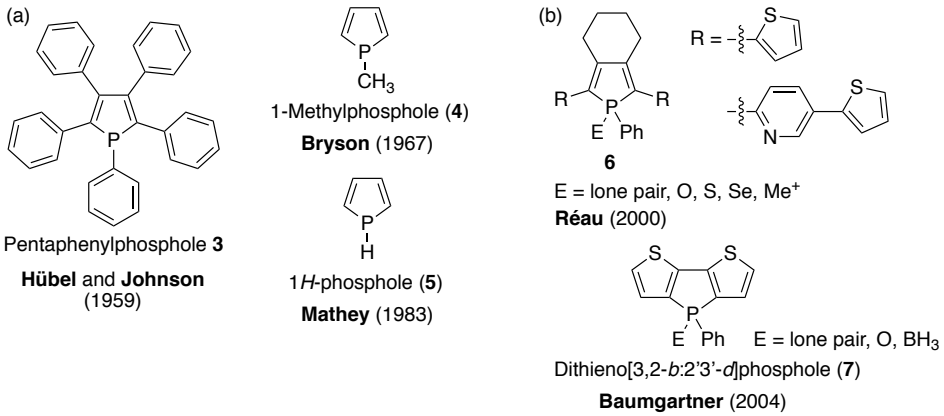

Figure 6. Examples of phosphole derivatives (a) in the early investigation, and (b) focusing physicochemical properties.

1-4-1. Benzene-fused Phospholes

One of the most studied phosphole based polycyclic aromatics is benzo[*b*]phosphole, which can be also regarded as heavy-atom analogue of indole. Some examples of benzo[*b*]phospholes have been reported from 1970s,[36] but their potential utility was not fully elucidated because of the limited synthetic accessibility for functionalized benzo[*b*]phospholes. In 2008 and 2009, Nakamura, Tanaka and Yamaguchi independently developed facile synthetic methodology for functionalized benzophospholes via intramolecular cyclization of alkynylarenes (Figure 7a).[37] Moreover, preparation of 2- or 3-bromobenzo[*b*]phospholes by Matano and Yamaguchi (Figure

7b) enables diverse benzo[*b*]phosphole derivatives through cross-coupling reaction.[38] These developments on synthetic accessibility allowed us to reveal intriguing optoelectronic properties of benzo[*b*]phosphole derivatives.

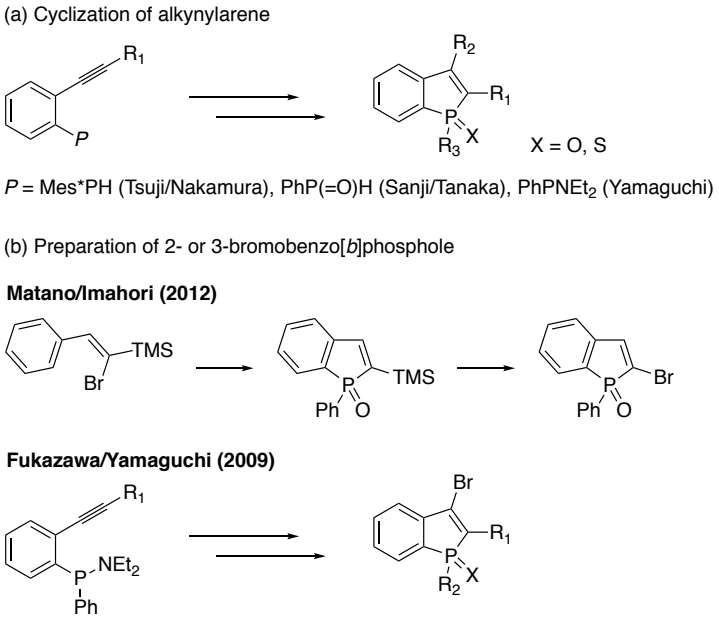

Figure 7. Synthetic methodology for benzo[*b*]phosphole derivatives.

Matano and co-workers synthesized a series of 2-functionalized benzo[*b*]phospholes **8** and elucidated their excellent fluorescence properties.[38b,e] It is worth noting that the introduction of electron donating substituents caused large bathochromic shifts by intramolecular charge-transfer interaction (ICT) without loss of fluorescence intensity, which is useful character for biological imaging. Actually, Yamaguchi and co-workers developed benzo[*b*]phosphole based fluorescence dye (**Ph-Bphox**, **C-Bphox**, and **C-Naphox**) for stimulated emission depletion (STED) microscopy.[38f] All dyes exhibited intense fluorescence even in polar and protic solvents with a large Stokes shifts and diarylmethylene-bridged analogues (**C-Bphox**, and **C-Naphox**) showed outstanding photostability under irradiation with a pulsed laser (λ_{ex} = 405 nm, 273 mW) and Xe lamp (300 W). This photostability derived from the low reactivity of central double-bond moiety with singlet O_2 and/or a hydroxyl radical generated during photoexcitation. Benzo[*b*]phospholes are also useful as an electron transporting material. Nakamura reported an amorphous film of bis(benzo[*b*]phosphole) sulfide **9a** (1:1 diastereomeric mixture) exhibited an electron mobility of 2×10^{-3} cm^2 V^{-1} s^{-1}, which was the highest value among n-type amorphous organic semiconductors at that time.[37a,39] On the other hand, the electron mobility of an amorphous film of bis(benzo[*b*]phosphole) oxide **9b**

was quite low, 5 × 10^{-6} cm^2 V^{-1} s^{-1}. This difference is originated from polarization of P=E moieties, which indicates that P=O acts as an electron trapping site because P=O is more polar than P=S.

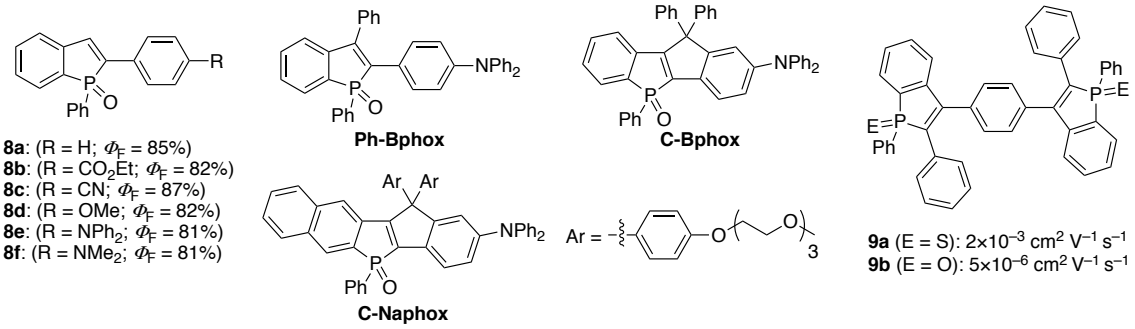

Figure 8. Molecular structures of benzo[*b*]phoshole derivatives.

Several research groups also developed doubly phosphole-fused scaffolds (Figure 9). Tanaka and co-workers reported the first synthesis of phenyl-substituted benzodiphosphole **10**.[37b] Then, Yamaguchi et al. also presented the synthesis and optical and electrochemical properties of phenyl-substituted benzodiphospholes **11**.[37c] These benzodiphospholes have been synthesized through intramolecular cyclization of bisalkynylarenes, as used in the synthesis of benzo[*b*]phospholes. It is notable that the benzodiphospholes **11** were applied to OPVs as a cathode buffer layer.[39b] Additionally, Liu and co-workers reported the synthesis of aromatic-fused benzodiphospholes **12** and **13** through a radical phosphanylation reaction.[40] With the assistance of synthetic methodologies for dibenzophospholes, doubly benzo-fused and naphtho-fused benzodiphospholes **14**–**16** have also been prepared.[41] Phosphoryl-bridged stilbenes **17** are also examples of doubly phosphole-fused scaffolds, and Yamaguchi and co-workers reported their excellent electron-accepting character and luminescent properties with a fluorescence quantum yield of 0.99.[42]

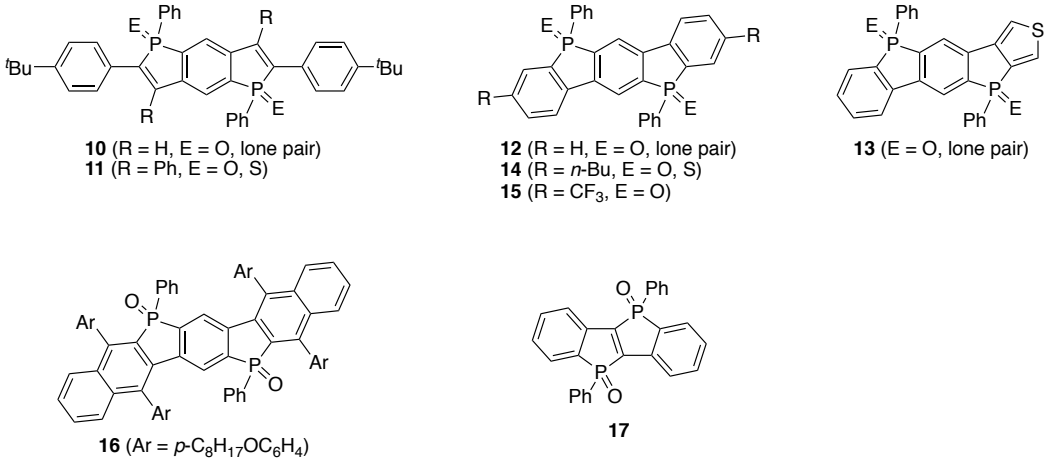

Figure 9. Examples of doubly phosphole-fused scaffolds.

1-4-2. Phosphole/Thiophene Hybrid Polycyclic Aromatics

Dithieno[3,2-*b*:2',3'-*d*]phospholes are represented examples of this class. The first synthesis was reported by Mathey and co-workers in 1974,[43] whereas Baumgartner and co-workers have pioneered their aspect of functional material since 2004.[35] They established efficient synthetic route for dithieno[3,2-*b*:2',3'-*d*]phosphole and demonstrated tuning of photophysical and electronic properties by various functionalization on the phosphorus center (Figure 10).[35f] Furthermore, the α-position of thiophene-rings can be modified to achieve diversity of their properties. Thus, wide color range of light emission maxima (415–631 nm) and high luminescence quantum efficiencies (up to 0.99) were realized.[35f,i]

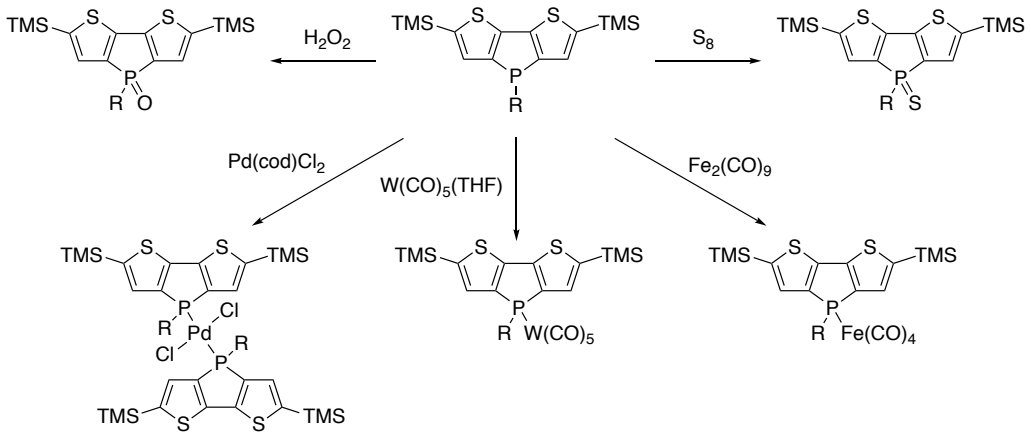

Figure 10. Examples of modification of dithieno[3,2-*b*:2',3'-*d*]phosphole on phosphorus atom.

Their facile functionality facilitates the design and synthesis of phosphole-based molecules for various applications. For example, Baumgartner and co-workers found diboryl dithienophosphole **18** acting as a fluoride ion sensor (Figure 11a).[35c] The emission color changes from blue (452 nm) to green (485 nm) upon coordination of fluoride ion and its sensitivity is in the parts-per-million regime. They also reported dithienophosphole-based liquid crystal **19** which exhibited external-stimuli responsibility (Figure 11b).[35d,e] Recently, Yam and co-workers applied dithienophosphole derivatives as active material in organic photovoltaics (PCE: up to 4.23%), organic light-emitting diode (EQE: up to 3.0%) and organic resistive memory devices (Figure 11c).[44]

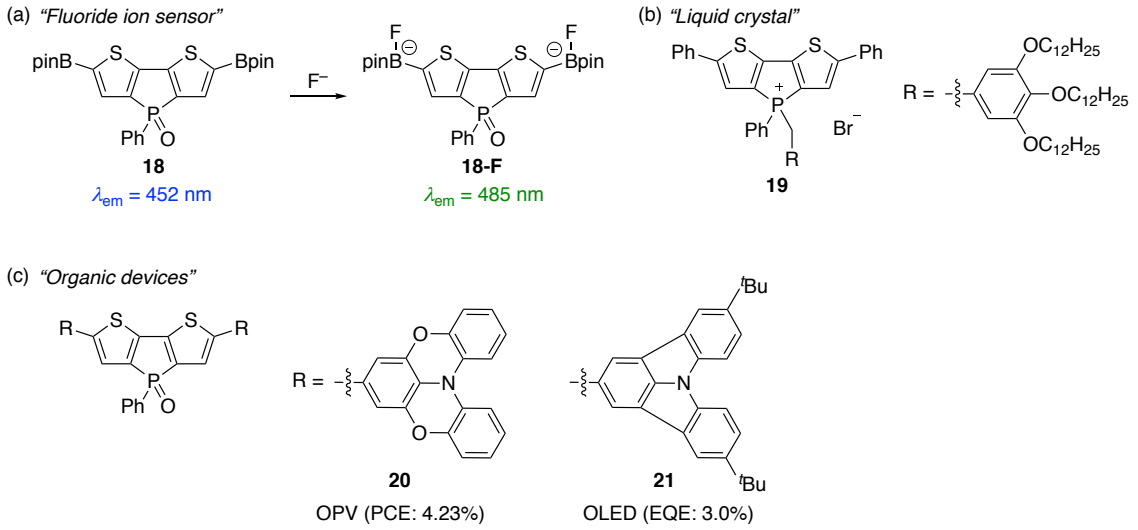

Figure 11. Applications of dithieno[3,2-*b*:2',3'-*d*]phosphole derivatives.

Baumgartner and co-workers reported P,S-bridged stilbene **22** in 2011, and demonstrated that the optical and electronic properties are dually switchable via independent modification of phosphorus and sulfur atoms (Figure 12).[45] The oxidation states of sulfur atom affects not only the conjugation pathway but also the electronic contribution of phosphorus atom. On the other hand, fluorescence quantum yield highly depends on the nature of phosphorus atom.

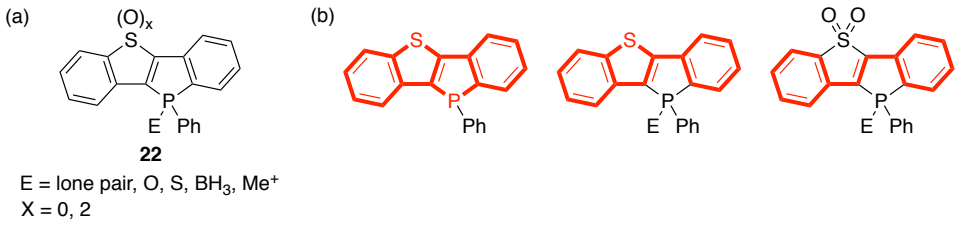

Figure 12. (a) Structure of P,S-bridged stilbene, and (b) change of the conjugation pathway (bold red bonds) upon P/S functionalization.

1-5. Overview of This Thesis

Incorporation of main group elements into the π-system has attracted much attention because of their unique properties derived by their electronical and structural diversity. In this context, phosphole-based PAHs have been rapidly developed in these two decades. Furthermore, a combination of phosphole and thiophene is effective approach to create novel functional material, such as emissive material, carrier transporting material and non-liner optical materials.

In Chapter 1, dithieno[3,4-*b*:3',4'-*d*]phosphole derivatives are reported as a new type of thiophene-fused phospholes. The hybrid character of electron-withdrawing phosphole and electron-donating thiophene is discussed.

In Chapter 2, dithieno[3,4-*b*:3',4'-*d*] phosphole is applied to π-linker of donor-π-acceptor type molecules. The position of substituents on the dithienophosphole moiety plays an important role in the frontier molecular orbitals, and the hybrid character of electron-withdrawing phosphole and electron-donating thiophene can be modulated by the substituents.

In Chapter 3, the unique characters of doubly thiophene-fused benzodiphospholes are described. Their two-photon absorption and charge-transporting ability as well as intriguing physicochemical properties are investigated.

In Chapter 4, a series of doubly thiophene-fused naphthodiphospholes have been synthesized. Effects of phosphole-fused structure to their structural and electronic properties are investigated from the view of optical/electrochemical properties, molecular arrangement in the solid state, and theoretical calculations.

Chapter 1. Dithieno[3,4-*b*:3',4'-*d*]phospholes as the New Type Thiophene-fused Phosphole

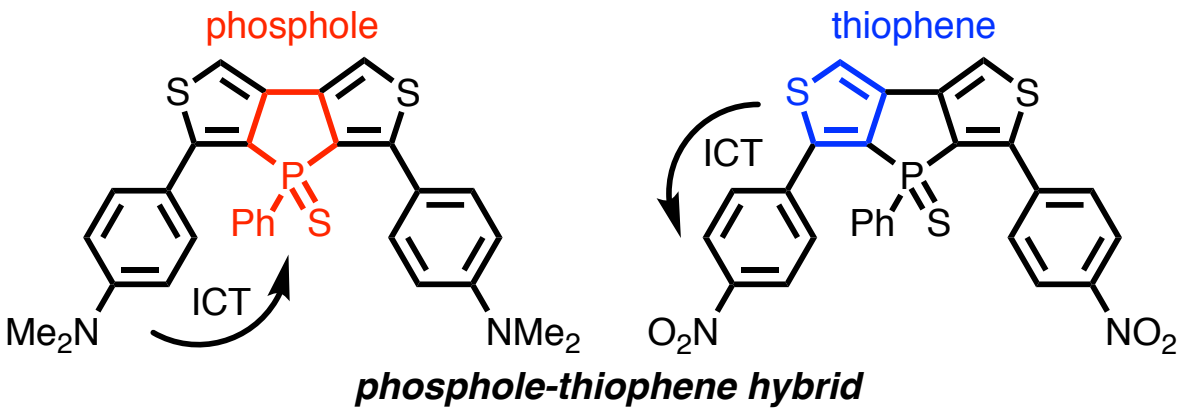

Contents

1-1. Introduction

As mentioned in General Introduction, phospholes have been actively studied owing to their intriguing optical and electrochemical properties as well as potential for diverse applications.[33,46] Among them, arene-fused phospholes, such as dibenzo[*b*,*d*]phosphole,[47] benzo[*b*]phospholes,[37-39] and the other phospholes,[48] are one of the attractive classes of phosphole-fused π-system (Figure 1-1a). In particular, some of their phosphorus(V) derivatives exhibit high electron mobility because of their intriguing electron affinity.[39,48f–h] Recently, heterocycle-fused phospholes have been synthesized as promising n-type organic materials (Figure 1-1b).[47a,49] Particularly, the presence of the nitrogen center allowed further functionalization with alkyl and aryl groups that result in their altered absorption and redox features.[49d,e] In addition, thiophene-fused phospholes have also been reported (Figure 1-1c).[35,50] Depending on the direction of the thiophene ring, the thiophene-fused structure provides regioisomers, of which the most intensively studied one is dithieno[3,2-*b*:2',3'-*d*]phosphole **7**.[35,51]

Importantly, the fused structures have a large impact on the properties of the aromatic-fused phospholes. In this regard, the author expected that the development of novel aromatic-fused phosphole derivatives would provide the useful insight for promising organic functional materials. Herein, the author designed and synthesized dithieno[3,4-*b*:3',4'-*d*]phosphole **23**, 3,3'-bithiophene derivative, as a new type of aromatic-fused phosphole. To the best of our knowledge, no examples of **23** have been reported. The author found the unprecedented character that they can act as both electron acceptor and donor, resulting from the phosphole-thiophene hybrid nature.

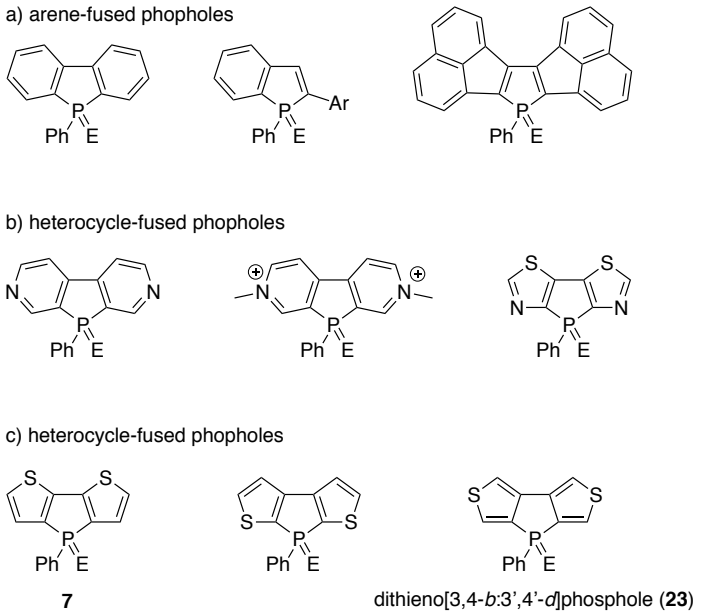

Figure 1-1. Representative examples of aromatic-fused phospholes. (E = lone pair, O, S, BH_3, CH_3^+, metal, etc.)

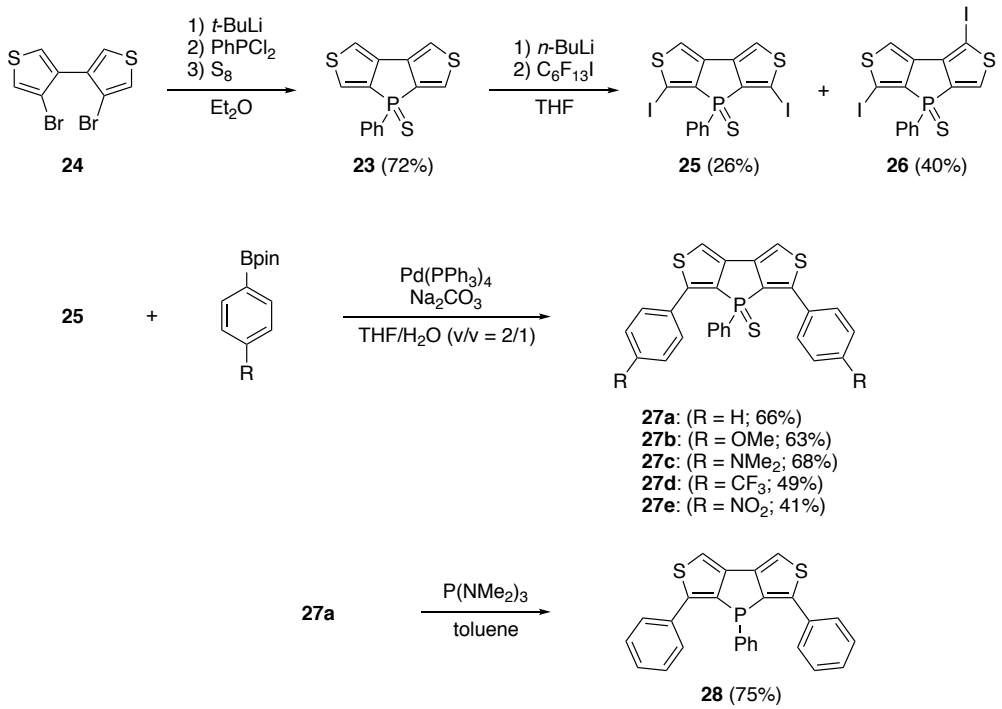

Scheme 1-1. Synthesis of the dithieno[3,4-*b*:3',4'-*d*]phospholes.

1-2. Synthesis of Dithieno[3,4-*b*:3',4'-*d*]phosphole Derivatives

The synthetic route of dithieno[3,4-b:3′,4′-d]phospholes is shown in Scheme1-1. 4,4'-Dibromo-3,3'-bithiophene **24** was prepared according to the literature.[52] Treatment of **24** with *t*-BuLi followed by the addition of dichlorophenylphosphine and elemental sulfur produced dithienophosphole **23** in 72% yield. Then, the halogenation of **23** was attempted for further functionalization. However, straightforward halogenation by *N*-bromosuccinimide or *N*-iodosuccinimide did not proceed. Fortunately, the author found that treatment of **23** with *n*-BuLi and $C_6F_{13}I$ gave 3,5-diiododithienophosphole **25** (26%) along with the regioisomer, 1,5-diiododithienothiophene **26** (40%). The structure of **25** was confirmed by single crystal X-ray diffraction analysis, which revealed the highly rigid and planar tricyclic structure (Figure 1-2). In the next step, the Suzuki-Miyaura coupling reaction of **25** with a variety of pinacol arylboronates afforded the 3,5-diaryldithienophospholes **27a-e** in moderate yields (41–68%). Additionally, treatment of **27a** with tris(dimethylamino)phosphine provided trivalent phosphole **28**. They were characterized by high-resolution mass spectrometry as well as ^{1}H and ^{13}C NMR spectroscopies. Whereas P-sulfides **27a-e** exhibit signals at δ = 21.2–23.3 ppm in the ^{31}P NMR, **28** displays the signal at δ = –31.8 ppm.

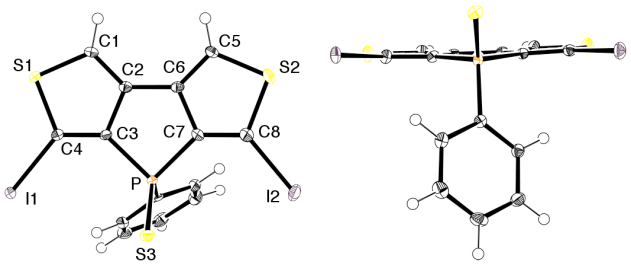

Figure 1-2. X-Ray crystal structure of **25**; top view (right) and side view (left). Thermal ellipsoids represent 50% probability.

1-3. Optical Properties

The UV/vis absorption spectra of phospholes **23**, **27**, and **28** were measured in CH_2Cl_2 (Table 1-1). The phosphole **23** displays a peak at 302 nm (Figure 1-3a), while the TMS-protected phosphole derivative **29** (Chart 1-1) has a peak at 374 nm.[35b] The blue-shifted absorption suggests the weak π-delocalization over the dithienophosphole structure of **23**. The phenyl-substituted **27a** shows red-shifted absorption and the absorption edge reaches up to 375 nm (Figure 1-3b). The red-shifted absorption indicates effective π-delocalization by the phenyl groups. Since the trivalent phosphole **28** displays almost the same absorption, the oxidation state of the phosphorus atom is trivial (Figure 1-3a). This is explicitly different from the phosphole **7** derivative, which exhibits a blue-shift for the trivalent analogue (338 nm, E = lone pair).[35b] The electron-donating group (**27b**,**c**) induces red-shift of the absorption and enhancement of the intensity for the lowest energy absorption. It is noteworthy that the dimethylamino-substituted **27c** shows the considerably red-shifted, broad peak around 380 nm. The spectral features suggest intramolecular charge-transfer (ICT) from the donor (i.e., dimethylaminophenyl) to the acceptor (i.e., dithienophosphole) units, which is consistent with other phosphole derivatives.[35g,38d,53] On the other hand, the trifluoromethyl group (**27d**) has a negligible impact on the absorption features. However, the nitro-substituted **27e** exhibits the red-shifted, broad absorption around 390 nm. This peak implies ICT from the dithienophosphole core to the nitrophenyl moiety. Although it is known that trivalent phospholes with the nitrophenyl group show ICT character, phosphorus(V) derivatives show little ICT character.[53b]

Chart 1-1. TMS-Protected phosphole derivative **29**.

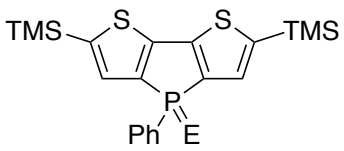

29

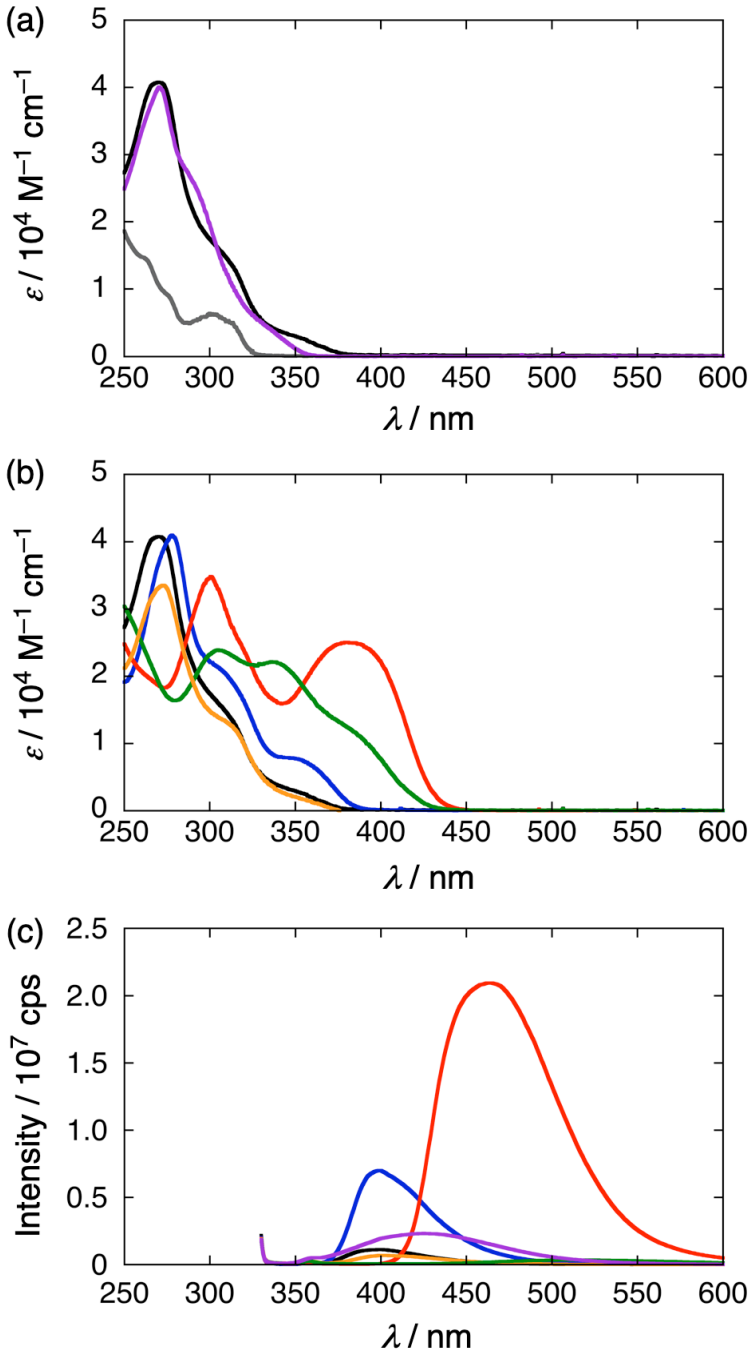

Figure 1-3. (a,b) UV/Vis absorption and (c) fluorescence spectra of **23** (gray), **27a** (black), **27b** (blue), **27c** (red), **27d** (orange), **27e** (green), and **28** (purple) in CH_2Cl_2. For fluorescence measurements, the absorbances at 323 nm were adjusted to be identical (0.1) and the samples were excited at 323 nm under the same condition for accurate intensity comparison.

Table 1-1. Optical properties of dithieno[3,4-*b*:3′,4′-*d*]phospholes in CH_2Cl_2.

	λ_{abs} / nm (ε / 10^4 $M^{-1}cm^{-1}$)	λ_{em} / nm[a]
23	260 (1.5), 302 (0.65)	–[b]
27a	270 (4.1), 310 (1.4), 355(sh) (0.23)	399
27b	279 (4.2), 308 (2.1), 351 (0.80)	399
27c	301 (3.5), 381 (2.5)	464
27d	273 (3.3), 314 (1.2), 350(sh) (0.22)	400
27e	307 (2.4), 336 (2.2), 385(sh) (1.2)	515
28	271 (4.0), 291 (2.6), 330(sh) (0.40)	429

[a]Wavelengths for emission maxima by exciting at 323 nm. [b]Fluorescence was not observed.

The fluorescence spectra were compared in CH_2Cl_2 under the same condition (Table 1-1). Although no fluorescence was detected for **23**, the fluorescence of **27a** was observed at 399 nm (Figure 1-3c). The trivalent phosphole **28** displays a red-shifted, broad peak around 430 nm. The methoxy-substituted **27b** shows red-shifted emission and the intensity is five times higher than that of **27a**. Moreover, the dimethylamino-substituted **27c** possesses the further enhanced emission at 464 nm with the fluorescence quantum yield of 0.11. The quantum yield of **27c** is remarkable considering that most of phosphole P-sulfides have the quantum yields less than 0.01.[47g,49c,54] In contrast, the trifluoromethyl-substituted **27d** shows the weaker fluorescence than **27a**. Notably, the nitro-substituted **27e** reveals the further weak, broad emission around 520 nm. To shed light on the ICT interaction for **27c** and **27e**, the author also measured the absorption and fluorescence spectra in various solvents and found their solvatochromism (Figure 1-4 and Table 1-2). The Stokes shifts ($\Delta\nu$) of **27c** and **27e** increased with increasing orientation polarizability (Δf) of the solvent. The Lippert-Mataga analyses gave moderate linear correlation with $\Delta\nu$ and the Δf values (Figure 1-5).[55] The slope of **27e** (24300 cm^{-1}) is larger than that of **27c** (9270 cm^{-1}), which reflects the ICT with opposite direction. Thus, the dithienophospholes **27** can exhibit two opposite types of the ICT interactions: (1) from the donor to the dithienophosphole, which is governed by the electron-accepting nature of the phosphole moiety, and (2) from the dithienophosphole to the acceptor, which is governed by the electron-donating nature of the thiophene moiety. To the best of our knowledge, this is the first example where phospholes with the phosphorus(V) center behave as both electron acceptor and donor.

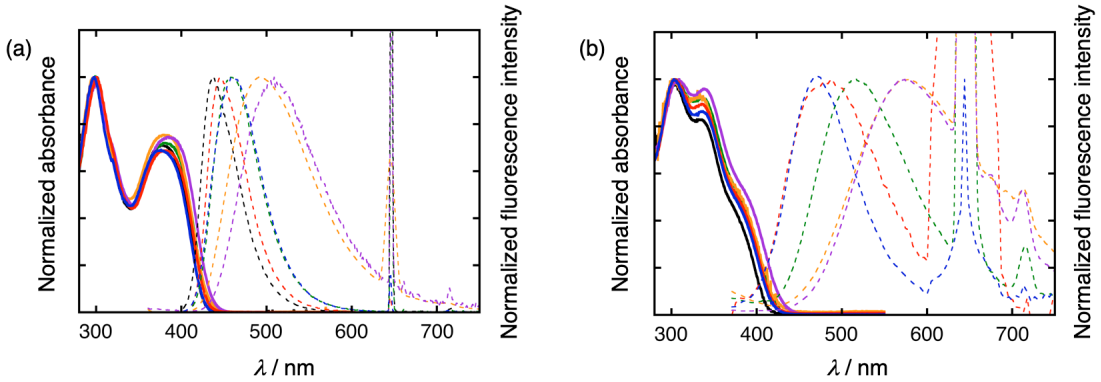

Figure 1-4. Normalized absorption (solid lines) and fluorescence spectra (dashed lines) of (a) **27c** and (b) **27e** in toluene, $CHCl_3$, THF, CH_2Cl_2, acetonitrile, and DMF. For fluorescence spectra, the absorbances at 323 nm were adjusted to be identical (0.1) and the samples were excited at 323 nm.

Table 1-2. Absorption and fluorescence maxima of **27c** and **27e** in various solvents.

		toluene	$CHCl_3$	THF	CH_2Cl_2	MeCN	DMF
27c	λ_{abs} / nm	378	381	376	381	382	386
	λ_{em} / nm	437	446	462	464	492	510
	Stokes shift / cm^{-1}	3570	3820	4950	4690	5850	6300
27e	λ_{abs} / nm	376	382	380	385	385	390
	λ_{em} / nm	n.d.[a]	482	473	515	576	573
	Stokes shift / cm^{-1}	–	5430	5170	6560	8610	8190

[a] Fluorescence was not detected.

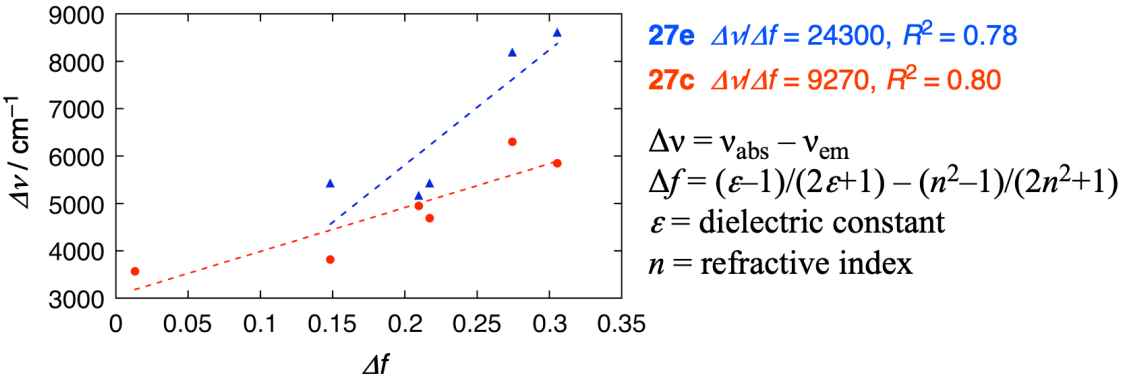

Figure 1-5. Lippert-Mataga plots for the solvatochromism of **27c** and **27e**. Calculated from the data listed in Table 1-2.

1-4. Electrochemical Properties

The electrochemical properties of **27a-e** were studied by cyclic voltammetry (CV) and differential pulse voltammetry (DPV) in acetonitrile with tetrabutylammonium hexafluorophosphate as an electrolyte (Figure 1-6). The first oxidation (E_{ox}) and reduction (E_{red}) potentials of **27a** were determined to be +1.12 and –2.26 V versus ferrocene/ferrocenium ion (Fc/Fc^+). Introduction of the electron-donating groups into the aryl groups shifts the redox potentials to the negative direction, while that of the electron-withdrawing groups shifts the redox potentials to the positive direction, which is in good agreement with the theoretical calculations below.

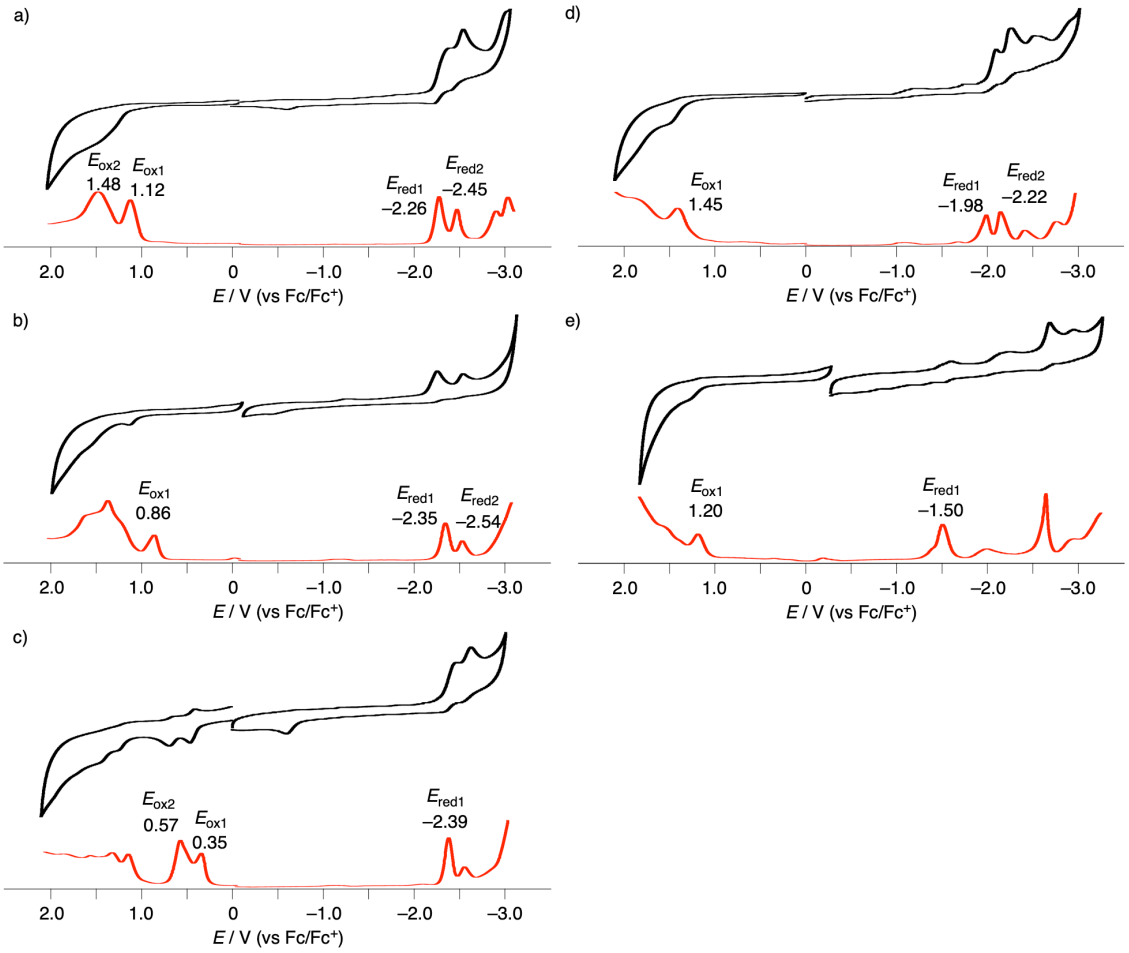

Figure 1-6. Cyclic voltammograms (black) and DPV curves (red) of a) **27a**, b) **27b**, c) **27c**, d) **27d**, and e) **27e**. Redox potentials were determined by DPV. Solvent: acetonitrile; scan rate: 0.05 V s^{-1}; working electrode: glassy carbon; reference electrode: Ag/Ag^+ (0.01 M $AgNO_3$); electrolyte: *n*-Bu_4NPF_6. Ferrocene (+0.081 V vs Ag/Ag^+ (0.01M $AgNO_3$)) was used as an external standard.

1-5. Theoretical Calculations

To obtain further insights into the structural and electronic properties of **27a-e**, the author performed density functional theory (DFT) calculations at the B3LYP/6-31G(d,p) level with C_s symmetry. Although the C–C bond lengths between the dithienophosphole core and the aryl group are virtually the same (ca. 1.46–1.47 Å), the dihedral angles for **27c** (33.1°) and **27e** (36.3°) are smaller than those for **27a**, **27b**, and **27d** (37.5–38.5°) on the optimized structures (Table 1-3). These small dihedral angles may enhance the ICT interactions in **27c** and **27e**. In addition, the author obtained optimized structures in various solvents with COSMO solvation model. In accordance with the increase of solvent polarity, the dihedral angles for **27c** and **27e** become slightly smaller, but those for **27a**, **27b**, and **27d** become larger (Table 1-3). These trends are consistent with the ICT character of **27c** and **27e**. Thus, the calculations also support that electron-donating dimethylamino and electron-withdrawing nitro groups induce ICT interactions.

Table 1-3. Structural parameters on optimized structures of **27a-e** with or without COSMO method.

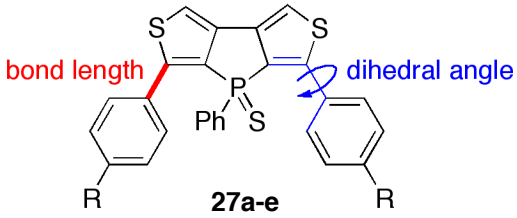

27a-e

27a (R = H)
27b (R = OMe)
27c (R = NMe_2)
27d (R = CF_3)
27e (R = NO_2)

	solvent	**27a**	**27b**	**27c**	**27d**	**27e**
bond length / Å	none	1.471	1.468	1.464	1.471	1.470
dihedral angle / º		38.5	38.3	33.1	37.5	36.3
bond length / Å	toluene	1.472	1.469	1.464	1.471	1.470
dihedral angle / º		39.3	38.8	34.1	38.4	36.7
bond length / Å	CH_2Cl_2	1.472	1.469	1.464	1.472	1.470
dihedral angle / º		40.0	39.7	33.9	39.4	36.7
bond length / Å	MeCN	1.472	1.469	1.464	1.472	1.469
dihedral angle / º		40.2	40.0	33.8	40.3	36.6

The selected Kohn-Sham orbitals are shown in Figure 1-7. The HOMO and LUMO of **27a** are delocalized over the dithienophosphole core and the aryl groups. Introduction of the electron-donating groups leads to an increase and decrease of the orbital distributions on the aryl groups for the HOMO and LUMO, respectively. It is notable that the HOMOs of **27b** and **27c** possess no orbital distribution on the P=S moiety, which may related to the increase of the fluorescence intensities of **27b** and **27c** relative to **27a**.[54a] In contrast, the HOMOs of **27d** and **27e** are localized on the dithienophosphole core. Whereas the LUMO of **27d** is similar to that of **27a**, the LUMO of **27e** is significantly localized on the aryl group. These localized HOMO and LUMO may be responsible for the ICT interaction in **27e**. Furthermore, the author performed time-dependent DFT (TD-DFT) calculations to evaluate the absorption. The lowest excitation energies of **27c** (3.25 eV) and **27e** (2.98 eV) are smaller than that of **27a** (3.78 eV), which is consistent with the red-shifted absorption. Given that the lowest energy absorption is mainly derived from the HOMO/LUMO transition, the TD-DFT calculations also support the ICT interactions in **27c** and **27e**.

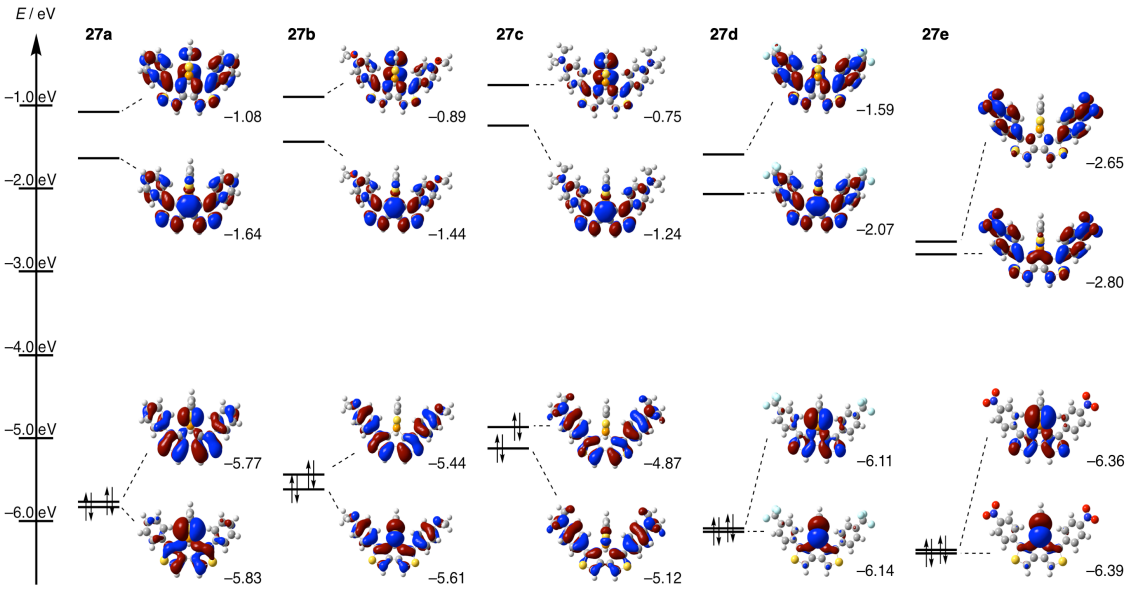

Figure 1-7. Selected Kohn-Sham orbitals of **27a**, **27b**, **27c**, **27d**, and **27e** on the optimized structures.

1-6. Summary

In summary, the author has synthesized dithieno[3,4-*b*:3',4'-*d*]phosphole **23** as a new type of thiophene-fused phospholes. A series of the diaryl-substituted dithieno[3,4-*b*:3',4'-*d*]phosphole **27a-e** have also been prepared to evaluate the fundamental properties. The dithienophospholes **27** were found to exhibit the different types of ICT interactions by introducing the electron-donating or withdrawing groups into the diaryl groups. Namely, the phosphole core behaves as the electron acceptor by introducing the electron-donating groups, while it behaves as the electron donor by introducing the electron-accepting group. Such hybrid character reflecting natures of electron-withdrawing phosphole and electron-donating thiophene is unprecedented and would be useful for extracting the full potential as organic functional materials.

Chapter 2. Modulation of Frontier Molecular Orbitals on Dithieno[3,4-*b*:3′,4′-*d*] -phosphole Derivatives by Donor-π-Acceptor Interaction

---

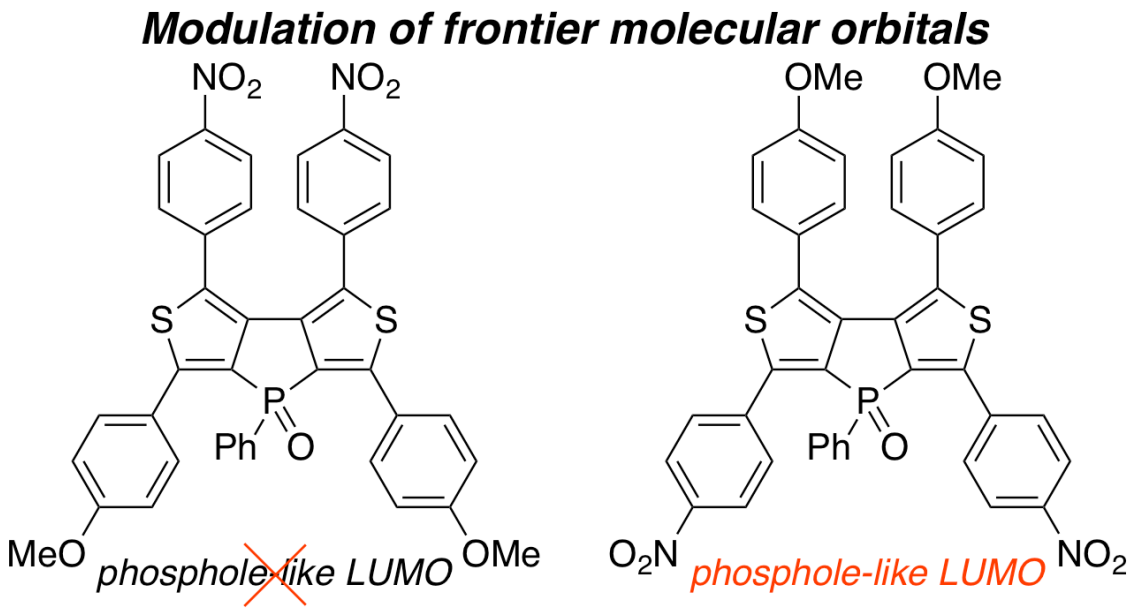

Contents

2-1. Introduction

In Chapter 1, the author reports the synthesis of dithieno[3,4-*b*:3',4'-*d*]phosphole which show intramolecular charge transfer (ICT) interaction by introducing electron-donating and electron-withdrawing groups (EDG and EWG, Figure 2-1). Namely, they exhibit the hybrid character of electron-withdrawing phosphole and electron-donating thiophene. Therefore, the author expected that introduction of the electron-withdrawing and/or electron-donating groups at appropriate positions of the dithieno[3,4-*b*:3',4'-*d*]phosphole core would control to exhibit the characters of phosphole and/or thiophene. Herein, the author designed two donor (D)-π-acceptor (A)-type dithieno[3,4-*b*:3',4'-*d*]phosphole derivatives, which possess electron-withdrawing and electron-donating groups (Scheme 2-1).[53b,56] The author examined their optical and electrochemical properties, and evaluated the contribution of the phosphole and thiophene moieties in their electronic structures by theoretical calculations.

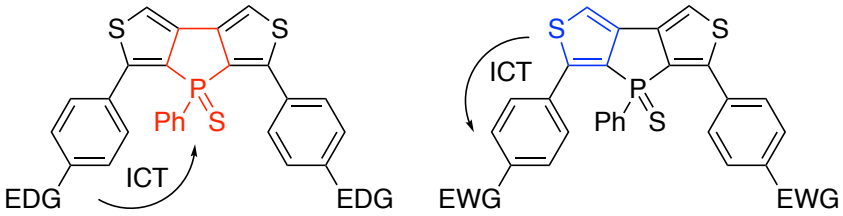

Figure 2-1. The illustration of hybrid nature of dithieno[3,4-*b*:3',4'-*d*]phosphole (EDG = electron-donating group, EWG = electron-withdrawing group).

2-2. Synthesis of D-π-A type Dithienophospoholes

The synthetic scheme of D-π-A-type dithieno[3,4-*b*:3',4'-*d*]phospholes is shown in Scheme 2-1. First the author attempted halogenation at the 1,7-positions of **27b** and **27e** with *N*-bromosuccinimide (NBS) or *N*-iodosuccinimide (NIS), but could not obtain the desired halogenated compounds because of the oxidation of phosphorus atom.[57] On the other hand, after the P=S moieties were converted to the P=O moieties by treatment with $P(NMe_2)_3$ and H_2O_2, halogenation of **30b** and **30e** with NIS afforded the corresponding halogenated derivatives **31** in 33–91% yields. Finally, Suzuki-Miyaura coupling reaction of **31** with pinacol arylboronates furnished D-π-A-type dithienophospholes **32** in good yields (76–85%). They were fully characterized by high-resolution mass spectrometry and ^{1}H, ^{13}C, and ^{31}P NMR spectroscopies.

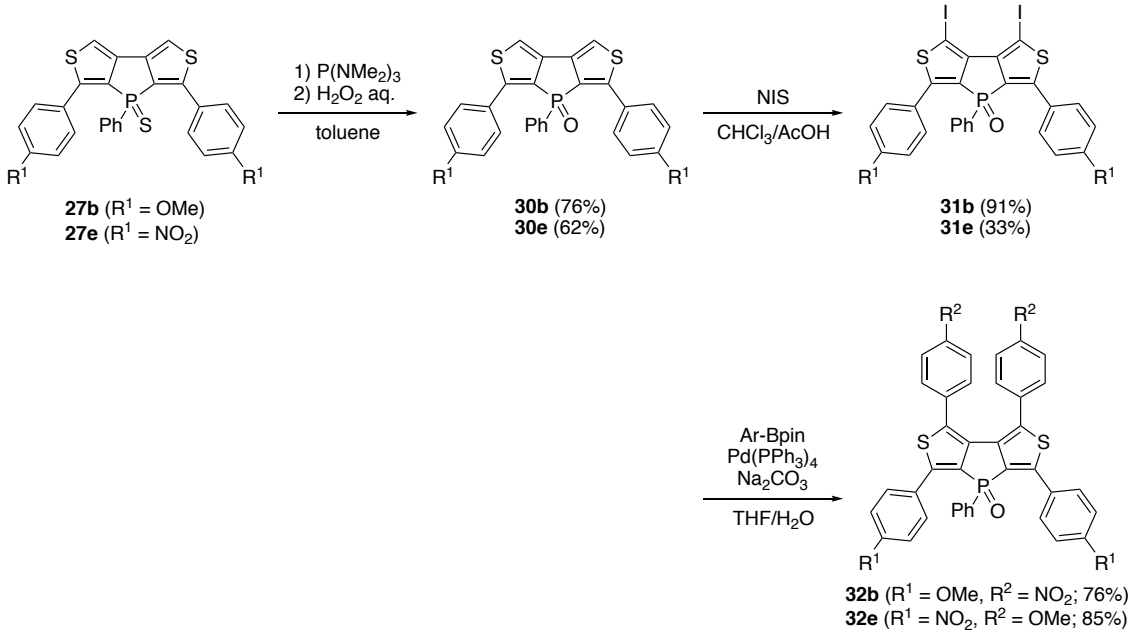

Scheme 2-1. Synthesis of D-π-A-type dithieno[3,4-*b*:3',4'-*d*]phospholes. (Ar = 4-nitrophenyl or 4-methoxyphenyl)

Fortunately, single crystals suitable for X-ray diffraction analysis were obtained by vapor diffusion of acetonitrile into $CHCl_3$ solutions of **32b** and **32e** (Figure 2-2, 2-3). The structural parameters of the dithienophosphole moiety for **32b** and **32e** are almost identical. Furthermore, the C–C bond lengths between the dithienophosphole moiety and aryl substituents for **32b** (1.468(5)–1.475(6) Å) and **32e** (1.463(4)–1.471(3) Å) are also comparable. The dihedral angles of the aryl substituents at the 1,7-positions are φ_1, φ_7 = 39–47°, reflecting the significant steric hindrance. The dihedral angles at the 3,5-positions for **32b** (φ_3 = 30° and φ_5 = 43°) are slightly larger than those for **32e** (φ_3 = 17° and φ_5 = 31°). The difference of the dihedral angles at the 3,5-positions may be attributed to the packing force (*vide infra*). Therefore, the position of the aryl substituents does not affect the structural properties.

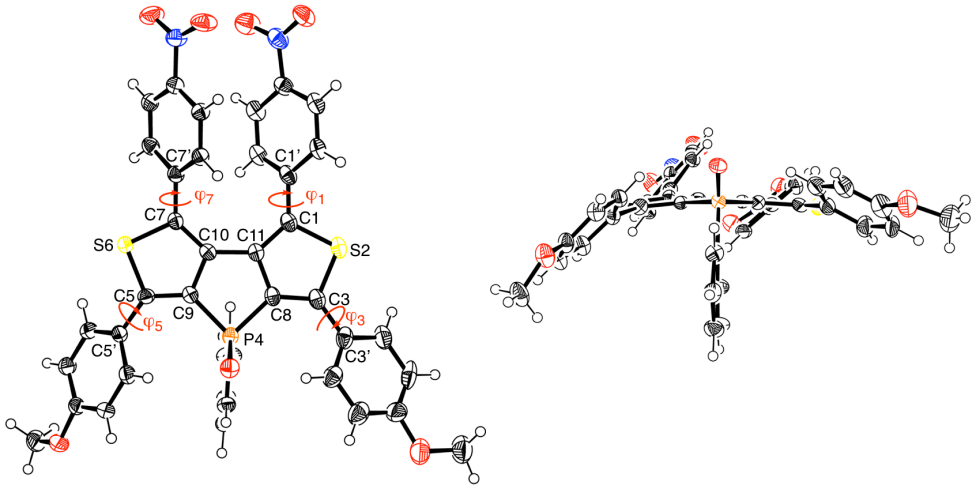

Figure 2-2. X-Ray crystal structure of **32b**: top view (left) and side view (right). Thermal ellipsoids represent 50% probability. Selected bond lengths (Å): C1–S2, 1.734(4); S2–C3, 1.731(4); C1–C11, 1.382(5); C3–C8, 1.388(5); C8–C11, 1.451(5); C5–S6, 1.727(4); S6–C7, 1.732(4); C5–C9; 1.375(5); C9–C10, 1.437(5); C7–C10, 1.384(5); P4–C8, 1.794(4); P4–C9, 1.788(4); C10–C11, 1.492(5); C1–C1', 1.468(5); C3–C3', 1.475(6); C5–C5', 1.473(5); C7–C7', 1.468(5). Selected dihedral angles: φ_1, 44.6°; φ_3, 29.7°; φ_5, 42.5°; φ_7, 45.6°.

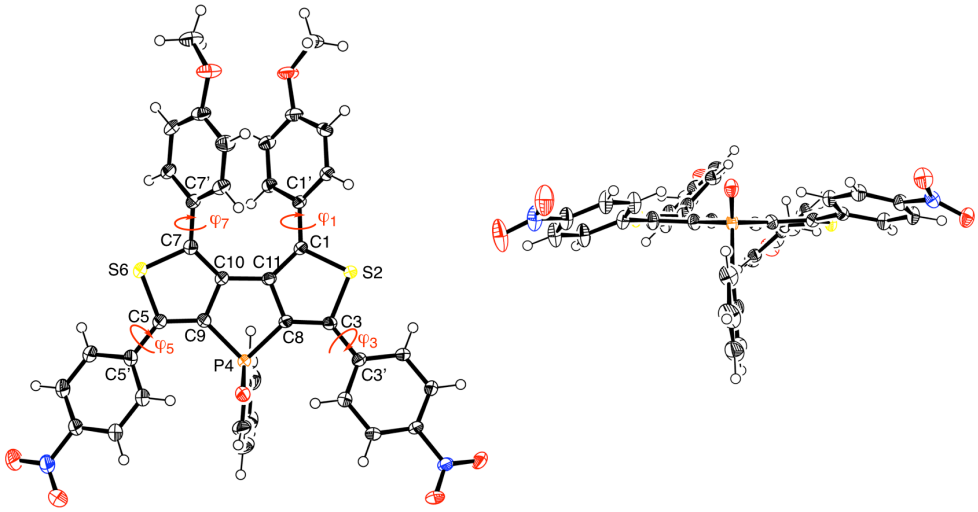

Figure 2-3. X-Ray crystal structure of **32e**: top view (left) and side view (right). Thermal ellipsoids represent 50% probability. Solvent molecules are omitted for clarity. Selected bond lengths (Å): C1–S2, 1.731(2); S2–C3, 1.730(3); C1–C11, 1.383(3); C3–C8, 1.378(3); C8–C11, 1.439(3); C5–S6, 1.728(3); S6–C7, 1.734(3); C5–C9; 1.388(3); C9–C10, 1.432(3); C7–C10, 1.386(3); P4–C8, 1.800(3); P4–C9, 1.794(3); C10–C11, 1.482(3); C1–C1', 1.463(3); C3–C3', 1.471(3); C5–C5', 1.463(4); C7–C7', 1.464(4). Selected dihedral angles: φ_1, 39.2°; φ_3, 16.9°; φ_5, 30.7°; φ_7, 47.3°.

2-3. Optical Properties

The UV-vis-NIR absorption and fluorescence spectra of **32b** and **32e** in CH_2Cl_2 are shown in Figure 2-4. The phosphole **32b** displays a peak at 358 nm, while the phosphole **32e** exhibits a peak at 376 nm with a shoulder at 425 nm. The red-shifted absorption of **32e** suggests more efficient intramolecular charge transfer (ICT) interaction because of the enhancement of D-π-A character. In accordance with this trend, the fluorescence peak of **32e** appears at 629 nm, while **32b** shows a peak at 606 nm. From the intersection of normalized absorption and fluorescence spectra, the optical HOMO–LUMO gaps were estimated to be 2.61 eV for **32b** and 2.57 eV for **32e**. The smaller optical HOMO–LUMO gap of **32e** supports the more effective ICT interaction for **32e** than **32b**.

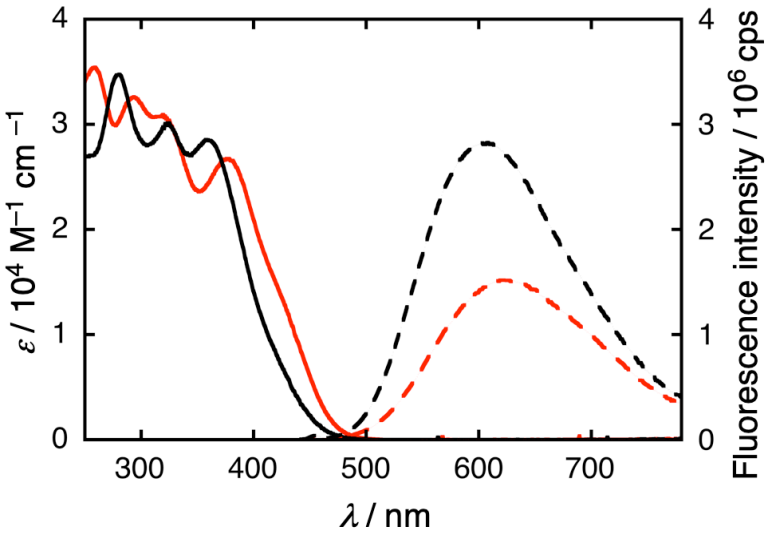

Figure 2-4. UV-vis-NIR absorption (solid lines) and fluorescence (dashed lines) spectra of **32b** (black) and **32e** (red) in CH_2Cl_2. For fluorescence measurements, the absorbances at 400 nm were adjusted to be 0.1 and the samples were excited at 400 nm under the same conditions for accurate intensity comparison.

2-4. Electrochemical Properties

The electrochemical properties of **32b** and **32e** were examined by cyclic voltammetry (CV) and differential pulse voltammetry (DPV) techniques in CH_2Cl_2 with tetrabutylammonium hexafluorophosphate (Bu_4NPF_6) as an electrolyte (Figure 2-5). The phosphole **32b** exhibits an irreversible oxidation peak at 1.03 V and two reversible reduction peaks at –1.42 and –1.80 V versus ferrocene/ferrocenium ion (vs. Fc/Fc^+). On the other hand, the phosphole **32e** exhibits an irreversible oxidation peak at 0.98 V and two reversible reduction peaks at –1.39 and –1.74 V. The electrochemical HOMO–LUMO gap of **32e** (2.37 eV) is smaller than that of **32b** (2.45 eV), which is consistent with the trend of the optical HOMO–LUMO gaps.

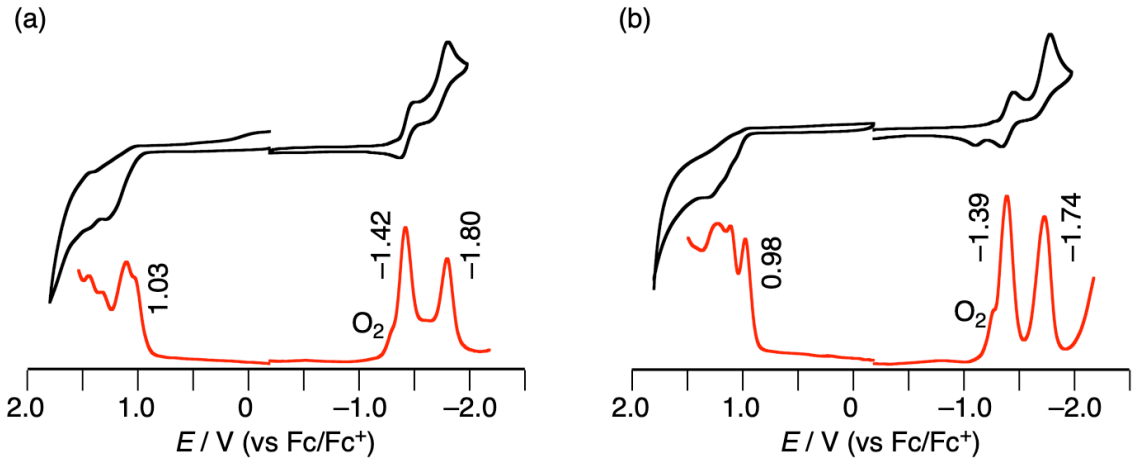

Figure 2-5. Cyclic voltammograms (black) and differential pulse voltammetry (DPV) curves (red) of dithienophospholes (a) **32b** and (b) **32e**. Redox potentials were determined by DPV. Solvent: CH_2Cl_2; scan rate: 0.05 V s^{-1}; working electrode: glassy carbon; reference electrode: Ag/Ag^+ (0.01 M $AgNO_3$); electrolyte: 0.1 M *n*-Bu_4NPF_6.

2-5. Theoretical Calculations

To understand the difference in the optical and electrochemical properties of D-π-A-type phospholes **32b** and **32e**, we performed density functional theory (DFT) calculations at the B3LYP/6-31G(d,p) level. The dihedral angles of the aryl substituents at the 1,7-positions on optimized structures for **32b** and **32e** are ca. 45°, which are consistent with those of their crystal structures (Figure 2-6). Meanwhile, the dihedral angles at the 3,5-positions are ca. 28° and 34°, respectively. These optimized structures also verify that the smaller dihedral angle for **32e** than **32b** is attributed to the packing force (*vide supra*). The selected Kohn-Sham orbitals of **32b**, **32e**, and unsubstituted dithienophosphole **23** are shown in Figure 2-7. The tendency on the calculated HOMO–LUMO gaps of **32b** and **32e** is inconsistent with those on the optical and electrochemical HOMO–LUMO gaps. Although the reason is unclear at this stage, the calculated HOMO–LUMO gaps at CAM-B3LYP/6-31G(d) and M06-2X/6-31G(d,p) cannot also reproduce the trend of the optical and electrochemical HOMO–LUMO gaps. In addition, we also performed the calculations using the X-ray crystal structures without optimization. The results are not consistent with those obtained from the optical and electrochemical measurements. Thus, it is difficult to explain the difference between **32b** and **32e** by the structural factors.

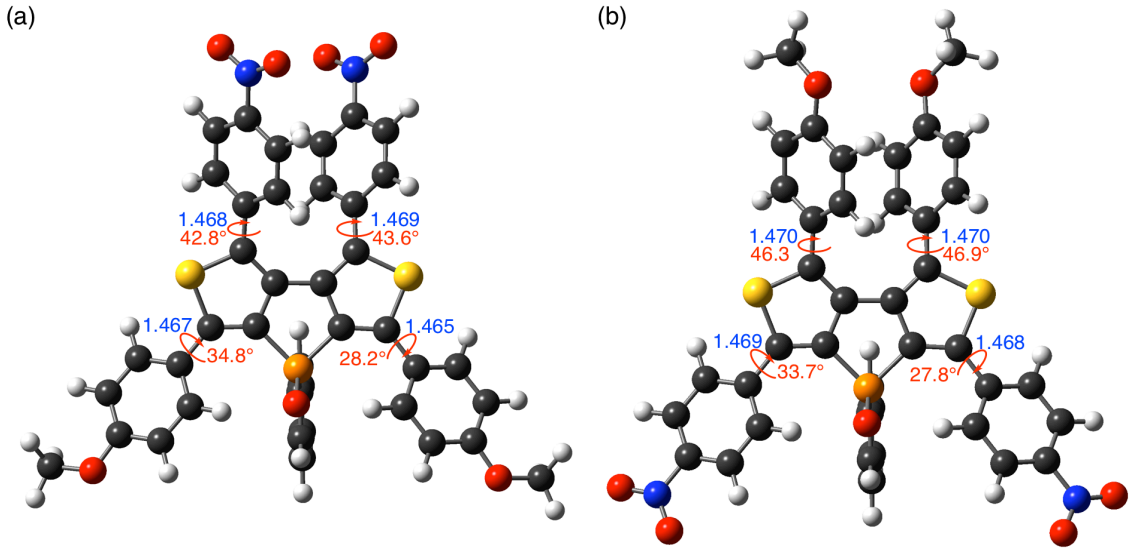

Figure 2-6. Optimized structures of (a) **32b** and (b) **32e** at the B3LYP/6-31G(d,p) level. Selected C–C bond lengths in Å (blue) and dihedral angles (red) are indicated.

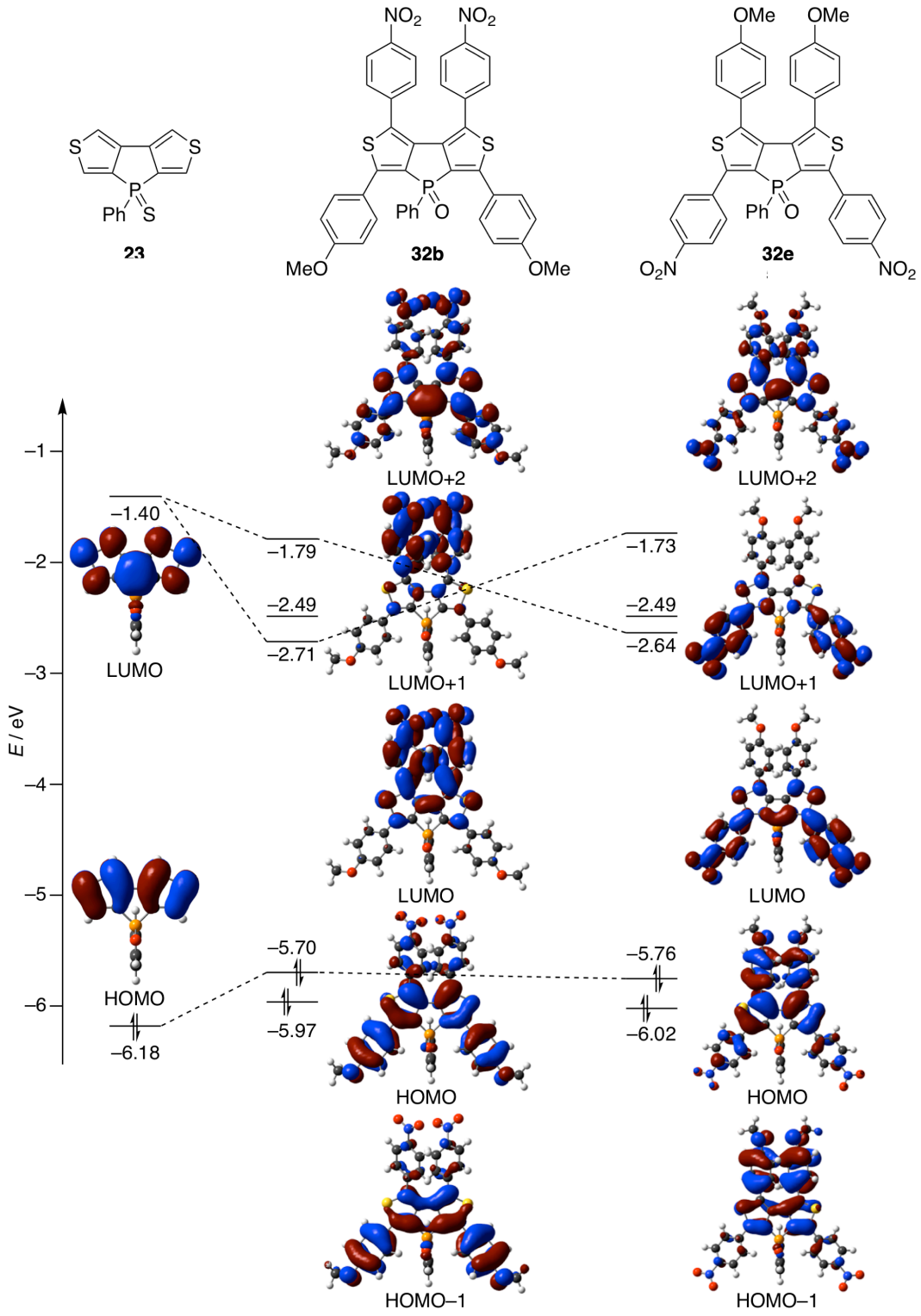

Figure 2-7. Selected Kohn-Sham orbitals of dithienophospholes **23**, **32b**, and **32e**.

The HOMO of **23** is localized on the thiophene rings, while the LUMO of **23** shows significant orbital distribution on the phosphorus atom, which indicates the effective σ*-π* interaction. Namely, the dithienophosphole **23** possesses thiophene-based HOMO and phosphole-based LUMO, which is responsible for the hybrid character of electron-donating thiophene and electron-withdrawing phosphole. The HOMO of **23** provides the HOMOs of **32b** and **32e**, which display large orbital distributions on the dithienophosphole moiety and the methoxyphenyl groups. Despite the moderate dihedral angles at the 1,7-positions (ca. 45°), the large orbital distributions on the methoxyphenyl groups for **32e** suggests the effective electronic communication between the dithienophosphole moiety and the methoxyphenyl groups. Thus, the electron-donating character of the thiophene can be enhanced by the methoxyphenyl groups for both **32b** and **32e**. In contrast, the LUMOs of **32b** and **32e** are mainly localized on the nitrophenyl groups. It is noteworthy that the LUMO of **32b** shows no orbital distribution on the phosphorus atom, whereas the LUMO of **32e** exhibits significant orbital distribution on the phosphorus atom, indicating the contribution of phosphole-like σ*-π* interaction.[33,46] Interestingly, the LUMO of **23** provides the LUMO and LUMO+2 for **32b** and **32e**. For **32b**, phosphole-like σ*-π* interaction is seen in LUMO+2. On the other hand, the LUMO+2 of **32e** reveals orbital distributions on the dithienophosphole moiety similar to the LUMO of **32b**. Consequently, the character of the electron-withdrawing phosphole would be weakened for **32b**, whereas the nitrophenyl groups enhance the phosphole character for **32e**. Therefore, the enhanced phosphole-like character for **32e** rationalizes the more effective ICT interaction for **32e** than **32b**. The position of the nitrophenyl group plays an important role in the frontier molecular orbitals, and the hybrid character of dithieno[3,4-*b*:3’,4’-*d*]phosphole.

2-6. Summary

In summary, we designed and synthesized two D-π-A-type dithieno[3,4-*b*:3',4'-*d*]phosphole derivatives to examine the effects of the D-π-A interaction. The phosphole **32e** exhibited red-shifted absorption and fluorescence, which suggests the more effective ICT interaction for **32e** than **32b**. The DFT calculations revealed that the HOMOs of **32b** and **32e** are originated from the thiophene-based HOMO of unsubstituted **23**. Meanwhile, the LUMO of **32b** possesses no orbital distribution on the phosphorus atom, whereas the LUMO of **32e** shows significant orbital distribution on the phosphorus atom. Accordingly, the position of substituents plays an important role in the frontier molecular orbital distributions. Overall, **32e** retains both character of the electron-donating thiophene and electron-withdrawing phosphole by introducing electron-donating and electron-withdrawing substituents at the appropriate positions of the dithieno[3,4-*b*:3',4'-*d*]phosphole core. Thus, the modulation of frontier molecular orbitals would be an effective strategy to explore organic functional materials based on dithieno[3,4-*b*:3',4'-*d*]phospholes.

Chapter 3. Pluripotent Features of Doubly Thiophene-Fused Benzodiphospholes as Organic Functional Materials

---

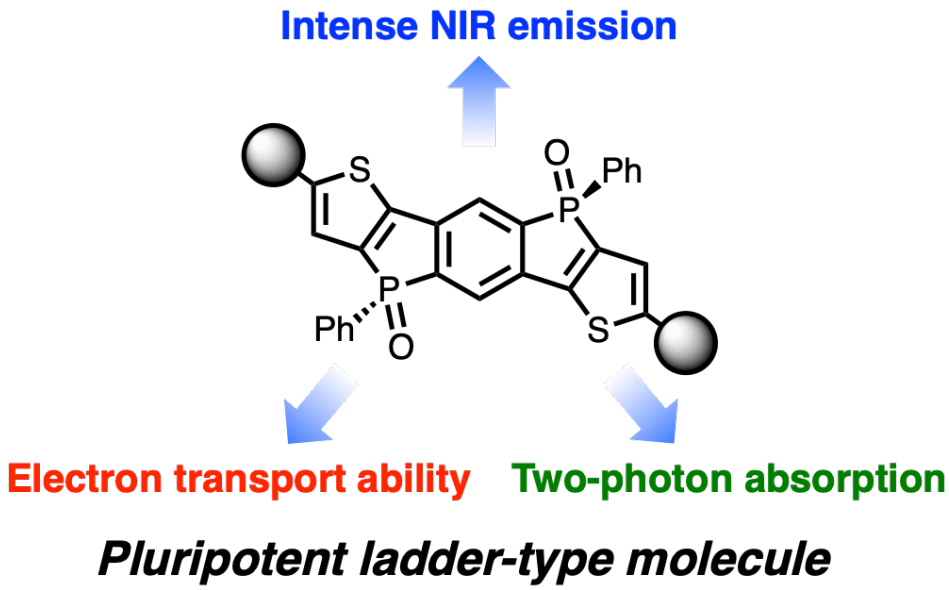

Contents

3-1. Introduction

As described in General Introduction, physcochemical properties of phosphole-fused π-conjugated molecules have been extensively investigated in this decade due to the development of facile synthetic methodology and their potential utilities in various fields have also been demonstrated.[46] Because several phosphorus(V) derivatives exhibit high electron mobility because of their excellent electron-accepting ability, they are expected to be used as n-type organic semiconducting materials that are applicable to OPVs [14g,h] and OLEDs.[47h] In addition, a zwitterionic ladder-type phosphole is known to possess a large two-photon absorption (TPA) cross section (ca. 780 GM at λ = 1200 nm).[58] However, to the best our knowledge, examples of benzodiphospholes have been still rare despite their potential utility as a leading platform to explore various phosphole-based ladder-type π-conjugated molecules. The synthetic difficulties, i.e., direct chemical modifications of the terminal phenyl rings and fused benzene rings, prevent further π-extension and functionalization. Nevertheless, to create a new class of phosphole-based ladder-type π-conjugated molecules, we need a breakthrough in their π-extension and functionalization. Considering the synthetic advantages of thiophene over benzene and phosphole, i.e., the high chemical stability and facile chemical modification at the α-position, the author focuses on doubly thiophene-fused benzodiphosphole **33** as the key leading platform (Figure 3-1). Fusion of electron-donating thiophene to electron-withdrawing benzodiphosphole would stabilize the electronic structure, creating the new platform depending on the substituents. Another important benefit of the thiophene-fused structure is plausible enhancement of intermolecular interactions involving the heteroatoms in the solid state. Unique three-dimensional (3D) packing structures of **33** in the solid state would be formed by combination of intermolecular hydrogen bondings and S–S interactions as well as π-π interactions derived from its rigid and planar structure, considering that phosphole-based molecules are known to exhibit intermolecular hydrogen bonds between P=O and C–H moieties in the solid state.[45,59] Therefore, the author envisioned that **33** would be an attractive platform for π-extension and functionalization to explore diverse potential applications. Herein, we report the synthesis and physicochemical properties of **33**–**36**, and its π-extension by conventional palladium-catalyzed coupling reactions (Figure 3-1). First, the author established the general synthetic route to doubly thiophene-fused benzodiphospholes ***trans*-33** and ***cis*-33** as the core unit and elucidated their unusual properties depending on the isomers. Then, the author introduced aryl, arylethenyl, and arylethynyl groups with electron-donating or electron-withdrawing substituents to the α-positions of the synthetic accessible fused-thiophene

moieties of ***trans*-33**, yielding the π-extend derivatives **34**–**36**. The systematic exploration was found to be effective to unveil their pluripotent features of doubly thiophene-fused benzodiphospholes as organic functional materials, i.e., intense near infrared (NIR) emission, excellent TPA cross-section, and remarkably high electron-transporting ability.

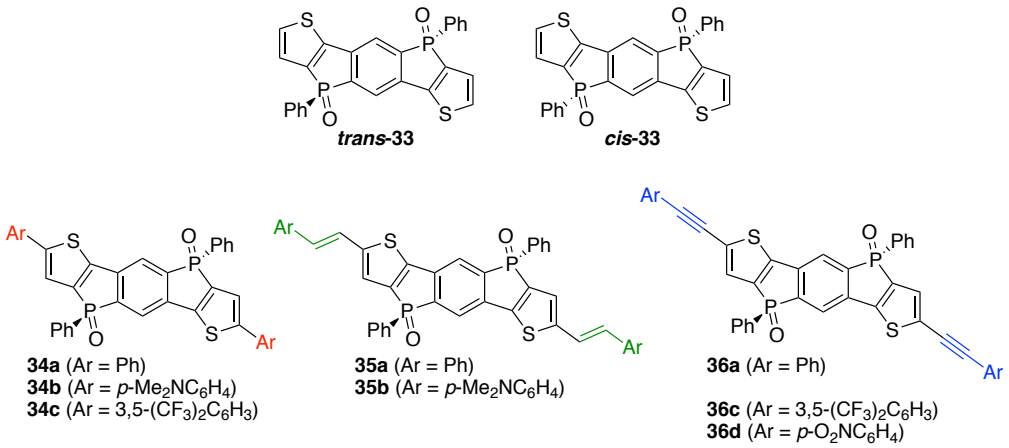

Figure 3-1. Structures of doubly thiophene-fused benzodiphospholes.

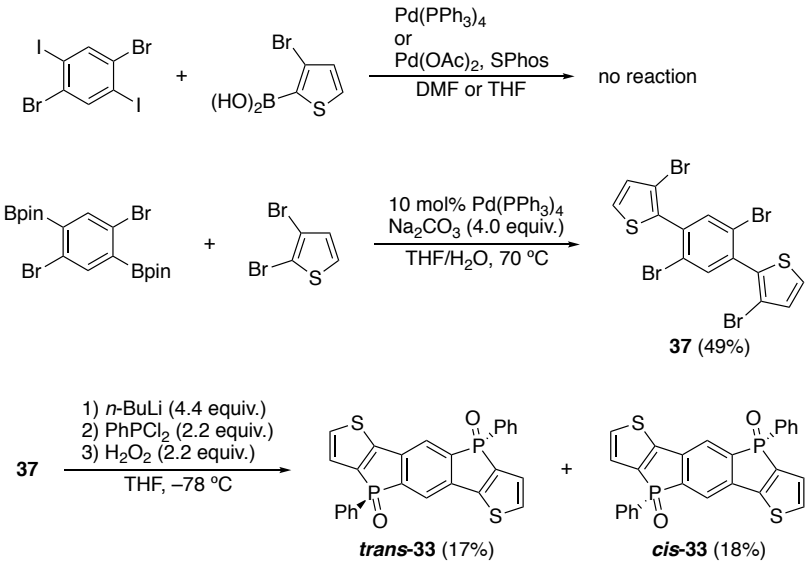

Scheme 3-1. Synthesis of doubly thiophene-fused benzodiphospholes.

3-2. Synthesis of Thiophene-fused Benzodiphospholes

At the first stage, the author aimed to establish the synthetic method of doubly thiophene-fused benzodiphosphole *via* halogen-lithium exchange of **37** (Scheme 3-1). When the author performed Suzuki-Miyaura coupling reaction of 1,4-dibromo-2,5-diiodobenzene with 3-bromo-2-thienylboronic acid in the presence of $Pd(PPh_3)_4$ or $Pd(OAc)_2$/SPhos as catalysts, the starting materials were recovered and the key precursor **37** was not obtained. On the other hand, Suzuki-Miyaura coupling reaction of 1,4-dibromo-2,5-bis(pinacolatoboryl)benzene with 2,3-dibromothiophene in the presence of $Pd(PPh_3)_4$ smoothly proceeded to afford **37** in acceptable yield (49%). In the next step, when a solution of *n*-BuLi was added to a THF solution of **37** at –78 °C, the solution immediately turned black and gave a complicated mixture. Conversely, the addition of a THF solution of **37** into a solution of *n*-BuLi afforded a clear solution containing tetralithiated species. Treatment of the lithiated species with $PhPCl_2$ and H_2O_2 provided ***trans*-34** and ***cis*-33** as a diastereomeric mixture. These diastereomers were successfully separated by silica-gel column chromatography to yield ***trans*-33** in 17% and ***cis*-33** in 18%. The doubly thiophene-fused benzodiphospholes **33** were characterized by ^{1}H, ^{13}C, and ^{31}P NMR spectroscopies and high-resolution mass spectrometry. The ^{31}P NMR spectra of ***trans*-33** and ***cis*-33** exhibit the peaks at 22.9 and 22.7 ppm, respectively. The upfield shifts relative to the doubly phenyl-substituted benzodiphosphole (33.7 ppm)[40] reflect their thiophene-fused structures. Fortunately, the structures with *trans*/*cis*-configurations were revealed by X-ray diffraction analysis. The crystal structure of ***trans*-33** shows a highly planar structure (Figure 3-2). On the other hand, ***cis*-33** reveals a slightly warped structure, probably originated from the packing forces (Figure 3-3). The C–C and C–P bond lengths on the benzodiphosphole unit are similar to those of reported benzodiphosholes,[37b,c,41a,b] indicating that the fusion of thiophene to the benzodiphosphole has little impact on their structural parameters (Figures 3-2 and 3-3). The trans and cis isomers reveal unusual contrast in the packing modes. The packing structure of ***trans*-33** displays a one-dimensional (1D) slip π-stacked alignment (Figure 3-2). The separation distance between two π-planes is ca. 3.5 Å, which implies effective intermolecular π-π interaction. In contrast, ***cis*-33** forms a face-to-face dimeric structure. The intermolecular separation distance is approximately 3.5 Å with effective overlapping with a small rotation angle between the two planes (ca. 7°) (Figure 3-3). Additionally, each dimeric structure is isolated by the phenyl groups on the phosphorus atoms in the molecular packing.

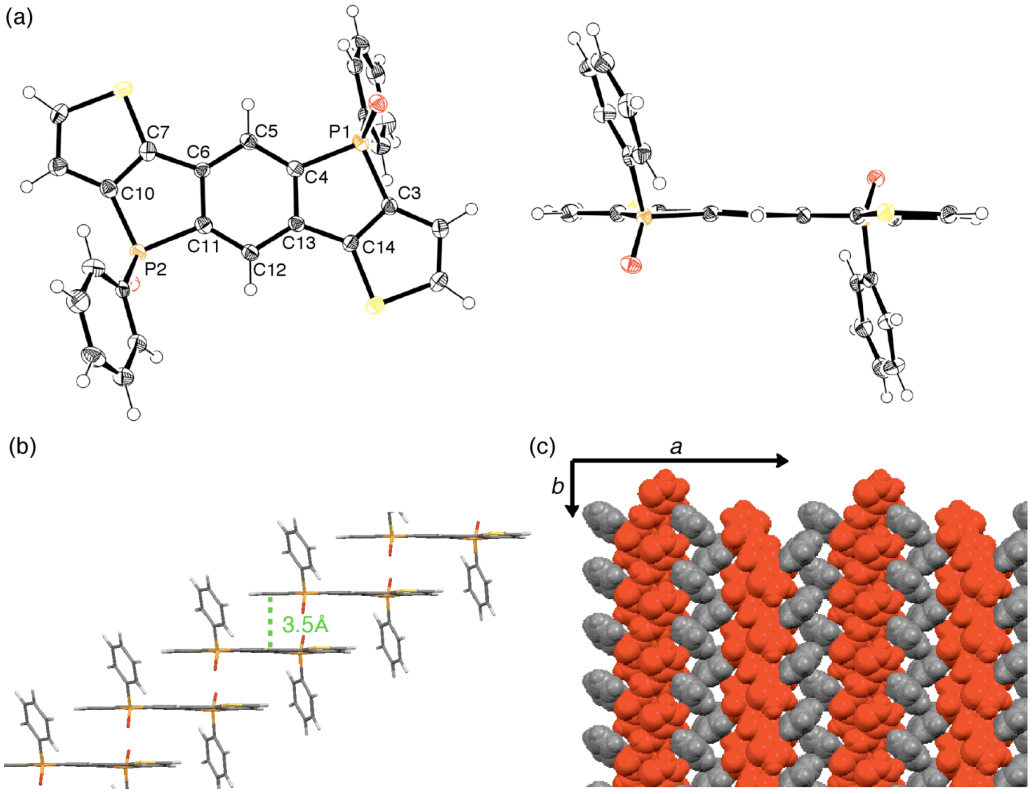

Figure 3-2. (a) X-Ray crystal structure of ***trans*-33**: top view (left) and side view (right). Thermal ellipsoids represent 50% probability. (b) 1D slip stacked arrangement of ***trans*-33** in the crystal structure (Intermolecular π-π interaction is shown in green dashed line with the separation distance). (c) Packing structure of ***trans*-33**. The doubly thiophene-fused benzodiphosphole cores are colored in red, whereas the phenyl groups and oxygen atoms on the P atoms are shown in grey color. Solvent molecules are omitted for clarity. Selected bond lengths (Å): C3–P1, 1.786(5); C3–C14, 1.378(6); C4–P1, 1.813(5); C4–C5, 1.387(7); C4–C13, 1.408(7); C5–C6, 1.393(7); C6–C7, 1.473(6); C6–C11, 1.408(7); C7–C10, 1.385(7); C10–P2, 1.788(5); C11–P2, 1.815(5); C11–C12, 1.381(7); C12–C13, 1.397(7); C13–C14, 1.469(6).

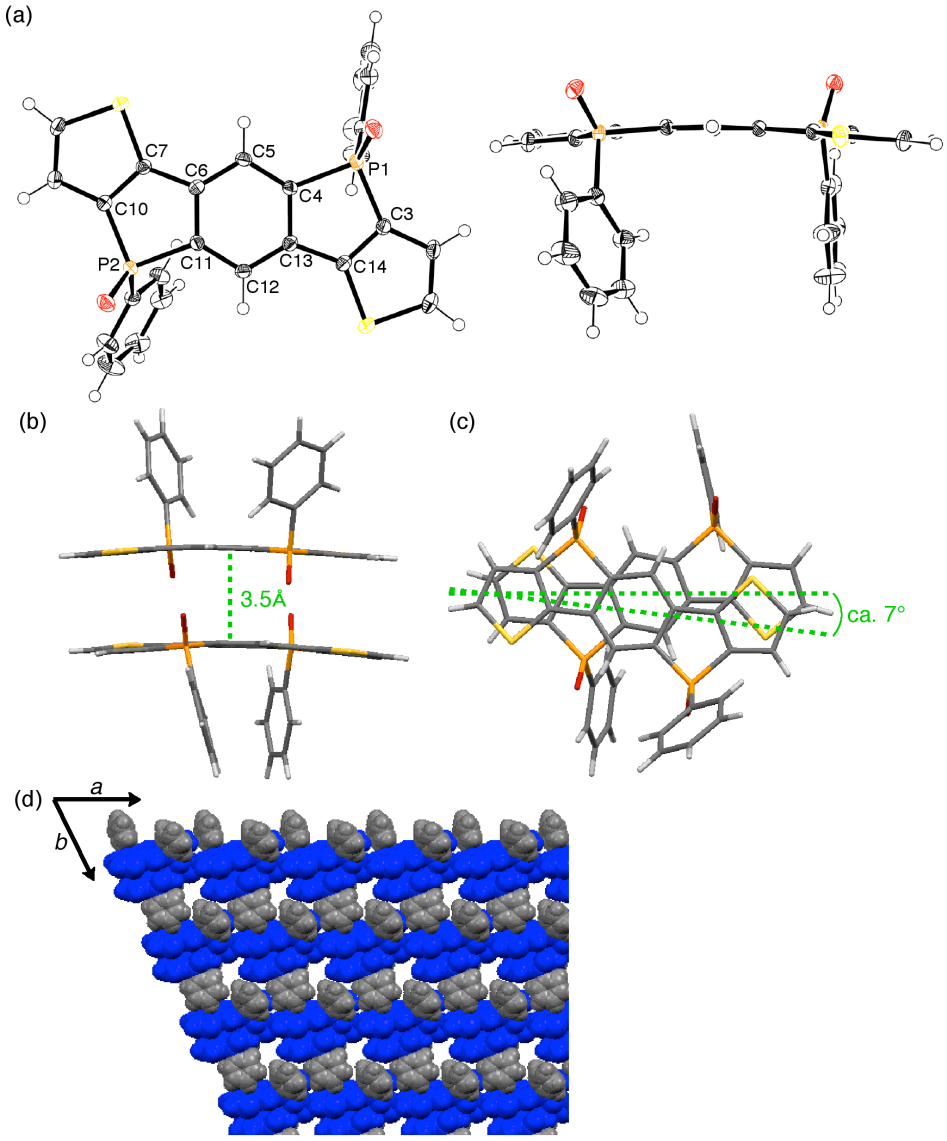

Figure 3-3. (a) X-ray crystal structure of ***cis*-33**: top view (left) and side view (right). Thermal ellipsoids represent 50% probability. One of the two independent molecules in the unsymmetric unit cell is shown. (b) Face-to-face dimeric structure with the π-π interaction (Intermolecular π-π interaction is shown in green dashed line with the separation distance). (c) Effective overlapping of two molecules (Molecular axes are shown in green dashed line with the rotation angle). (d) Packing structure of ***cis*-33**. The doubly thiophene-fused benzodiphosphole cores are colored in blue, whereas the phenyl groups and oxygen atoms on the P atoms are shown in grey color. Solvent molecules are omitted for clarity. Selected bond lengths (Å): C3–P1, 1.797(3); C3–C14, 1.383(4); C4–P1, 1.820(3); C4–C5, 1.387(4); C4–C13, 1.411(4); C5–C6, 1.397(4); C6–C7, 1.463(4); C6–C11, 1.413(4); C7–C10, 1.386(4); C10–P2, 1.789(3); C11–P2, 1.830(3); C11–C12, 1.387(4); C12–C13, 1.394(4); C13–C14, 1.469(4).

Taking into account the more extensive intermolecular π-π interactions in ***trans*-33** than that in ***cis*-33** in the solid state, the author chose ***trans*-33** as the platform for the π-extension and functionalization. First, the author attempted halogenation of ***trans*-33**. However, the reaction of ***trans*-33** with 2 equivalent of *N*-bromosuccinimide (NBS) resulted in the complete recovery of ***trans*-33**. After trial-and-error optimization of reaction conditions, the author succeeded to obtain dibrominated benzodiphosphole **38** as the important intermediate quantitatively by treatment of ***trans*-33** with 10 equivalent of NBS in a mixture of chloroform and acetic acid (Scheme 3-2). It is noteworthy that the α-positions of the thiophene rings were brominated with complete selectivity irrespective the large excess of NBS. Then, the author carried out palladium-catalyzed cross-coupling reactions of **38** to obtain versatile π-extended doubly thiophene-fused benzodiphospholes (Scheme 3-2). The Suzuki-Miyaura coupling reaction of **38** with arylboronates afforded aryl-substituted **34** in high yields (67–88%). The Mizoroki-Heck reaction of **38** with styrene also proceeded to give **35a**, but the yield was low (27%). On the other hand, the Suzuki-Miyaura coupling reaction with alkenylboronates afforded arylethenyl-substituted **35a** and **35b** in high yields (65 and 78%, respectively). In addition, the Sonogashira coupling reaction with arylacetylenes gave arylethynyl-substituted **36a**,**c**,**d** in moderate to high yields (32–86%), although the reaction with dimethylaminophenylacetylene resulted in the complete recovery of **38**. These results unambiguously corroborate that various π-extended doubly thiopene-fused benzodiphospholes are accessible by conventional palladium-catalyzed cross-coupling reactions of **38** converted from ***trans*-33** as the platform.

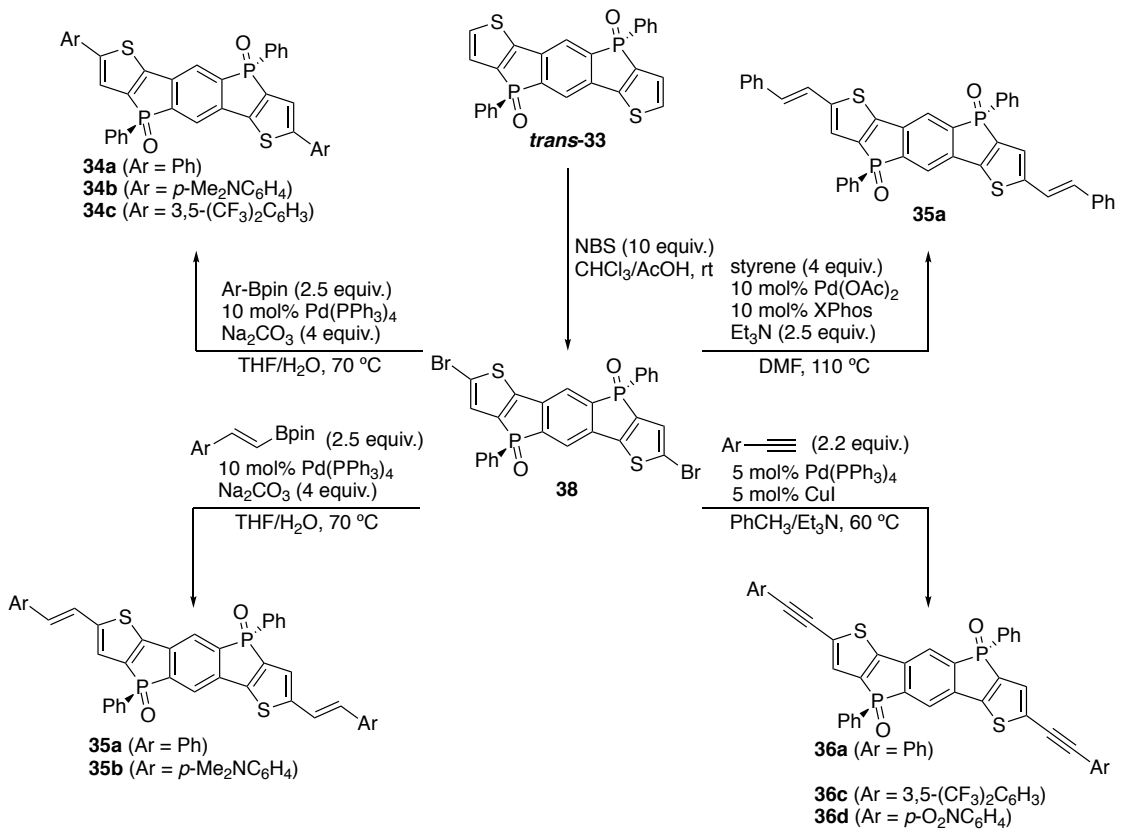

Scheme 3-2. Coupling reactions of **38** to produce versatile π-extended doubly thiophene-fused benzodiphospholes **34**–**36**.

Fortunately, the author obtained single crystals of **34a** (Figure 3-5) and **36a** (Figure 3-4) suitable for X-ray crystallographic analysis. The C–C and C–P bond lengths on the benzodiphosphole unit of **34a** and **36a** are comparable to those of the unsubstituted ***trans*-33**. The torsion angles of the terminal phenyl rings relative to the benzodiphosphole core are small (11~22°), implying effective π-extension through the substituents. The packing structure of **36a** signifies a 1D slip π-stacked alignment, which is similar to the packing structure of ***trans*-33**. The separation distance between two π-planes is enlarged (ca. 3.7 Å), indicating the weakened π-π interaction by the introduction of the phenylethynyl group (Figure 3-4b). Meanwhile, the packing structure of **34a** is unique. It displays an ununiform 1D slip π-stacked alignment with independent molecules A and B (Figure 3-5b). The molecule A shows high planarity with a mean plane deviation (MPD) of the thiophene-fused benzodiphosphole core (18 atoms, 0.039 Å), while the molecule B reveals a slightly distorted structure with a MPD of 0.060 Å. The separation distances between the terminal phenyl group and thiophene-fused benzodiphosphole core are 3.6–3.7 Å, suggesting the reduced intermolecular π-π interactions by the direct introduction of the phenyl groups. Importantly, the doubly thiophene-fused benzodiphosphole

core of **34a** exhibits a 2D herringbone structure with a short intermolecular S-S contact of 3.64 Å (Figure 3-5c).[60] Moreover, there are short distances between the oxygen atoms of the P=O moieties and the hydrogen atoms of the thienyl and the terminal phenyl groups (2.3–2.5 Å), indicating the presence of multiple hydrogen bondings. Thus, the terminal phenyl rings attached directly to the fused-thiophene moieties play an important role in the formation of 2D herringbone structure of **34a** with the assistance of the versatile intermolecular interactions involving the heteroatoms, unlike ***trans*-33**, ***cis*-33**, and **36a**. This unique packing structure encouraged us to further examine the charge-transporting ability of the doubly thiophene-fused benzodiphospholes in the solid state (vide infra).

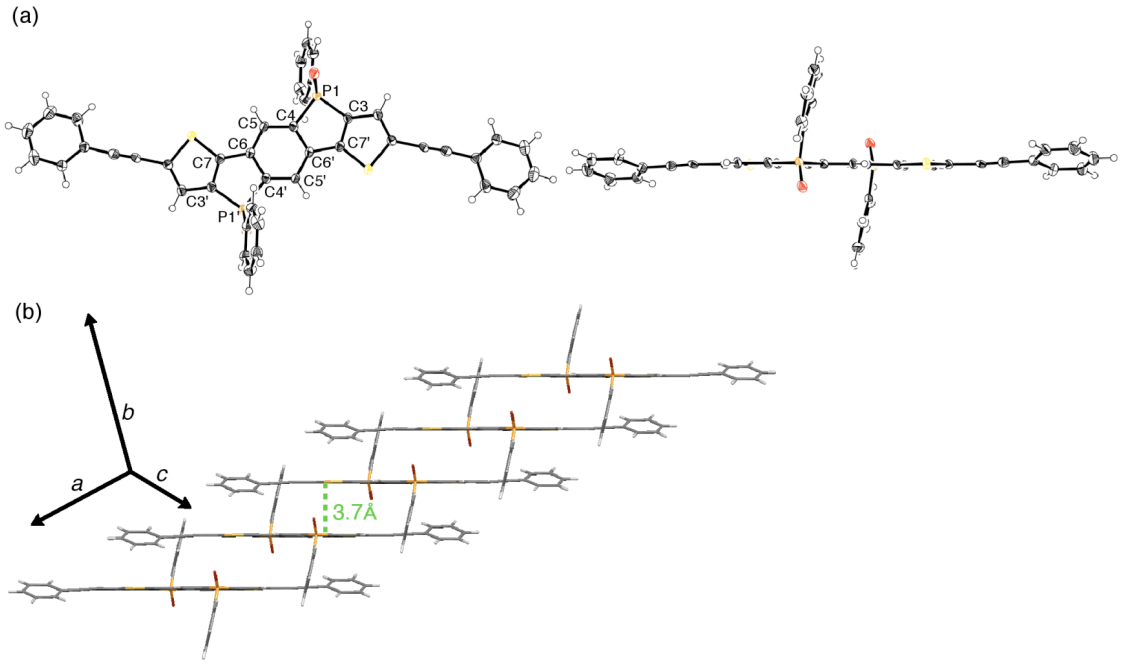

Figure 3-4. (a) X-ray crystal structure of **36a**: top view (left) and side view (right). Thermal ellipsoids represent 50% probability. (b) 1D slip stacked arrangement of **36a** in the crystal structure (Intermolecular π-π interaction is shown in green dashed line with the separation distance). Solvent molecules are omitted for clarity. Selected bond lengths (Å): C3–P1, 1.803(3); C3–C7', 1.372(4); C4–P1, 1.816(3); C4–C5, 1.387(4); C4–C6', 1.411(4); C5–C6, 1.409(4); C6–C7, 1.464(4).

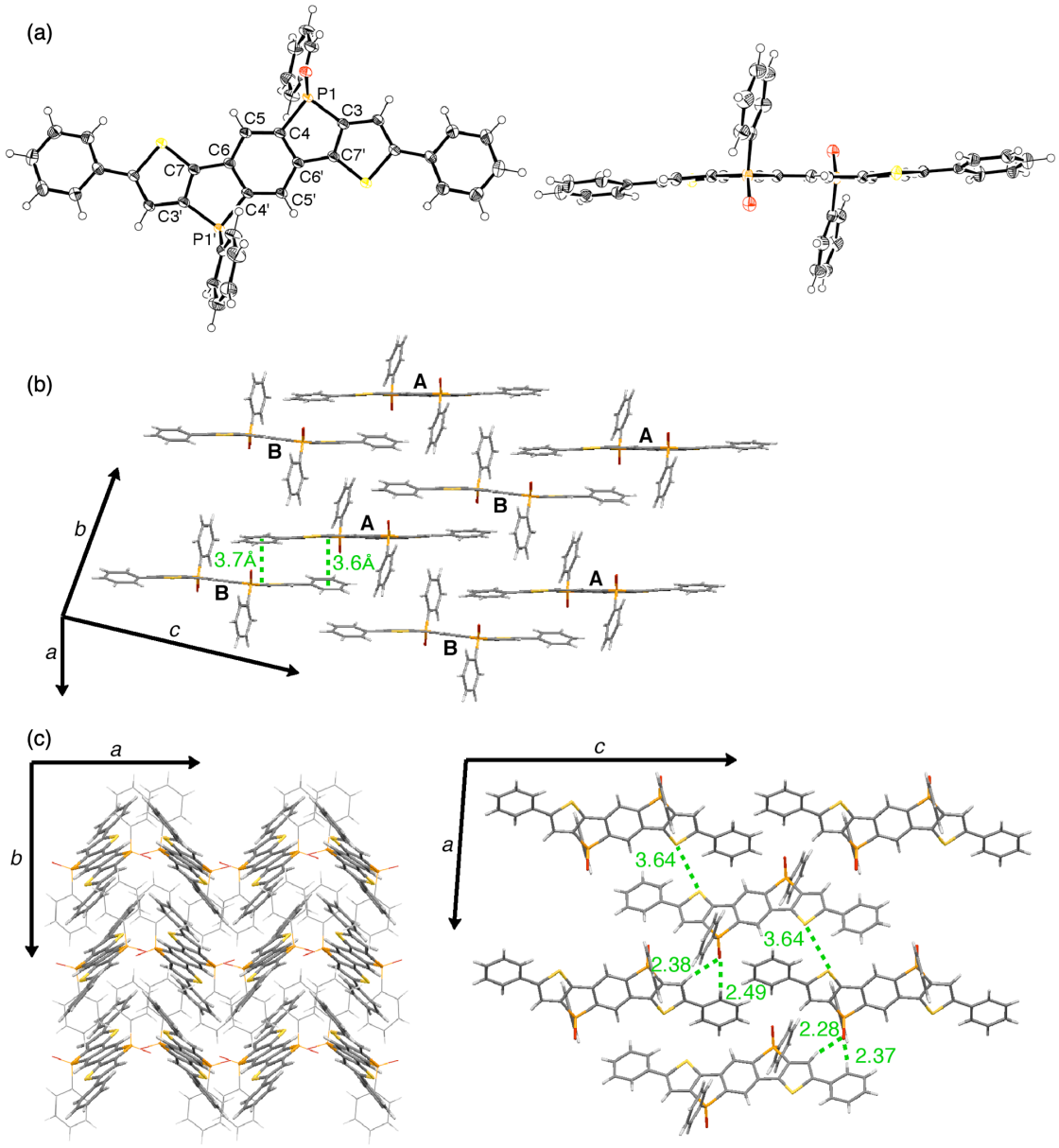

Figure 3-5. (a) X-ray crystal structure of **34a**: top view (left) and side view (right). Thermal ellipsoids represent 50% probability. One of the two independent molecules in the unsymmetric unit cell is shown. (b) Ununiform 1D slip p-stacked arrangement of **34a** in the crystal structure (Intermolecular π-π interactions are shown in green dashed line with the separation distances). (c) The packing structure of **34a** along with *c*-axis (left) and *b*-axis (right). S-S contacts and hydrogen bonds are indicated (dashed green lines) with the distances between S···S and O···H (Å). Selected bond lengths (Å): C3–P1, 1.798(2); C3–C7', 1.382(3); C4–P1, 1.8311(19); C4–C5, 1.384(3); C4–C6', 1.410(3); C5–C6, 1.400(3); C6–C7, 1.459(3).

3-3. Optical Properties

The author examined the optical properties of doubly thiophene-fused benzodiphospholes **33**–**36** (Table 3-1). UV/Vis absorption and fluorescence spectra of ***trans*-33** and ***cis*-33** were measured in CH_2Cl_2. The absorption spectra of ***trans*-33** and ***cis*-33** display the lowest energy absorption at 404 nm (Figure 3-6a), which are red-shifted compared to those of aromatic-fused benzodiphospholes (ca. 380 nm).[40] These red-shifts can be attributed to ICT interaction as a result of fusion of the electron-rich thiophene rings to the electron-deficient benzodiphosphole core. The solvatochromism of their absorption spectra supports their ICT interactions (Figure 3-6c and 3-6d). The benzodiphospholes ***trans*-33** and ***cis*-33** exhibit blue fluorescence with similar emission maxima at 481 and 478 nm, respectively (Figure 3-6b). The fluorescence peaks are remarkably shifted to long wavelengths relative to the benzene-fused dibenzophosphole (420 nm).[40] Namely, the Stokes shifts of ***trans*-33** and ***cis*-33** (4000 and 3800 cm^{-1}) are much larger than that of the benzene-fused dibenzophosphole (2300 cm^{-1}).[40] Notably, ***trans*-33** and ***cis*-33** are highly fluorescent. The fluorescence quantum yields (Φ_F) of ***trans*-33** and ***cis*-33** are 0.92 and 0.91, which are higher than that of the benzene-fused dibenzophosphole (0.81).[40] The fluorescence lifetimes (τ_F) were measured by the time-correlated single-photon counting (TCSPC) technique. The τ_F values in CH_2Cl_2 were determined to be 11.9 ns and 12.0 ns, respectively. Although no fluorescence lifetimes of benzodiphospholes have been reported, these values are similar to those of phosphole-based ladder-type molecules.[42,61] The radiative (k_r) and nonradiative (k_{nr}) rate constants are calculated from the τ_F and Φ_F values. The k_r and k_{nr} values are 7.6–7.7 $\times 10^7$ and 6.7–7.5 $\times 10^6$ s^{-1}, respectively. The k_{nr} values are one order of magnitude smaller than those of typical benzo[*b*]phospholes ($\sim 10^7$ s^{-1}). These small k_{nr} values relative to k_r values are responsible for the high Φ_F values in spite of the large Stokes shifts. Although the large Stokes shifts and rather strong fluorescence are counterintuitive, the unusual fluorescence properties of doubly thiophene-fused benzodiphospholes are beneficial for biological imaging to avoid background fluorescence (vide infra).

Fluorescence spectra of ***trans*-33** and ***cis*-33** were also measured in the solid state (Figure 3-6b). The fluorescence spectra in the solid state are red-shifted considerably in comparison with those in solution. Remarkably, the red-shift of ***cis*-33** (55 nm) is much larger than that of ***trans*-33** (10 nm). The fluorescence quantum yields of ***trans*-33** and ***cis*-33** in the solid state were determined to be 0.16 and 0.10, respectively. The remarkable red-shift of fluorescence in the solid state may result from the isolated unique dimeric structure of ***cis*-33**, as observed in the packing structure, which reveals an excimer emission solely in the solid state. In accordance

with this interpretation, no red-shift of fluorescence was observed in the solution even at high concentrations. Although the solid-state excimer emission is often observed in polyaromatic hydrocarbons (i.e., anthracene[62] and pyrene[63]), the examples of excimer emission of phosphole derivatives have been limited to dithienophosphole derivatives.[35d,59,64] Thus, the subtle change, i.e., the mutual orientation of the phenyl groups and oxygen atoms on the phosphorous atoms, has a large influence on the packing structure in the solid state, altering the photophysics in the excited states of ***trans*-33** and ***cis*-33** in the solid state.

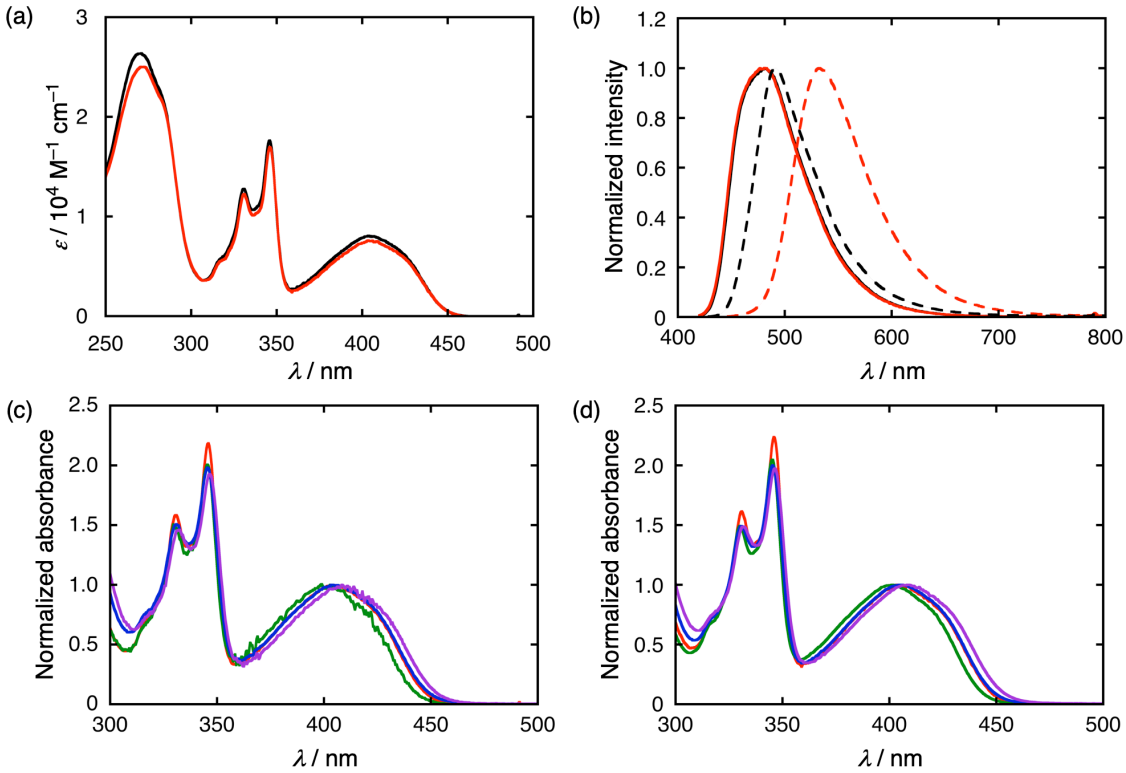

Figure 3-6. (a) UV/Vis absorption and (b) normalized fluorescence spectra of doubly thiophene-fused benzodiphospholes ***trans*-33** (black) and ***cis*-33** (red) in CH_2Cl_2 (solid lines) and in the solid state (dashed lines). Normalized absorption spectra of (c) ***trans*-33** and (d) ***cis*-33** in various solvents; THF (green), CH_2Cl_2 (red), DMF (blue), and DMSO (violet). For fluorescence measurements, the samples were excited at 415 nm.

Table 3-1. Optical properties of doubly thiophene-fused benzodiphospholes in CH_2Cl_2.

	λ_{abs} / nm[a] (ε / $M^{-1}cm^{-1}$)	λ_{abs} / nm[b] (Φ_F)[c]	E_{opt} /eV[d]	τ_F /ns	k_r /10^7 s^{-1}	k_{nr} /10^7 s^{-1}	$\Delta\nu$ /cm^{-1}[e]
***trans*-33**	404 (8000)	481 (0.92)	2.76	11.9	7.7	0.67	4000
***cis*-33**	404 (7600)	478 (0.91)	2.76	12.0	7.6	0.75	3800
34a	443 (19000)	525 (0.50)	2.50	3.6	14	14	3500
34b	505 (33000)	650 (0.51)	2.14	4.6	11	11	4400
34c	434 (27000)	496, 514 (0.28)	2.58	1.6	18	45	2900
35a	470 (15000)	556 (0.27)	2.33	1.6	17	46	3300
35b	520 (37000)	699 (0.22)	2.05	1.7	13	46	4900
36a	445 (31000)	520 (0.37)	2.49	1.8	21	35	3200
36c	439 (31000)	501, 520 (0.34)	2.53	1.4	24	47	2800
36d	445 (42000)	505, 532 (0.30)	2.50	0.9	33	78	2700

[a] Absorption maxima at the longest wavelength. [b] The samples were excited at 415 nm. [c] Absolute fluorescence quantum yields. [d] Optical HOMO–LUMO gaps from the intersection of normalized absorption and fluorescence spectra. [e] Stokes shift.

The phenyl-substituted doubly thiophene-fused benzodiphospholes **34a-c** display red-shifted absorption and fluorescence spectra compared to the unsubstituted ***trans*-33** (Figure 3-7). The thiophene-fused structure is responsible for the red-shifted absorption of **34a** (443 nm) relative to those of the phenyl-substituted benzodiphospholes (ca. 425 nm).[37b,c] The dimethylaminophenyl-substituted **34b** reveals a red-shifted intense absorption at 505 nm in comparison with **34a**, indicating effective ICT interaction between the electron-donating dimethylamino moiety and electron-withdrawing benzodiphosphole unit. Strikingly, **34b** shows a moderate fluorescence with a peak at 650 nm and wavelengths exceeding 900 nm (Figure 3-7b). Therefore, the push-pull D-A-D structure of **34b** is an effective molecular design to achieve the small HOMO–LUMO gap and NIR fluorescence. On the other hand, the bis(trifluoromethyl)phenyl-substituted **34c** exhibits rather blue-shifted absorption and fluorescence relative to those of **34a**. There may be a trade-off between the electron-withdrawing nature of the trifluoromethyl group and electron-donating nature of the fused-thiophene ring, eliminating the effect of ICT interaction in **34c**. The direct introduction of the aryl groups into ***trans*-33** lowers the Φ_F values (**34a**: 0.50, **34b**: 0.51, **34c**: 0.28). In fact, the k_{nr} values of **34a-c** (1.1–4.5 $\times 10^8$ s^{-1}) become two orders of magnitude larger than that of ***trans*-33** (6.7 $\times 10^6$ s^{-1}), whereas the k_r values of **34a-c** (1.1–1.7 $\times 10^8$ s^{-1}) are rather comparable

to that of ***trans*-33** (7.7×10^7 s^{-1}). The significant enhancement in the k_{nr} values of **34a-c** is interpreted by the increased vibrational and rotational degrees of freedom owing to the introduced aryl substituents.

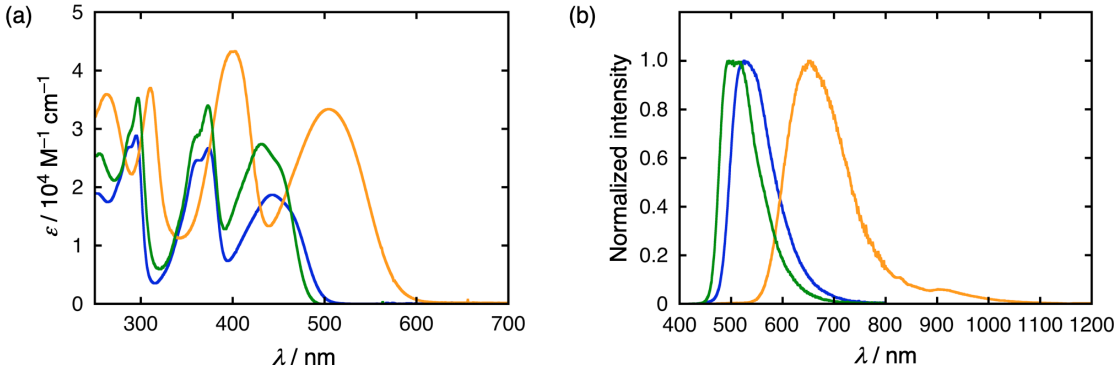

Figure 3-7. (a) UV/Vis absorption and (b) normalized fluorescence spectra of aryl-substituted doubly thiophene-fused benzodiphospholes **34a** (blue), **34b** (yellow), and **34c** (green) in CH_2Cl_2. For fluorescence measurements, the samples were excited at 415 nm. To obtain the whole fluorescence spectra, we used two detectors, one for wavelengths less than 850 nm, and the other one for wavelengths more than 850 nm.

The author also compared the absorption and fluorescence spectra of arylethenyl-substituted **35** and arylethynyl-substituted **36** (Figures 3-8) together with those of **34a**. The absorption maximum of phenylethynyl-substituted **36a** (445 nm) is almost identical to that of **34a** (443 nm), whereas phenylethenyl-substituted **35a** exhibits significant red-shifted absorption (470 nm). The corresponding fluorescences show the same trend (**34a**: 525 nm, **35a**: 556 nm, **36a**: 520 nm). More effective π-conjugation through the vinylene linker than the ethynylene linker causes the smaller HOMO–LUMO gap of **35a** than **36a**, as seen in the significant red-shifts in **35a**. The Φ_F value decreases in the order of **34a** (0.50) > **36a** (0.37) > **35a** (0.27). This trend reflects that of the vibrational and rotational degrees of freedom. Indeed, the k_{nr} value increases in the same order of **34a** (1.4×10^8 s^{-1}) < **36a** (3.5×10^8 s^{-1}) < **35a** (4.6×10^8 s^{-1}), while the k_r value remains similar. Relative to **35a** and even **34b**, **35b** exhibits more enhanced red-shifted absorption (520 nm) and fluorescence (699 nm). Surprisingly, the fluorescence of **35b** is extended into the NIR region deeply (~1200 nm). NIR emissive compounds have drawn much attention because of their potential applications in biological imaging.[16c–f] However, compared to numerous organic dyes with intense visible fluorescence, the NIR fluorescent organic dyes with a high Φ_F are still scarce.[65] Although the Φ_F value of **35b** (0.22) has not been optimized yet, it is comparable to that of a representative BODIPY-based molecule with an emission at 684 nm (Φ_F = 0.19).[65c]

Importantly, the large Stokes shift (4900 cm^{-1}, $\Delta\lambda$ = 179 nm) can avoid interference by excitation source, self-absorption, and autofluorescence.[66] The rather high Φ_F and large Stokes shift of **35b** demonstrate that push-pull D-A-D type, doubly thiophene-fused benzodiphospholes are excellent candidates as an efficient NIR fluorescent organic dye for biological imaging. In the cases of arylethynyl-substituted **36c** and **36d** with electron-withdrawing substituents, blue-shifted absorption and fluorescence relative to those of **36a** are observable, which is the same behavior as described in **34a** and **34c** (Figure 3-8c,d).

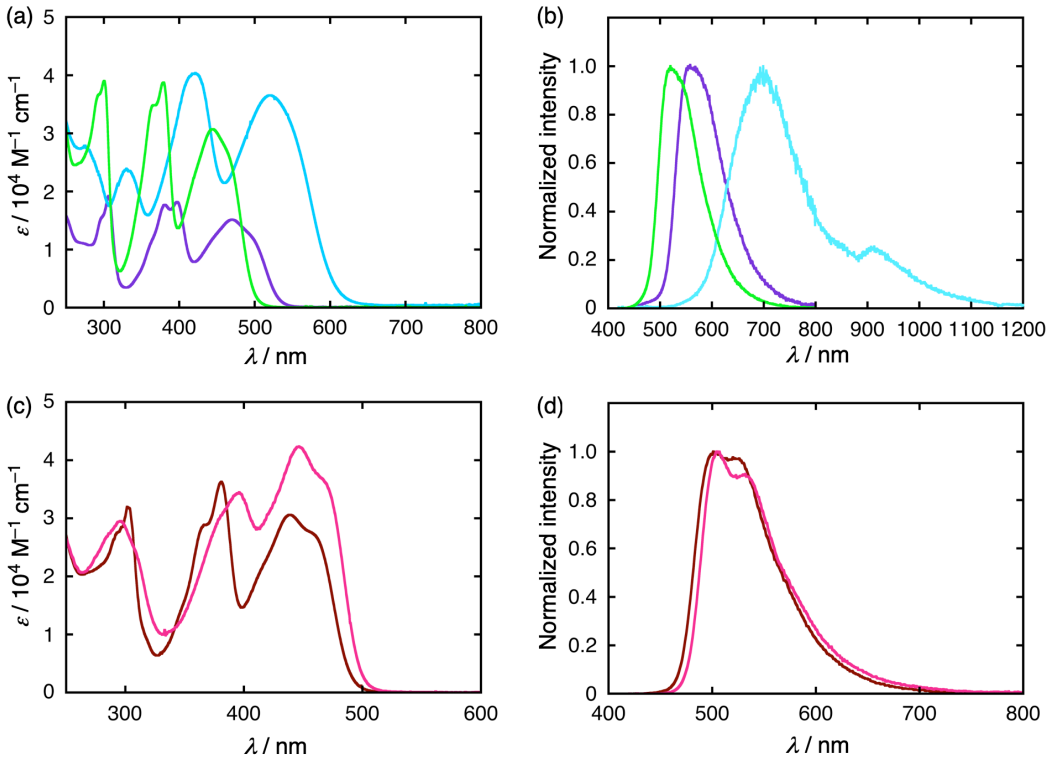

Figure 3-8. (a,c) UV/Vis absorption and (b,d) normalized fluorescence spectra of arylethenyl- and arylethynyl-substituted doubly thiophene-fused benzodiphospholes **35a,** (purple), **35b** (cyan), **36a** (light green), **36c** (brown), and **36d** (pink) in CH_2Cl_2. For fluorescence measurements, the samples were excited at 415 nm. To obtain the whole fluorescence spectra, we used two detectors, one for wavelengths less than 850 nm, and the other one for wavelengths more than 850 nm.

3-4. Electrochemical Properties

The electrochemical properties of doubly thiophene-fused benzodiphospholes **33**–**36** were assessed by CV and DPV technique in CH_2Cl_2 with Bu_4NPF_6 as an electrolyte versus ferrocene/ferrocenium ion (Fc/Fc^+) (Figure 3-9). Although ***trans*-33** and ***cis*-33** exhibit the reversible reduction peaks at –1.90 V, they reveal the irreversible oxidation peaks at +1.22 and +1.29 V, respectively. The reversible reduction peaks of **33** substantiate the excellent electron-accepting character of doubly thiophene-fused phospholes. The *trans*/*cis*-configurations have little impact on the oxidation potentials (E_{ox}) and reduction potentials (E_{red}).

Meanwhile, the E_{ox} values of **34a**, **35a**, and **36a** are shifted to a negative direction relative to that of ***trans*-33**, while the E_{red} values are moved to a positive direction. Consequently, the smaller electrochemical HOMO–LUMO gaps of **34a** (2.74 eV), **35a** (2.51 eV), and **36a** (2.72 eV) than that of ***trans*-33** (3.12 eV) agree with the corresponding optical HOMO-LUMO gaps (Table 3-1). For dimethylamino-substituted **34b** and **35b**, the quasi-reversible oxidation peaks are observed at +0.28 and +0.18 V, respectively, which are assigned to oxidations of the dimethylaminophenyl moiety. The E_{red} value becomes more positive in the order of **34a** (–1.81 V) < **35a** (–1.75 V) < **36a** (–1.71 V), which reflects the degree of the electron-donating effect of the aryl moiety through the linkers. As expected, introduction of the electron-withdrawing trifluoromethyl moieties on the aryl groups leads to more positive E_{red} values (–1.67 V for **34c** and –1.63 V for **36c**) than those of **34a** and **36a**. Given the energy level of Fc/Fc^+ is –4.8 eV under vacuum, the LUMO level of **34a** is estimated to be –2.99 eV.[67] This level is slightly higher than those of the phenyl-substituted benzodiphospholes (ca. –3.05 eV),[37c] which is used as a cathode buffer layer in OPV.[39b] The LUMO levels of **34c**, **36a**, and **36c** are also calculated to be –3.13, –3.09, and –3.17 eV, respectively, which are comparable to or even lower than those of the phenyl-substituted benzodiphospholes. Accordingly, introduction of electron-withdrawing groups on the aryl moiety and use of the ethynylene linkers are effective to enhance the high electron-accepting ability of doubly thiophene-fused benzodiphospholes. This information would be very useful for the exploitation of electron-transporting materials.

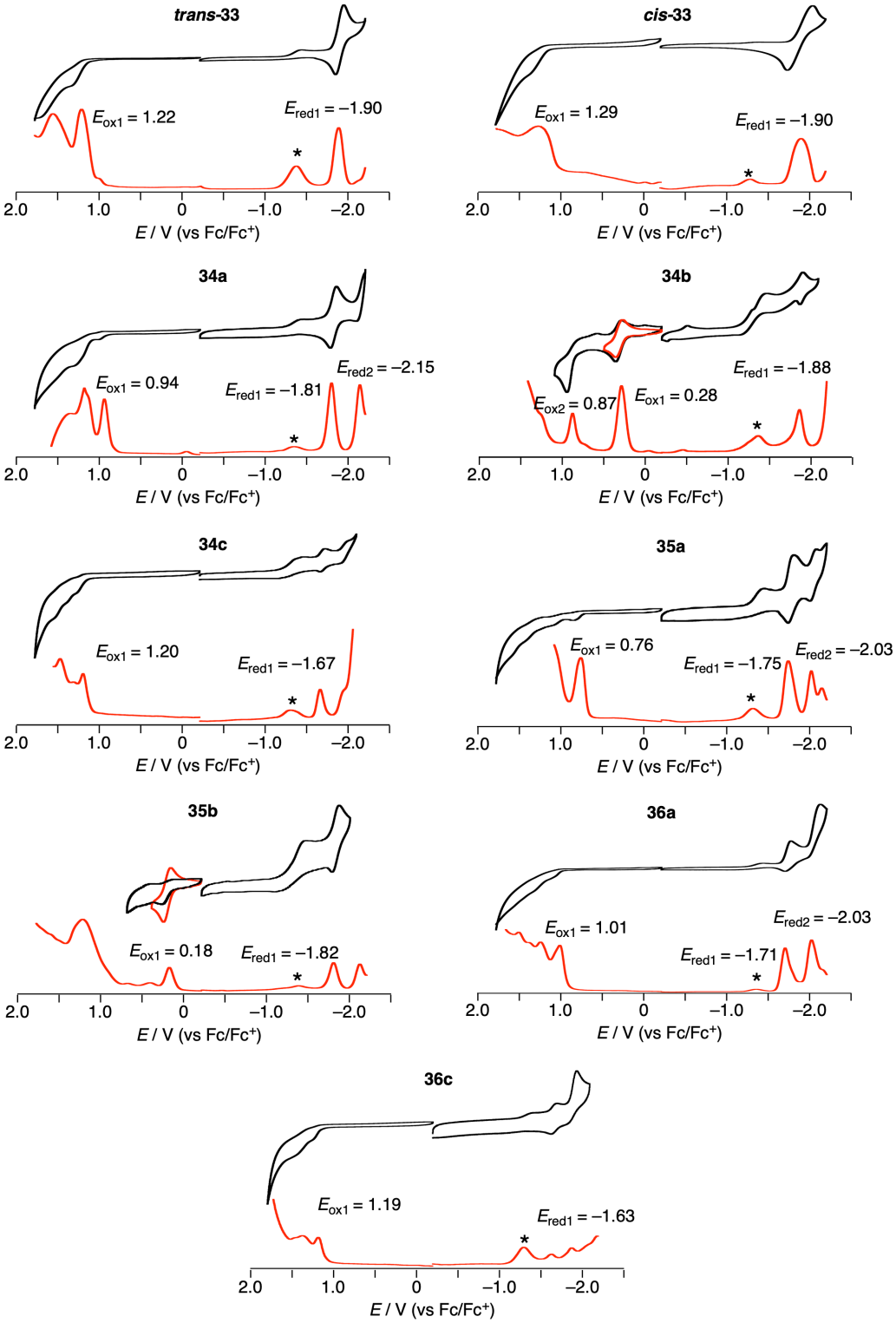

Figure 3-9. Cyclic voltammograms (black) and differential pulse voltammetry (DPV) curves (red) of naphthodiphospholes. Redox potentials were determined by DPV. Solvent: CH_2Cl_2; scan rate: 0.05 V s^{-1}; working electrode: glassy carbon; reference electrode: Ag/Ag^+ (0.01 M $AgNO_3$); electrolyte: 0.1 M *n*-Bu_4NPF_6.

3-5. Theoretical Calculations

To obtain the insight into the structural and electronic properties of doubly thiophene-fused benzodiphospholes **33**–**36**, we performed DFT calculations at the B3LYP/6-31G(d,p) level. The optimized structures of ***trans*-33**, **34a**, **35a**, and **36a** exhibit highly coplanar structure of the doubly thiophene-fused benzodiphosphole unit (Figure 3-10). The phenyl group of **34a** is slightly tilted (28°), whereas the styryl group of **35a** and phenylethynyl group of **36a** adopt completely coplanar structures.

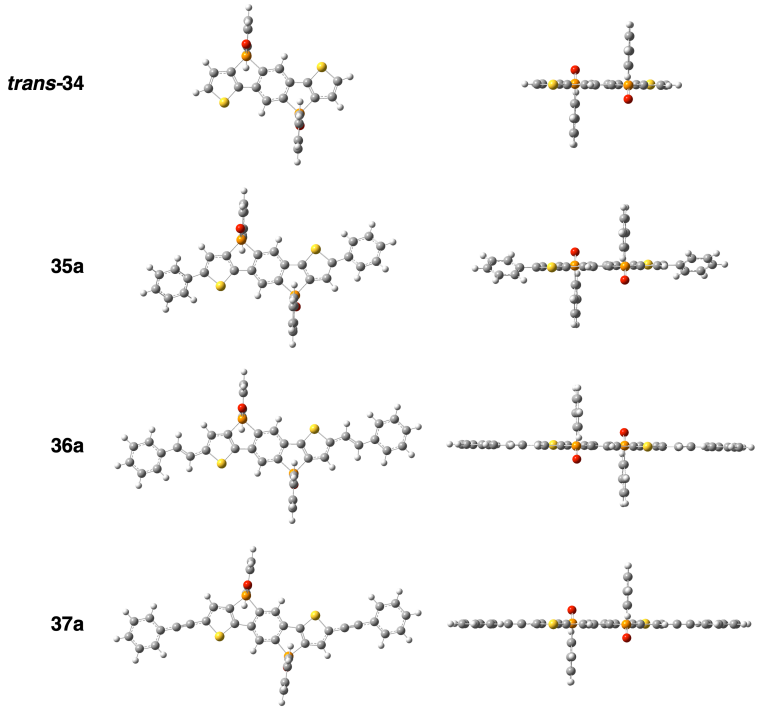

Figure 3-10. Optimized structures of doubly thiophene-fused benzodiphospholes ***trans*-33**, **34a**, **35a**, and **36a** at the B3LYP/6-31G(d,p) level: top view (left) and side view (right).

The orbital distributions of HOMO and LUMO of **33** are well delocalized over the whole π-conjugated system (Figure 3-11). The HOMO possesses almost no distribution on the phosphorus atom. In contrast, the LUMO possesses a large distribution on the phosphorus atom, indicating effective σ*–π* interaction that is unique in phospholes. To support the excimer emission of ***cis*-33** in the solid state, we carried out calculations on the dimeric structure taken from its crystal structure (Figure 3-11). Although the HOMO shows no interaction between the two doubly thiophene-fused benzodiphosphole units, the LUMO visualizes the effective interaction through the space. The calculated HOMO–LUMO gap of the dimer (3.28 eV) is

smaller than that of the monomer (3.52 eV), which is consistent with the red-shifted fluorescence stemming from the dimeric structure of ***cis*-33** in the solid state.

For the π-extended doubly thiophene-fused benzodiphospholes, the HOMOs of **34a**, **35a**, and **36a** are delocalized over the whole π-system, while their LUMOs are mainly localized on the doubly thiophene-fused benzodiphosphole unit (Figures 3-12−3-14). The energy levels of LUMO are lowered in the following order: **34a**: –2.33 eV > **35a**: –2.44 eV > **36a**: –2.52 eV, which matches with the trend on the E_{red} values. The introduction of the electron-donating dimethylamino moieties decreases the orbital distributions of LUMO on the dimethylaminophenyl groups in **34b** and **35b**, while those of HOMO on the dimethylaminophenyl groups are increased. Consequently, these orbital distributions support efficient ICT interactions in **34b** and **35b** (Figures 3-12 and 3-13). In marked contrast, the HOMOs and LUMOs of **34c** and **36c**,**d** with electron-withdrawing substituents on the aryl groups are similar to those of **34a** and **36a** to a great extent. The comparable orbital distributions are consistent with the their rather similar optical properties irrespective of the electron-withdrawing substituents (Figures 3-12 and 3-14). Importantly, the introduction of electron-withdrawing groups on the aryl groups stabilizes the LUMO levels and enhances their electron-accepting ability.

The author also carried out TD-DFT calculations to evaluate the absorption (Figure 3-11–3-14). For all the doubly thiophene-fused benzodiphospholes, the lowest excitations are derived from HOMO/LUMO transitions. The lowest excitation energies largely match with the absorption spectra. It should be noted here that the HOMO/LUMO transitions with large oscillator strengths for **34b** (f = 0.9596) and **35b** (f = 1.7015) agree with the efficient ICT interactions.

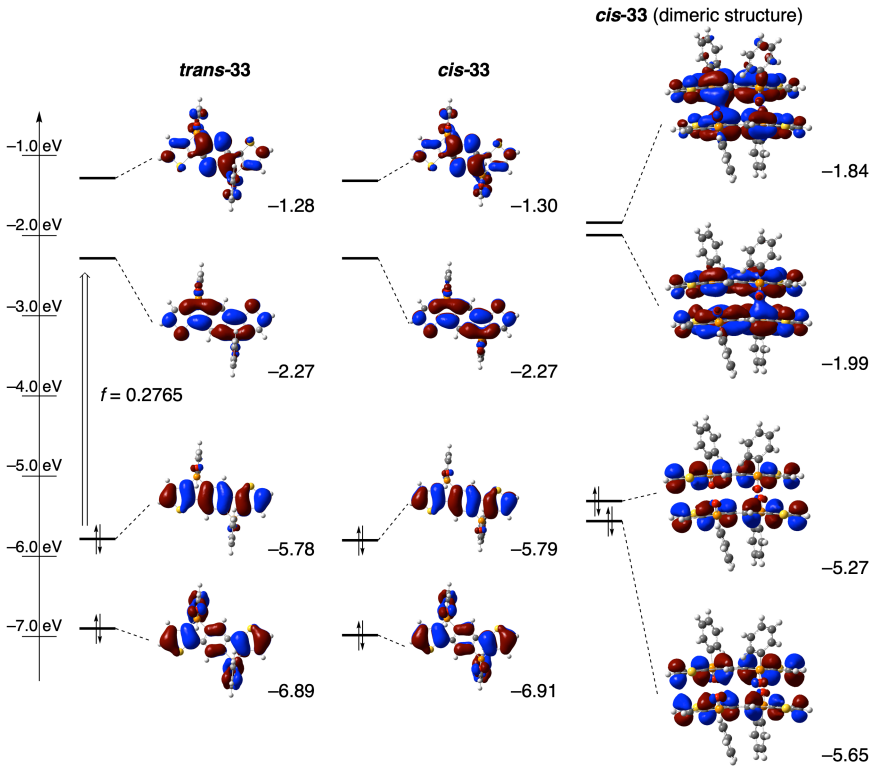

Figure 3-11. Selected Kohn-Sham orbitals of ***trans*-33**, ***cis*-33** on the optimized structures and the dimeric structure of ***cis*-33** obtained from the crystal structure. *f*: oscillator strengths

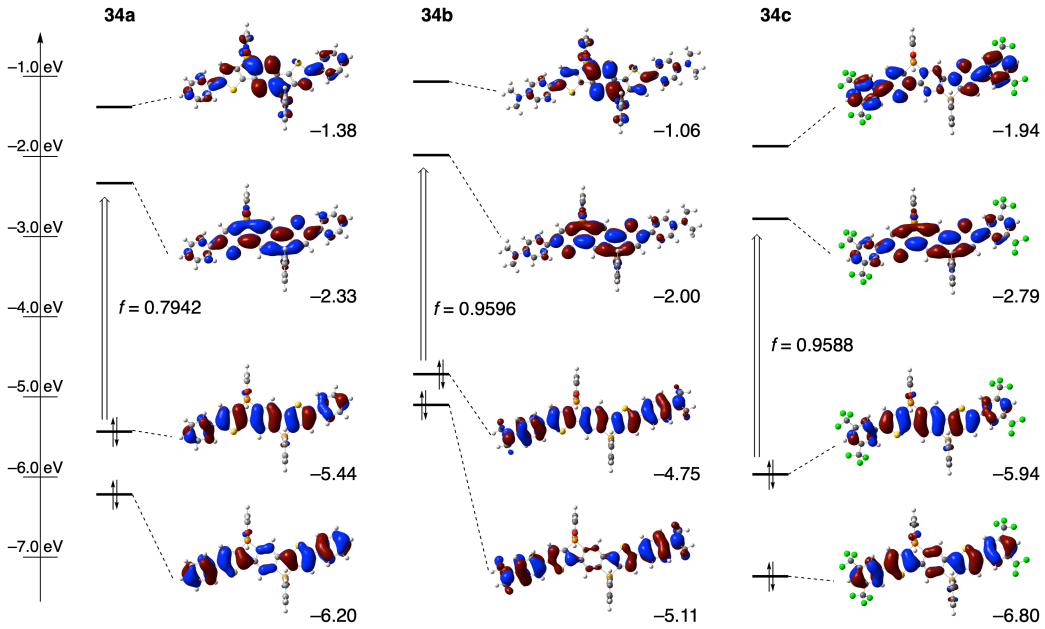

Figure 3-12. Selected Kohn-Sham orbitals of **34a**, **34b,** and **34c** on the optimized structures. *f*: oscillator strengths

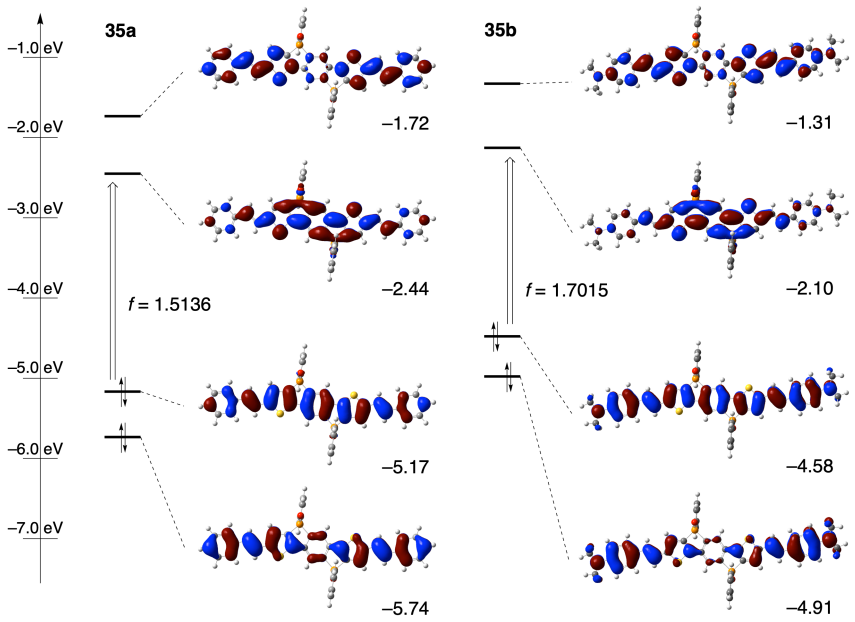

Figure 3-13. Selected Kohn-Sham orbitals of **35a** and **35b** on the optimized structures. *f*: oscillator strengths

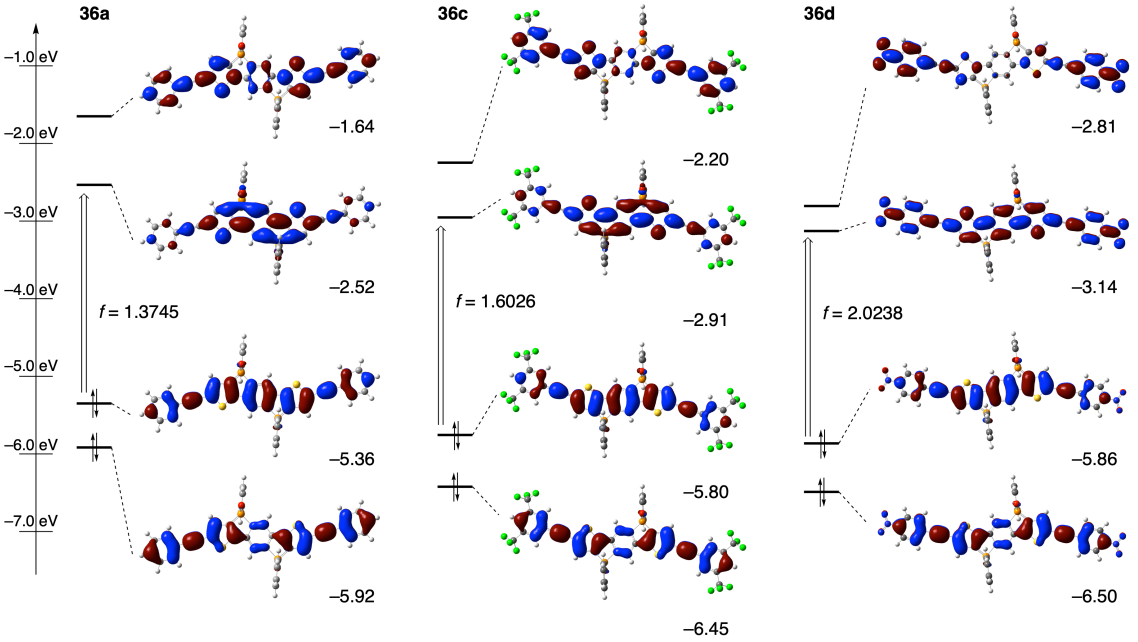

Figure 3-14. Selected Kohn-Sham orbitals of **36a, 36b** and **36c** on the optimized structures. *f*: oscillator strengths

3-6. Two-photon Absorption properties

Motivated by intense absorption of **35b** at 520 nm as a result of the enhanced ICT interaction originated from the push-pull D-A-D structure with the electron-donating substituents, we selected **35b** to evaluate the TPA properties. The author expected that the large π-conjugated system and D-A-D quadrupole would afford large TPA cross sections ($\sigma^{(2)}$). The TPA measurements of **35b** in CH_2Cl_2 were conducted by using the open-aperture Z-scan method (Figure 3-15). The TPA spectrum exhibits two broad peaks at around 900 and 650 nm (Figure 3-16a). The $\sigma^{(2)}$ values at 855 and 654 nm were determined to be 970 ± 190 and 2200 ± 420 GM, respectively, which are significantly larger than those of other phosphole-based molecules (~800 GM).[55b,58] To understand the origin of the TPA transitions, we performed the DFT calculations for the TPA spectral simulation of **35b**. The simulated one-photon absorption (OPA) and TPA spectra are displayed in Figure 3-16b. Although the transition energies are overestimated (i.e. the peaks are blue-shifted) at the CAM-B3LYP/6-31+G(d) level of calculations, the simulation largely reproduces the experimental spectral shapes. The lowest-energy TPA peak is located at the different transition energy from the OPA peaks in both simulation and experiment, reflecting alternating selection rule of symmetry between OPA and TPA for centrosymmetric molecules. From these comparisons with the simulated spectra, the TPA peaks at 880 and 650 nm in the experiment are assigned to the transitions, respectively, to S_2 and S_4 excited states both having *gerade* symmetry. These results corroborate that the introduction of electron-donating arylethenyl groups into doubly thiophene-fused benzodiphosphole is an effective means to create novel TPA materials.

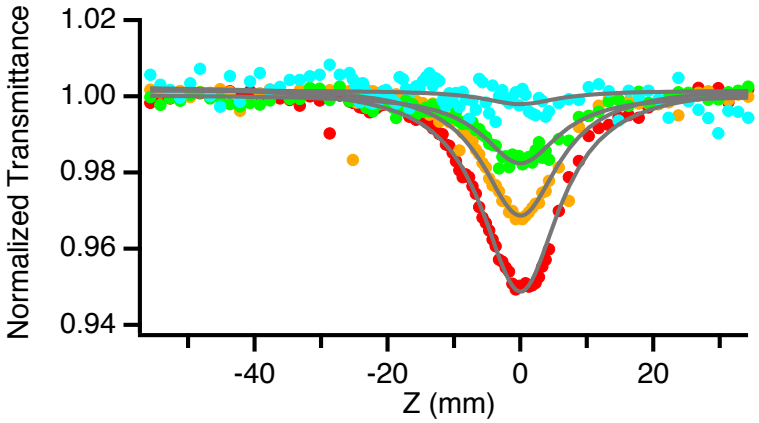

Figure 3-15. The open-aperture Z-scan traces of **35b** (0.3 mM) in CH_2Cl_2 (filled circles) at 855 nm for different incident powers (0.1–0.5 mW from top to bottom) together with the theoretical fitting curves (solid lines). Rayleigh range was 6.9 mm.

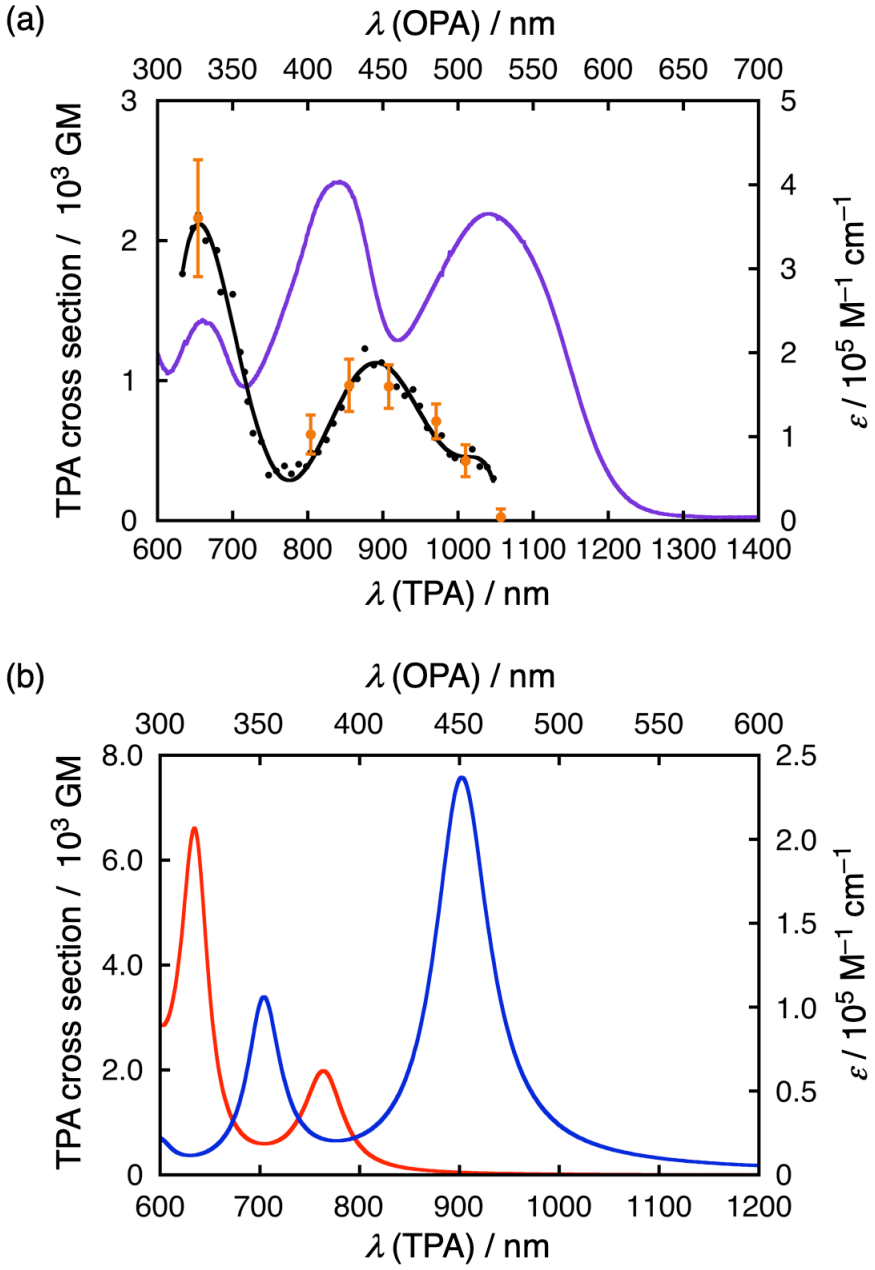

Figure 3-16. (a) TPA spectrum (bottom and left axes) of **35b** in CH_2Cl_2 measured at an excitation power of 0.4 mW (black dots, with solid curve of eye guide) and by changing the power (orange dots with error bars). The OPA spectrum (top and right axes, purple curve) is also overlapped with the half scale in the horizontal axis so that the same transition energies of OPA and TPA fall at the same position. b) Simulated TPA (red) and OPA (blue) spectra calculated at the CAM-B3LYP/6-31+G(d) level in CH_2Cl_2 with PCM plotted in the same manner.

3-7. Charge-transporting abilities

Finally, we evaluated the potential utility of the π-extended doubly thiophene-fused benzodiphosphole as electron-transporting materials. The author measured the photoconductivity of ***trans*-33**, **34a**, **35a**, and **36a** using the flash-photolysis time-resolved microwave conductivity (FP-TRMC) method.[68] The FP-TRMC profiles for drop-cast films of ***trans*-33**, **34a**, **35a**, and **36a** upon irradiation at λ = 355 nm are displayed in Figure 3-17a. The maximum transient conductivity $(\phi\Sigma\mu)_{max}$ for ***trans*-33** was determined to be 1.2×10^{-5} $m^2 V^{-1} s^{-1}$, where ϕ and $\Sigma\mu$ represent the charge carrier generation efficiency and the sum of the charge carrier mobilities, respectively. The $(\phi\Sigma\mu)_{max}$ values for **34a** (13×10^{-5} $m^2 V^{-1} s^{-1}$), **35a** (3.1×10^{-5} $m^2 V^{-1} s^{-1}$), and **36a** (6.2×10^{-5} $m^2 V^{-1} s^{-1}$) are larger than that for ***trans*-33**, suggesting that the π-extension can enhance the intrinsic charge-transporting ability greatly. The powder X-ray diffraction measurements of drop-cast films of ***trans*-33**, **34a**, and **36a** show sharp diffraction peaks, which are largely consistent with their unit cells (Figure 3-18). Importantly, the highest $(\phi\Sigma\mu)_{max}$ value for **34a** is rationalized by effective electronic communication in the packing derived from the 2D herringbone structure, which is realized by the multiple intermolecular interactions including S–S contacts and hydrogen bonds between P=O and C–H groups (Figure 3-5c),[25d,60a] in addition to the 1D slip π-stacked interactions (Figure 3-5b). Such S–S interactions are known to play an important role in providing an alternative charge-transporting pathway in the organic semiconductors.[60] Since the FP-TRMC measurements under air provide the sum of the electron and hole mobilities, we sought to determine the main contributor by the measurements under SF_6, electron scavenger gas. The $(\phi\Sigma\mu)_{max}$ value for **34a** under SF_6 is decreased to ca. 20% of that under air (Figure 3-17b). Moreover, the $(\phi\Sigma\mu)_{max}$ value under air is recovered to the initial value even after exposure to SF_6. These results indicate that the observed electrical conductivity of **34a** is largely contributed from electron transport. We also measured the photoconductivity of **36c**,**d**. Their FP-TRMC profiles are displayed in Figure 3-17c. Since the observed $(\phi\Sigma\mu)_{max}$ value for nitro-substituted **36d** (10×10^{-5} $m^2 V^{-1} s^{-1}$) is larger than those of **36a** and **36c** (6.7×10^{-5} $m^2 V^{-1} s^{-1}$), introduction of suitable electron-withdrawing groups on the phenylethenyl-substituted **36a** can also enhance photoconductivity as well as electron-accepting ability. Remarkably, the $(\phi\Sigma\mu)_{max}$ values for **34a** and **36d** surpass those of previously reported materials based on perylenediimide derivatives ($4–5 \times 10^{-5}$ $m^2 V^{-1} s^{-1}$),[68c,d] a representative n-type organic semiconducting motif. Therefore, the author verifies that π-extended doubly thiophene-fused benzodiphospholes with suitable substituents possess the potential utility as excellent electron-transporting materials.

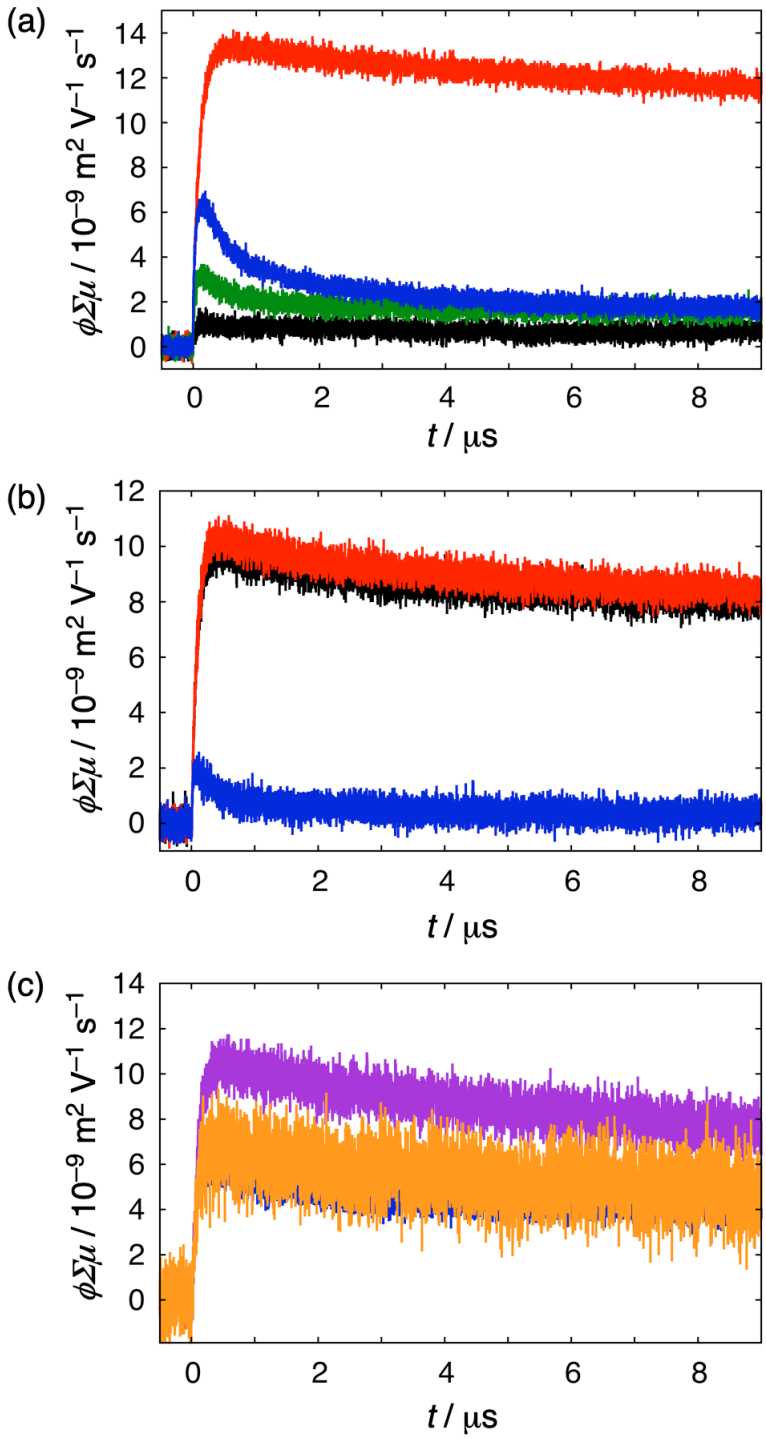

Figure 3-17. (a) Flash-photolysis time-resolved microwave conductivity (FP-TRMC) profiles (a) for drop-cast films of ***trans*-33** (black), **34a** (red), **35a** (green), and **36a** (blue) from $CHCl_3$ solution under air, (b) for drop-cast films of **34a** from $CHCl_3$ solution under air (black), SF_6 (blue), and air after exposure to SF_6 (red), and (c) of powders in PVA matrix films for **36a** (blue), **36c** (orange), and **36d** (purple) under air, upon 355 nm photoexcitation at 4.6 $\times 10^{15}$ photons cm^{-2}.

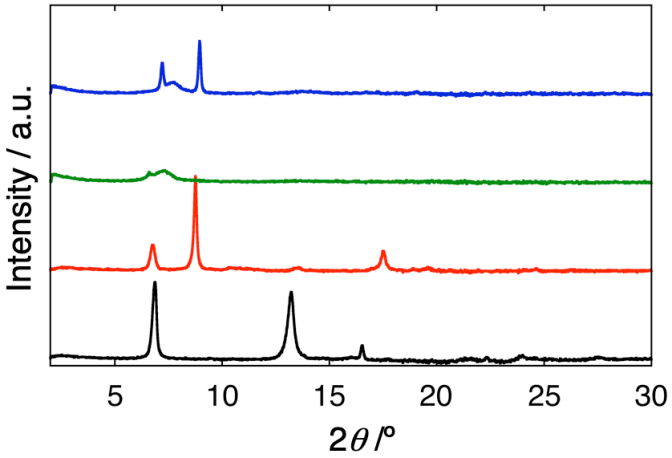

Figure 3-18. Powder X-ray diffraction patterns of drop-cast films of ***trans*-33** (black), **34a** (red), **35a** (green), and **36a** (blue) used for FP-TRMC measurements. Diffraction peaks: 2θ = 6.88, 13.22, and 16.54° (*d* = 12.8, 6.69, and 5.35 Å) for ***trans*-33**; 2θ = 6.76, 8.76, and 17.50° (*d* = 13.1, 10.1, and 5.06 Å) for **34a**; 2θ = 7.32° (*d* = 12.1 Å) for **35a**; 2θ = 7.22, 7.68, and 8.96° (*d* = 12.2, 11.5, and 9.8 Å) for **36a**.

3-8. Summary

In this chapter, the author established the synthetic methodology of doubly thiophene-fused benzodiphosphole and their π-extended derivatives as a new class of linear ladder-type π-conjugated molecules. Systematic investigation on the physicochemical properties of doubly thiophene-fused benzodiphospholes revealed that their pluripotent features for various potential applications could be extracted by rational π-extension with the introduction of aryl, arylethenyl, and arylethynyl groups with electron-donating or electron-withdrawing substituents to the α-positions of the synthetic accessible fused-thiophene moieties. The author summarizes the highlight on their pluripotent features as follows: The 1D slip π-stacked arrangement of ***trans*-33** in the solid state suggested effective π-π interaction through the 1D chain. On the other hand, ***cis*-33** exhibited the isolated face-to-face dimeric structure with effective overlapping of the doubly thiophene-fused benzodiphosphole cores. The doubly thiophene-fused benzodiphosphole ***trans*-33** and ***cis*-33** were highly florescent (Φ_F = 0.92 and 0.91). Notably, ***cis*-33** exhibited solid-state excimer fluorescence owing to its unique isolated dimeric structure. More importantly, the packing structure of the directly phenyl-substituted **34a** in the solid state showed the unique 2D herringbone structure created from the fusion of the phosphole and thiophene moieties. Namely, the structure is generated by multiple intermolecular interactions including S–S contacts and hydrogen bondings between P=O and C–H groups, which is beneficial for enhancing the electron-transporting properties. As expected, the π-extended doubly thiophene-fused benzodiphospholes exhibited smaller optical HOMO-LUMO gaps than that of ***trans*-33**. It is noteworthy that dimethylamino-substituted **34b** and **35b** showed enhanced red-shifted absorption and fluorescence extending into the NIR region (700–1200 nm) with rather high quantum yields. Especially, the NIR fluorescence of **35b** (up to 1200 nm) and its large Stokes shift ($\Delta\lambda$ = 179 nm) are suitable for efficient NIR fluorescent organic dye for biological imaging. Furthermore, **35b** revealed large TPA cross section (970 GM) at 855 nm, which demonstrated the potential for novel TPA materials. Meanwhile, phenyl-substituted **34a** displayed the highest $(\phi\Sigma\mu)_{max}$ value of 13×10^{-5} $m^2 V^{-1} s^{-1}$ in the FP-TRMC measurements. The 2D herringbone and 1D slip π-stacked structures in the solid state may be responsible for the highest $(\phi\Sigma\mu)_{max}$ value of **34a**. It is notable that the observed conductivity of **34a** was largely contributed from electron transport. In addition, electron-withdrawing nitro-substituted **36d** also showed the higher $(\phi\Sigma\mu)_{max}$ value (10×10^{-5} $m^2 V^{-1} s^{-1}$) than that of unsubstituted reference **36a**. The $(\phi\Sigma\mu)_{max}$ values for **34a** and **36d** exceed those of previously reported representative electron-transporting materials based on perylenediimide derivatives. Thus, π-extended doubly

thiophene-fused benzodiphospholes with suitable substituents possess the potential utility as excellent electron-transporting materials. Overall, these doubly thiophene-fused benzodiphospholes as the platform were found to be highly attractive ladder-type π-conjugated molecules as NIR fluorescent organic dyes, TPA materials, and electron-transporting materials. The author believes that this report unveils the pluripotent features of doubly thiophene-fused benzodiphospholes as promising organic functional materials in various fields, e.g. biological imaging, nonlinear optics, organic transistors, and organic photovoltaics.

Chapter 4. Thiophene-Fused Naphthodiphospholes: Modulation of the Structural and Electronic Properties of Polycyclic Aromatics by Precise fusion of Heteroles

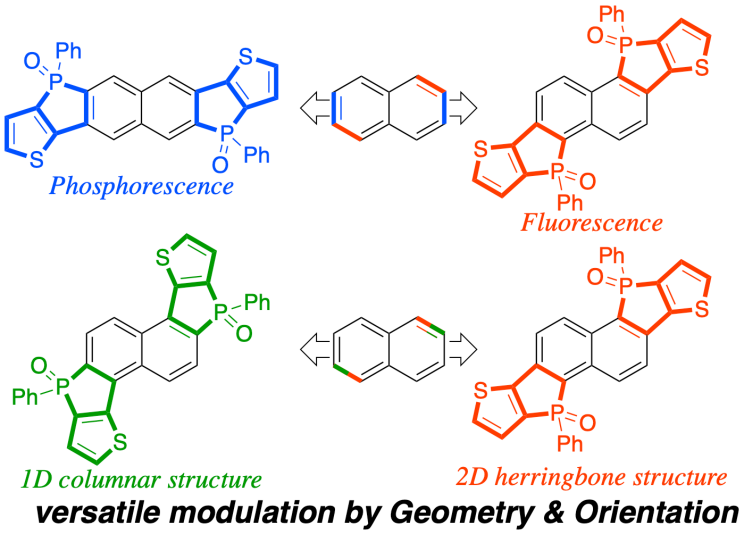

Contents

4-1. Introduction

As mentioned in General Introduction, fused polycyclic aromatics have been vigorously pursued over the years because of their attracting structural, electronic, and photophysical features associated with the rigid and planar π-conjugated frameworks. A unique advantage of fused polycyclic aromatics is that the molecule can be tailored through rational design and synthesis for various applications, such as organic semiconductors for organic field-effect transistors (OFETs),[4e,69] organic photovoltaics (OPVs)[14] and organic light-emitting diodes (OLEDs),[70] and scaffolds for supramolecular assemblies.[71]

Polycyclic aromatic hydrocarbons (PAHs) play central roles in material sciences.[72] At first glance, PAHs constitute a uniform class of very similar molecules, which are composed of solely sp^2 carbon atoms and hydrogen atoms. However, depending the size and geometry, PAHs exhibit dramatically different physicochemical properties. For example, tetracene,[4f,g,6b,e,73] which consists of four benzene rings, is a widely investigated molecule as organic semiconductors (Figure 4-1a). On the other hand, its isomers chrysene[74] and pyrene[75] have attracted attention as photofunctional molecules because of their fascinating photophysical properties. In contrast, triphenylene derivatives possess almost no absorption in visible region, but have been used as a component for discotic liquid crystals.[76]

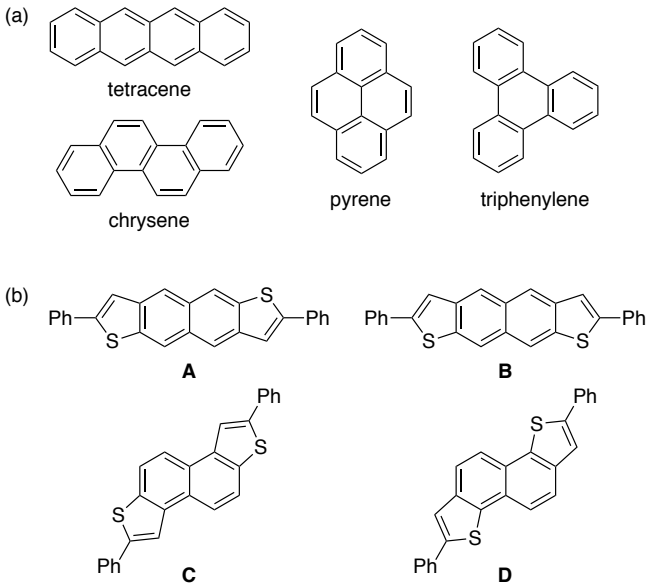

Figure 4-1. (a) Polycyclic aromatic hydrocarbons (PAHs) consisting of four benzene rings. (b) Isomers of naphthodithiophenes originated from the positions and orientations of thiophene rings.

Meanwhile, the incorporation of a range of heteroatoms into polycyclic aromatics is effective means to modulate their electronic structures,[13] and, especially, sulfur and phosphorus are promising candidate as described in General Introduction. In this context, a variety of polycyclic aromatics with both sulfur and phosphorus atoms have been developed and exhibited both features.[35f,45,61] However, placing different heteroatoms (i.e., sulfur and phosphorus) precisely in the same π-frameworks is still a challenge.

For polycyclic aromatics with heteroatoms, the orientation of the heterole rings as well as the geometry of the fused structure has a large impact on the physicochemical properties.[77] For instance, naphthodithiophene gives four isomers; 2,3/6,7-fused position (**A** and **B**) or 1,2/5,6-fused position (**C** and **D**) on the naphthalene core (Figure 4-1b).[77b] Reflecting the fused positions of thiophene rings on the naphthalene unit, the isomers **A** and **B** exhibited red-shifted absorption relative to the isomers **C** and **D**. On the other hand, the isomer **A** showed one-order magnitude higher hole mobility than the isomer **B** in the OFET devices because of more effective intermolecular interaction of **A** than **B** in the solid state. Thus, the fused position of heterole rings affects the electronic structure, while the orientation of fused heterole rings is crucial to determine the molecular arrangement in the solid state.

In this regard, the author expected that introducing two phosphorus atoms into polycyclic aromatics precisely would provide an assortment of isomers originated from not only the position and orientation of the phosphole rings, but also the orientation of substituents on the phosphorus atoms (*trans*/*cis* configurations) (Figure 4-2). In Chapter 3, the author described the potential utility of thiophene-fused benzodiphospholes as organic functional materials for various purposes. Precisely controlled fusion of heteroles into an aromatic core could be a useful approach to uncover their intrinsic properties that may create the possibility of new applications as organic functional materials.

Herein, the author reports the synthesis and physicochemical properties of six isomers of thiophene-fused naphtho[2,3-*b*:6,7-*b*']diphosphole **39**, naphtho[1,2-*b*:5,6-*b*']diphosphole **40**, and naphtho[2,1-*b*:6,5-*b*']diphosphole **41** with their *trans*/*cis* configurations (Figure 4-2). The author found that the fused position of phosphole rings influences their electronic properties greatly. In particular, **39** exhibited phosphorescence at 77K, whereas **40** and **41** showed no phosphorescence. More importantly, the author revealed that the orientation of phosphole rings and the substituents on the phosphorus atoms affect the molecular arrangement in the solid state. The systematic investigation unveiled the explicit impact of heterole-fused structures on their structural and electronic properties.

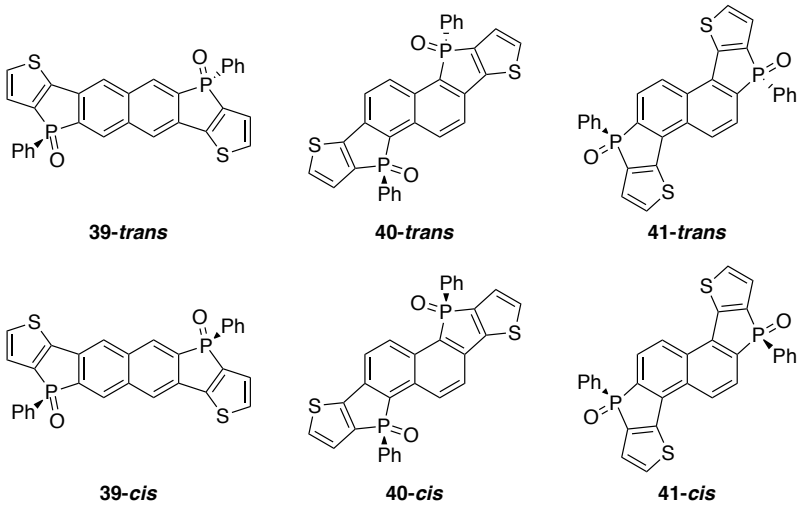

Figure 4-2. An assortment of isomers of thiophene-fused naphthodiphospholes derived from the positions and orientations of heterole rings and the orientations of substituents on the phosphorus atoms.

4-2. Synthesis of Thiophene-fused Naphthodiphospholes

The synthetic schemes for naphthodiphospholes are shown in Scheme 4-1. First, the author conducted the synthesis of **39**. The treatment of 2,6-dibromonaphthalane with lithium tetramethylpiperidide (Li-TMP) and B(O*i*-Pr)$_3$ afforded boronic acid **42**, and the boronic acid groups of **42** were converted to boronic ester groups of **43**. The Suzuki-Miyaura coupling of **43** with 2,3-dibromothiophene gave thienylnaphthalene **44** as a key precursor for **39**. Treatment of **44** with *n*-BuLi followed by the addition of dichlorophenylphosphine and H_2O_2 provided **39-*trans*** and **39-*cis*** as a diastereomeric mixture. These diastereomers were easily separated by silica-gel column chromatography to give **39-*trans*** in 19% and **39-*cis*** in 21% yield. In the next step, the author carried out the synthesis of **40**. 2,6-Dibromonaphthalene was transformed to bis-borylated naphthalene **45**. The Suzuki-Miyaura coupling of **45** with 2,3-dibromothiopehene yielded thienylnaphthalene **46**. The treatment of **46** with *t*-BuLi followed by the addition of dichlorophenylphosphine and H_2O furnished **47** as a key precursor for **40**. The author attempted Pd-catalyzed dehydrogenative cyclization of **47** using Pd(OAc)$_2$.[78] However, the reaction did not proceed and almost all of **47** was recovered. Then, the author applied the Tf_2O-mediated intramolecular phospha-Friedel-Crafts-type reaction[79] to **47** and succeeded in isolation of **40-*trans*** and **40-*cis*** in 18% and 17% yields, respectively. Finally, the author performed the synthesis of **41**. After the bromo groups of 1,5-dibromonaphthalene were converted to the boryl groups of **48**, the Suzuki-Miyaura coupling with 2,3-dibromothiophene provided thienylnaphthalene **49**. The treatment of **49** with *t*-BuLi followed by the addition of dichlorophenylphosphine and H_2O gave **50** as a key precursor for **41**. The Tf_2O-mediated intramolecular phospha-Friedel-Crafts-type reaction of **50** afforded **41-*trans*** and **41-*cis*** in 23% and 21% yields, respectively. All compounds were characterized by means of ^{1}H, ^{13}C and ^{31}P NMR spectroscopies and high-resolution mass spectrometry. The ^{31}P NMR spectra of **39**–**41** exhibit signals at δ = 22.5–24.6 ppm, suggesting that the difference in the positions of phosphole rings has little impact on the chemical shifts. Fortunately, the author obtained single crystals of **39-*trans***, **40-*trans***, **40-*cis*** and **41-*cis*** suitable for X-ray crystallographic analysis and the positions of phosphole rings for **39**–**41** were confirmed unambiguously by the crystal structures (Figure 4-3 and 4-4). The crystal structures of **39-*trans*** and **40-*trans*** display highly planar structures. On the other hand, the crystal structures of **40-*cis*** and **41-*cis*** exhibit slightly warped structures, which may be stemmed from the packing forces in the single crystals. The C–C and P–C bond lengths on the naphthodiphosphole core are comparable to those of reported naphthodiphosphole.[80] Thus, the positions of phosphole rings have negligible effect on their structural parameters.

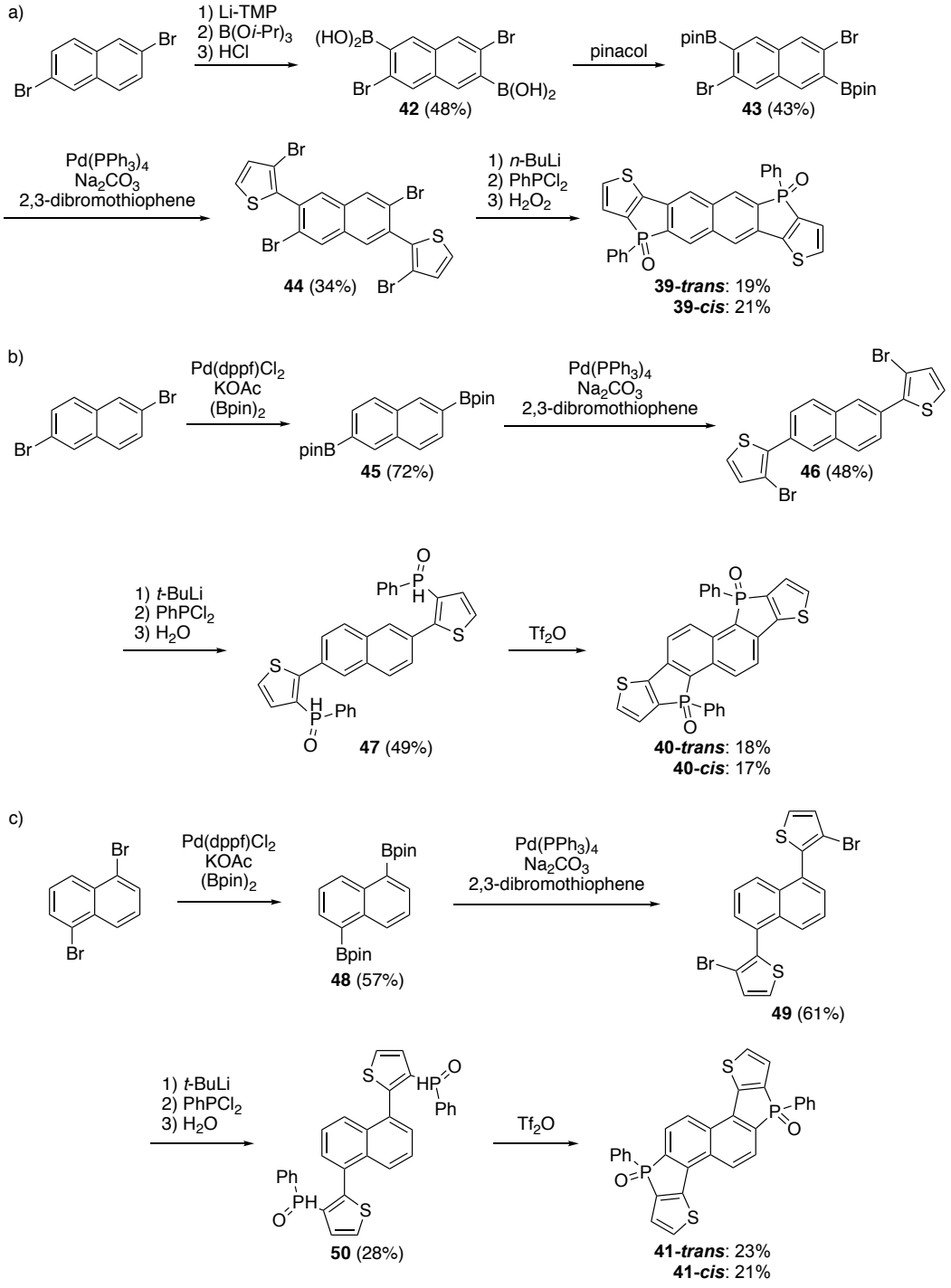

Scheme 4-1. Synthesis of thiophene-fused naphthodiphospholes (a) **39**, (b) **40**, and (c) **41**.

It is noteworthy that the packing structures reflect the positions and orientations of phosphole rings and *trans*/*cis* configurations of substituents on the phosphorus atoms. The packing structures of **39-*trans*** and **40-*trans*** illustrate one-dimensional (1D) slipped π-stacked alignments (Figure 4-3). For **39-*trans***, the separation distance between two π planes is about 3.7 Å, which is slightly longer than that for **40-*trans*** (ca. 3.6 Å). Furthermore, the overlap of the neighboring molecules for **39-*trans*** is smaller than that for **40-*trans***. Considering these features, the π-π interaction in the solid state of **39-*trans*** is weaker than that of **40-*trans***. On the other hand, the packing structures of **40-*cis*** and **41-*cis*** display no 1D slipped π-stacked alignments. The thiophene-fused naphthodiphosphole core of **40-*cis*** exhibits a 2D herringbone structure (Figure 4-4a). The multiple hydrogen bonds are visible between oxygen atoms of P=O moieties and hydrogen atoms of neighboring thienyl and phenyl moieties (Figure 4-4c). Thus, the multiple hydrogen bonds play an important role in the formation of 2D herringbone structure (*vide infra*). Meanwhile, the packing structure of **41-*cis*** shows a columnar structure based on a face-to-face dimeric structure, which is induced by a strong hydrogen bond (1.94 Å) with a water molecule (Figure 4-4b). Because of the presence of a cavity with the separation distance of 4.3 Å in the columnar structure, **41-*cis*** seems to be promising as molecular capsules or cages. Unfortunately, the author has not succeeded in encapsulation of any solvents or molecules in the cavity at this stage.

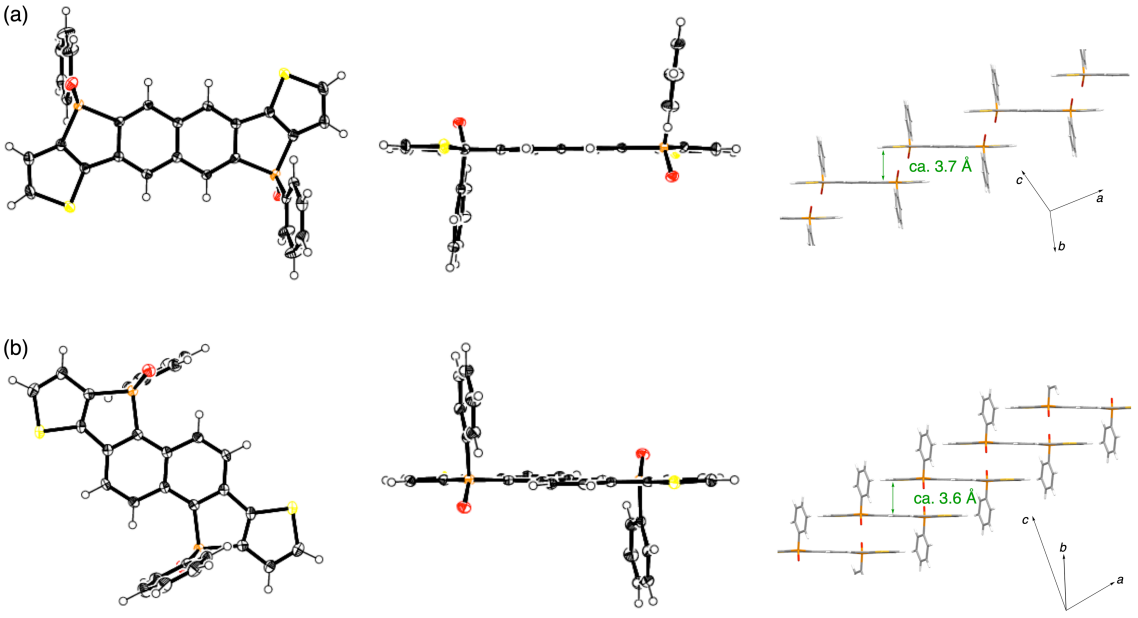

Figure 4-3. X-Ray crystal structures of (a) **39-*trans***, and (b) **40-*trans***: top view (left), side view (middle), and packing structure (right). Thermal ellipsoids represent 50% probability. Solvent molecules are omitted for clarity.

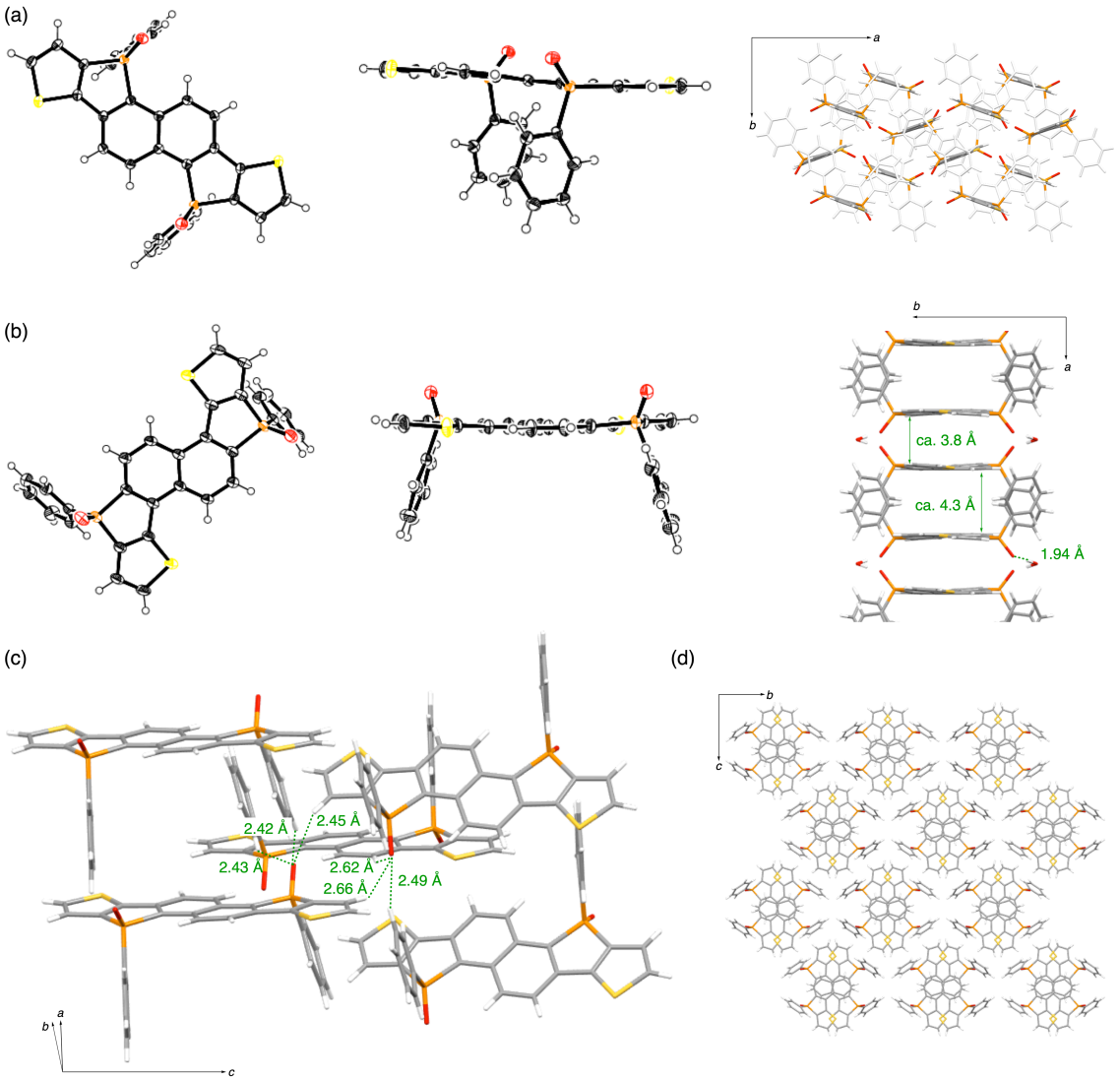

Figure 4-4. X-Ray crystal structures of (a) **40-*cis***, and (b) **41-*cis***: top view (left), side view (middle), and packing structure (right). Thermal ellipsoids represent 50% probability. Solvent molecules are omitted for clarity. Phenyl groups on the phosphorus atoms are shown in grey color for clarity in **40-*cis***. (c) Multiple hydrogen bonding natures of **40-*cis***. (d) The packing structure of **41-*cis*** along the *a*-axis. The hydrogen bonds with a water molecule are indicated (dashed green line) with the distance between O…H.

4-3. Optical Properties

The author examined the optical properties of naphthodiphospholes **39**–**41**. UV/Vis absorption and fluorescence spectra of **39**–**41** were measured in CH_2Cl_2 (Figure 4-5 and Table 4-1). The *trans*/*cis* configurations and the direction of substituents on the phosphorus atom have negligible impact on the absorption and fluorescence spectra, whereas the position of fused phosphole rings influences the optical properties remarkably. The absorption spectra of **39-*trans*/*cis*** display intense peaks at 294, 349, and 367 nm, and weak absorption band around 413 nm. In contrast, the absorption spectra of **40-*trans*/*cis*** show intense peaks at 295 and 307 nm, while those of **41-*trans*/*cis*** exhibit intense peaks at 286 and 294 nm. Moreover, they display lowest energy absorptions at λ = 438 and 441 nm, respectively. The significant red-shift of **40** and **41** relative to **39** indicates that the fused structure on 1,2/5,6-positions of a naphthalene core is more effective for efficient π-expansion than 2,3/6,7-positions. The isomers **39-*trans*/*cis*** show relatively weak blue fluorescence with a maximum at λ = 431 nm, whereas **40-*trans*/*cis*** and **41-*trans*/*cis*** display intensified red-shifted fluorescence with maxima at λ = 462 and 467 nm, respectively. The small Stokes shifts (1010–1270 cm^{-1}) reflect their highly rigid structures. The fluorescence quantum yields (Φ_F) were determined using thiophene-fused benzo-diphosphole (Φ_F = 0.91) as a standard. The Φ_F values of **39-*trans*** (0.04) and **39-*cis*** (0.06) were much smaller than those of **40** and **41** (0.20–0.26). In addition, we measured the fluorescence lifetimes (τ_F) by means of time-correlated single-photon counting (TCSPC) technique. The τ_F values of **39** in CH_2Cl_2 (1.1–1.5 ns) are smaller than those of **40** and **41** (2.0–2.9 ns). These values are similar to those of naphtho[2,3-*b*]phosphole derivatives.[80] The radiative (k_r) and nonradiative (k_{nr}) rate constants are calculated from the values of τ_F and Φ_F. The k_r and k_{nr} values for **40** and **41** are largely comparable. Compared to those values, the k_r values of **39-*trans*** ($3.8 \times 10^7\ s^{-1}$) and **39-*cis*** ($4.0 \times 10^7\ s^{-1}$) are smaller, but the k_{nr} values of **39-*trans*** ($6.3 \times 10^8\ s^{-1}$) and **39-*cis*** ($8.7 \times 10^8\ s^{-1}$) are larger. Thus, both k_r and k_{nr} values of **39** contribute to the low Φ_F value of **39**. The small k_r values of **39** imply that the phosphole-like character may be weakened because of the lack of efficient σ^*-π^* interaction (*vide infra*). Moreover, the large k_{nr} values of **39** can be ascribed to the enhanced intersystem crossing (ISC). Indeed, naphtho[2,3-*b*]phospholes showed phosphorescence at 77 K, which was interpreted by their relatively large k_{nr} values (ca. $2 \times 10^8\ s^{-1}$).[38e] We also measured the phosphorescence spectra of **39**–**41** in 2-methyltetrahydrofuran (2-MeTHF) at 77 K. Under these conditions, **39-*trans*** and **39-*cis*** exhibit apparent phosphorescence peaks at 571 and 623 nm (Figure 4-5c). In contrast, **40** and **41** display no phosphorescence peak. Therefore, the introduction of fused

structures into 2,3/6,7-positions is an effective strategy to increase the efficiencies of ISC process by small energy difference between S_1 and specific T_n states (ΔE_{ST}) and the corresponding enhanced spin-orbit coupling (*vide infra*).

Table 4-1. Optical properties of thiophene-fused naphthodiphospholes in CH_2Cl_2.

	λ_{abs} / nm[a] (ε / $M^{-1}cm^{-1}$)	λ_{abs} / nm[b] (Φ_F)[c]	E_{opt} /eV[d]	τ_F /ns	k_r /10^7 s^{-1}	k_{nr} /10^7 s^{-1}	$\Delta\nu$ /cm^{-1}[e]
39-*trans*	413 (3000)	431, 452 (0.06)	2.95	1.5	3.8	63	1010
39-*cis*	413 (2800)	431, 450 (0.04)	2.95	1.1	4.0	87	1010
40-*trans*	438 (11000)	462, 484 (0.26)	2.75	2.3	11	32	1180
40-*cis*	439 (9600)	462, 485 (0.24)	2.75	2.0	12	38	1180
41-*trans*	441 (7900)	467, 488 (0.23)	2.74	2.9	7.8	27	1270
41-*cis*	441 (8300)	467, 487 (0.20)	2.74	2.4	8.4	33	1270

[a] Absorption maxima at the longest wavelength. [b] The samples were excited at 367 nm for **39-*trans*/*cis*** and at 415 nm for **40-*trans*/*cis*** and **41-*trans*/*cis***. [c] Absolute fluorescence quantum yields (Φ_F) were determined using thiophene-fused benzodiphosphole (Φ_F = 0.91) as a standard (see Chapter 3). [d] Optical HOMO–LUMO gaps from the intersection of normalized absorption and fluorescence spectra. [e] Stokes shifts.

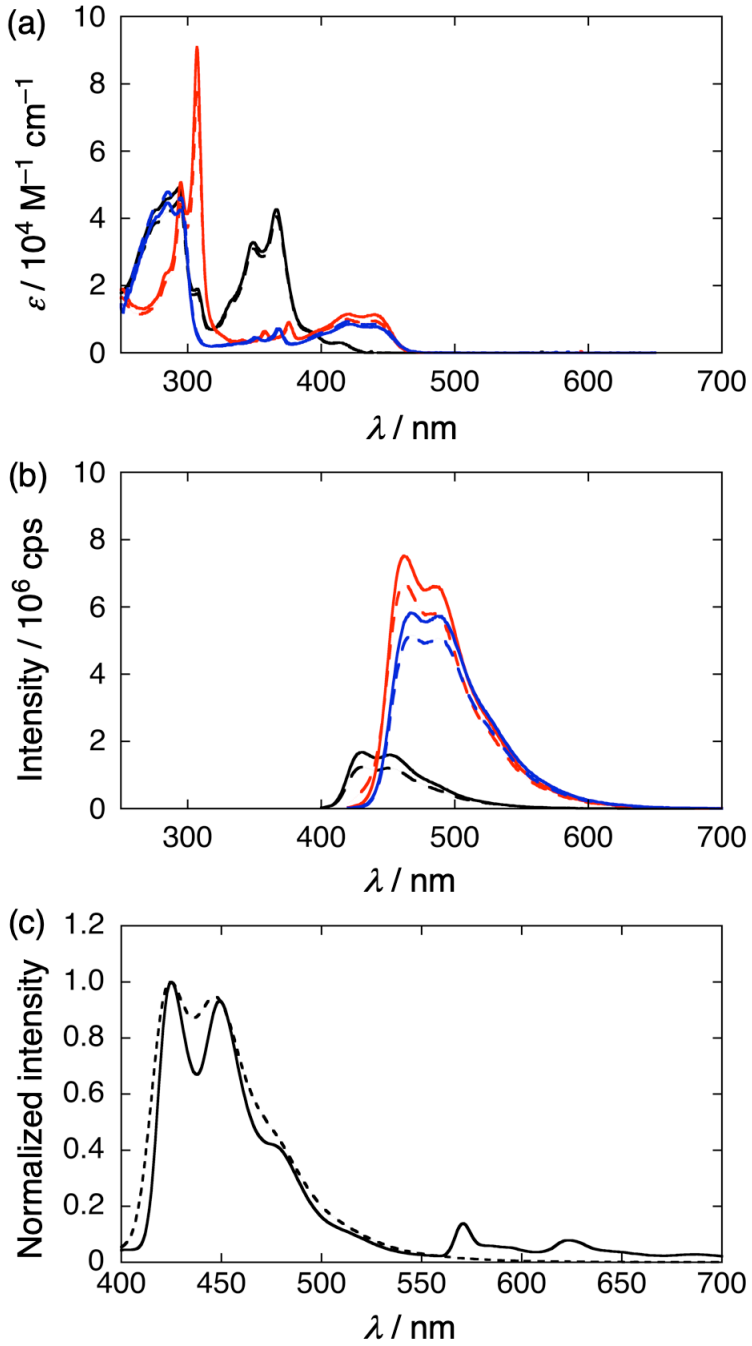

Figure 4-5. (a) UV/Vis absorption and (b) fluorescence spectra of thiophene-fused naphthodiphospholes **39-*trans*** (black, solid line), **39-*cis*** (black, dashed line), **40-*trans*** (red, solid line), **40-*cis*** (red, dashed line), **41-*trans*** (blue, solid line) and **41-*cis*** (blue, dashed line). (c) Emission spectra of **39-*cis*** in 2-MeTHF at r.t. (dashed line) and –190 ºC (solid line). For fluorescence measurement, the samples were excited at λ = 367 nm for **39** and λ = 415 nm for **40** and **41**. The absorbances at the excitation wavelengths were adjusted to be 0.1 for comparison.

4-4. Electrochemical Properties

The electrochemical properties of **39**–**41** were assessed by cyclic voltammetry (CV) and differential pulse voltammetry (DPV) technique in CH_2Cl_2 with tetrabutylammonium hexafluorophosphate (Bu_4NPF_6) as an electrolyte versus ferrocene/ferrocenium ion (Fc/Fc^+) (Figure 4-6). All of oxidation peaks are irreversible, whereas the reversible reduction peaks appear at –2.12 V for **39**, –1.82 V for **40**, and –1.75 V for **41**. The *trans*/*cis* configurations have almost no influence on the oxidation (E_{ox}) and reduction (E_{red}) potentials. The electrochemical HOMO–LUMO gaps of **39** (3.33 and 3.22 eV) are larger than those of **40** (2.98 and 2.87 eV) and **41** (2.91 and 2.89 eV). This trend agrees with that in the optical HOMO–LUMO gaps. Notably, the E_{red} value of **39** is significantly shifted in a negative direction compared to **40** and **41**. The less positive E_{red} value of **39** is consistent with the reduced phosphole-like electron accepting ability of **39** in comparison with **40** and **41**. Given that the energy level of Fc/Fc^+ is –4.8 eV under vacuum, the LUMO levels are estimated to be –2.98 eV for **40** and –3.05 eV for **41**. These LUMO levels are almost comparable to those of phosphole derivatives exhibiting high electron-transporting ability.[39,47h,48g,h,49a] Accordingly, the introduction of phosphole rings into 1,2/5,6-positions may be useful to extract the full potential as electron-transporting materials.

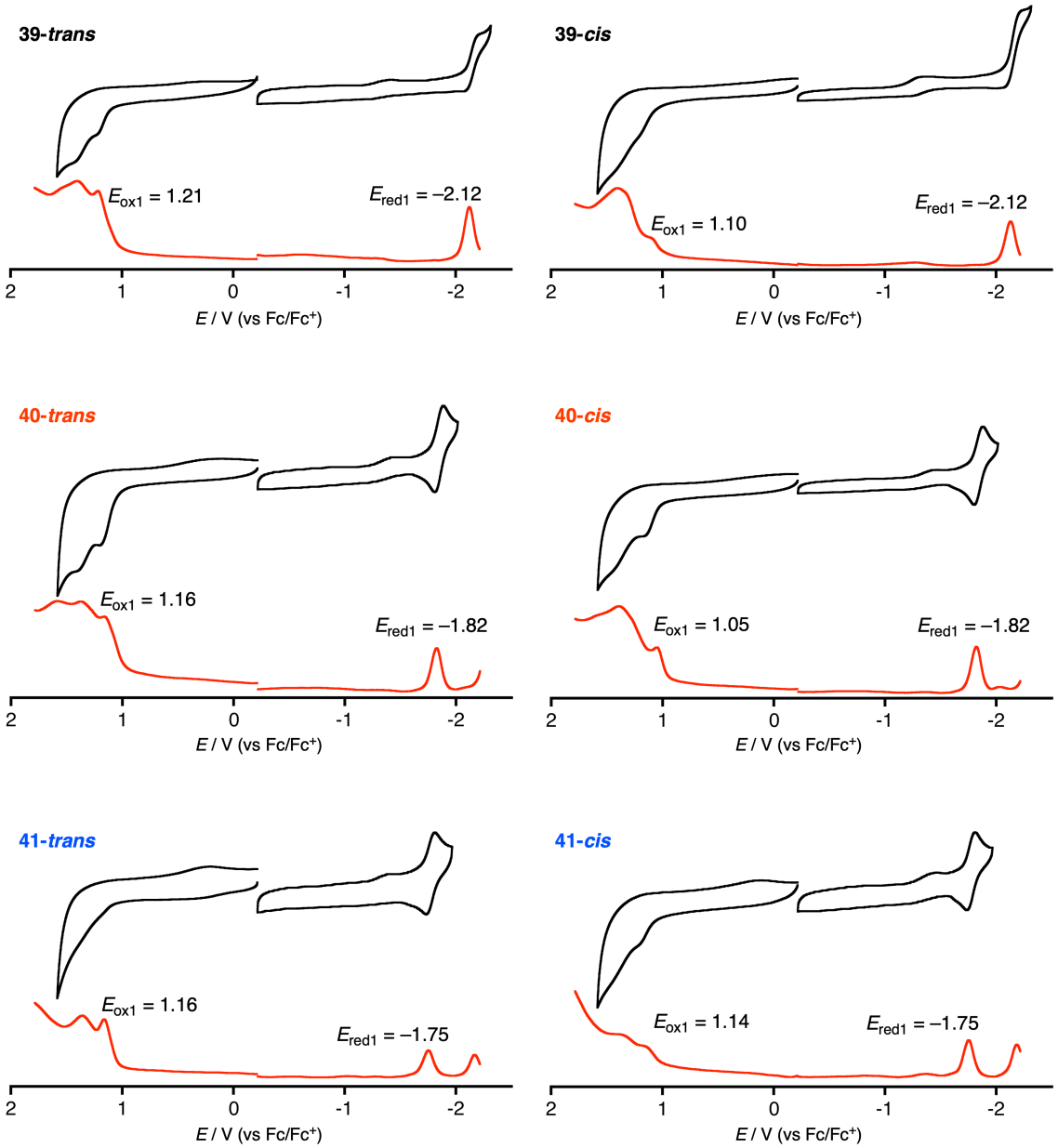

Figure 4-6. Cyclic voltammograms (black) and differential pulse voltammetry (DPV) curves (red) of naphthodiphospholes. Redox potentials were determined by DPV. Solvent: CH_2Cl_2; scan rate: 0.05 V s^{-1}; working electrode: glassy carbon; reference electrode: Ag/Ag^+ (0.01 M $AgNO_3$); electrolyte: 0.1 M *n*-Bu_4NPF_6.

4-5. Theoretical Calculations

The author carried out DFT calculations at the B3LYP/6-31G(d,p) level to obtain the further insight into the effects of the position of fused structures. The optimized structures adopt highly planar structure of naphthodiphospholes. The orbital distributions of HOMOs are delocalized over the whole π-conjugated systems except the phosphorus atoms (Figure 4-7 and 4-8). Meanwhile, the LUMOs of **40** and **41** possess large distributions on the phosphorus atom, indicating the phosphole-like effective σ*–π* interaction. On the other hand, the LUMO of **39** possesses almost no distribution on the phosphorus atom. Therefore, the phosphole-like character of **39** is limited because of little contribution of the phosphorus atoms to both HOMO and LUMO. Consequently, the LUMOs of **40** and **41** are significantly stabilized compared to the LUMO of **39**. The trend of LUMO energy levels (**39** (–2.12 eV) > **40** (–2.33 eV) > **41** (–2.47 eV)) agrees well with that in the E_{red} values. Accordingly, the introduction of phosphole-fused structure into 1,2/5,6-positions is crucial to retain phosphole-like features.

The author also calculated the spin-orbit coupling matrix element values (SOCMEVs) and the ISC rate constants (k_{ISC}) of **39**, **40**, and **41** by using the ADF2019 package[81] (Tables 4-2–4-4). The estimated k_{ISC} values of **39** (1.6×10^8 s^{-1} for **39-*trans*** and 1.7×10^8 s^{-1} for **39-*cis***) are one order larger than the corresponding k_r values (3.8×10^7 s^{-1} for **39-*trans*** and 4.0×10^7 s^{-1} for **39-*cis***, Table 4-1). In contrast, k_{ISC} values are more than one order smaller than the k_r values of **40** and **41** (see Tables 4-1, 4-3, and 4-4). The results well explain the relatively high efficiency of the ISC and low Φ_F of **39**. These calculations corroborate that the position of heterole rings possesses remarkable influence on the electronic properties of **39**–**41**.

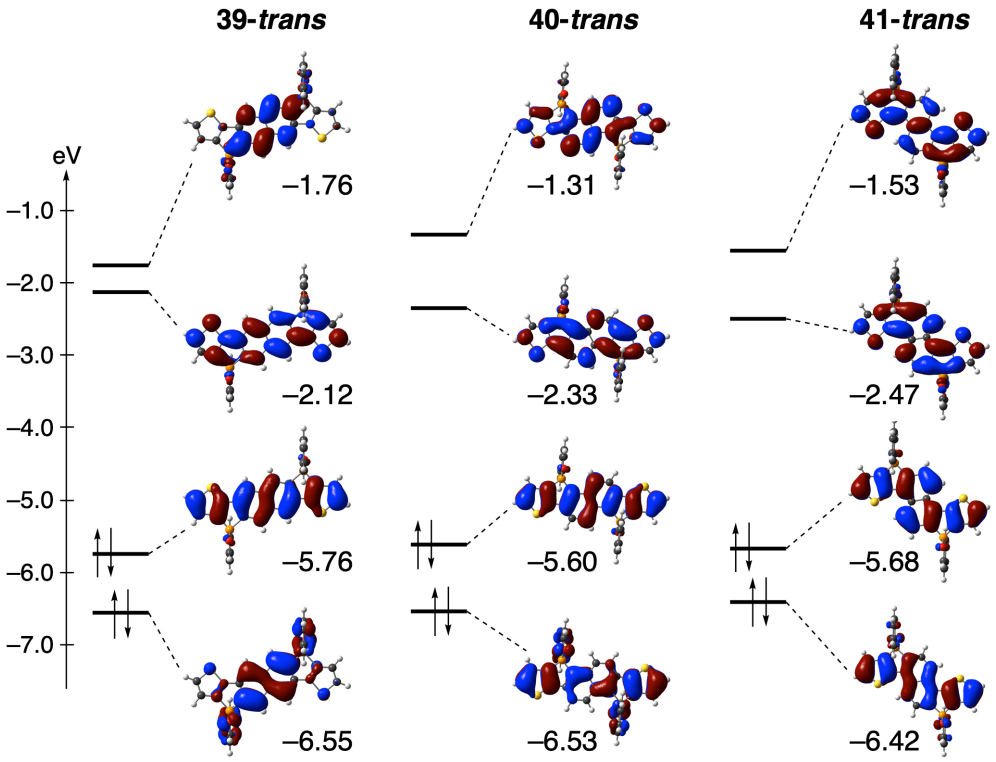

Figure 4-7. Selected Kohn-Sham orbitals of trans isomers of **39**–**41**.

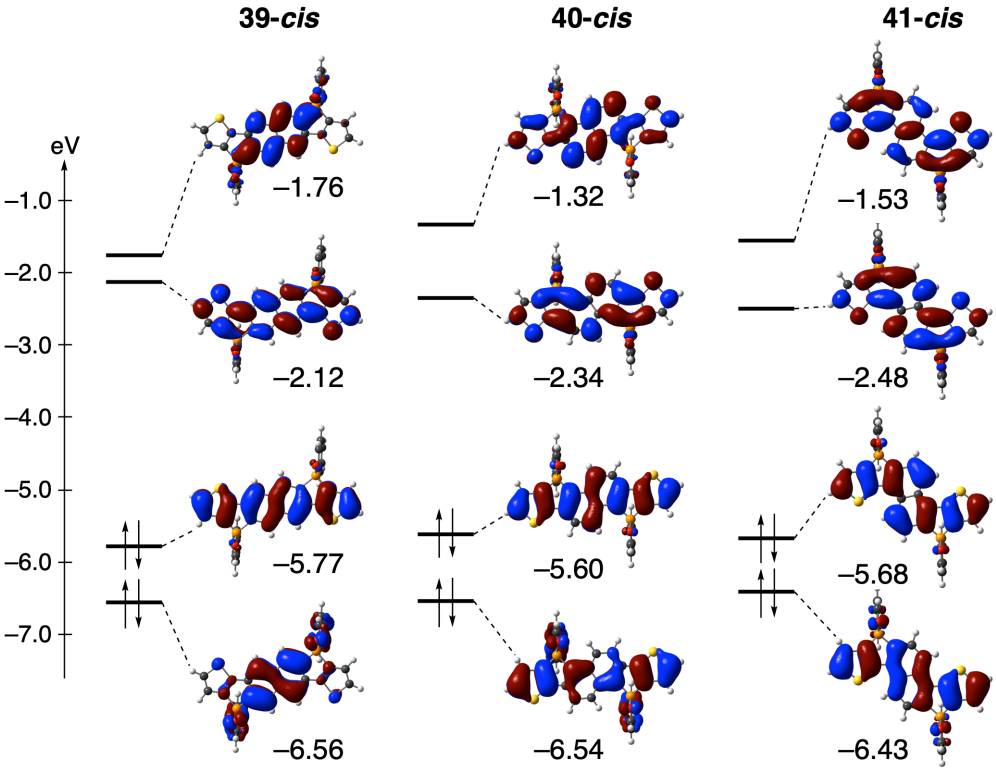

Figure 4-8. Selected Kohn-Sham orbitals of cis isomers of **39**–**41**.

Table 4-2. SOCMEVs and estimated k_{ISC} values between S_1 and T_n states for **39-*trans*** and **39-*cis***.

39-*trans*	T_1	T_2	T_3	T_4	T_5
SOCMEV/ cm^{-1}	1.92	1.03	0	1.15	0
k_{ISC}/ s^{-1}	8.8×10^{-18}	4.3×10^{5}	0	$\mathbf{1.6\times10^{8}}$	0

39-*cis*	T_1	T_2	T_3	T_4	T_5
SOCMEV/ cm^{-1}	0.90	0.58	1.51	1.15	0.34
k_{ISC}/ s^{-1}	2.2×10^{-18}	1.4×10^{5}	3.2×10^{7}	$\mathbf{1.7\times10^{8}}$	1.0×10^{-15}

Table 4-3. SOCMEVs and estimated k_{ISC} values between S_1 and T_n states for **40-*trans*** and **40-*cis***.

40-*trans*	T_1	T_2	T_3	T_4	T_5
SOCMEV/ cm^{-1}	0.40	0	1.05	1.8	0
k_{ISC}/ s^{-1}	2.2×10^{-23}	0	$\mathbf{2.0\times10^{7}}$	2.2×10^{0}	0

40-*cis*	T_1	T_2	T_3	T_4	T_5
SOCMEV/ cm^{-1}	0.30	0.51	0.61	1.17	0.73
k_{ISC}/ s^{-1}	1.9×10^{-19}	$\mathbf{3.5\times10^{7}}$	6.7×10^{6}	8.2×10^{-1}	4.3×10^{-24}

Table 4-4. SOCMEVs and estimated k_{ISC} values between S_1 and T_n states for **41-*trans*** and **41-*cis***.

41-*trans*	T_1	T_2	T_3	T_4	T_5
SOCMEV/ cm^{-1}	0.31	0	1.53	1.62	0
k_{ISC}/ s^{-1}	3.7×10^{-25}	0	$\mathbf{8.6\times10^{-2}}$	3.0×10^{-7}	0

41-*cis*	T_1	T_2	T_3	T_4	T_5
SOCMEV/ cm^{-1}	1.64	0.28	4.43	8.39	13.98
k_{ISC}/ s^{-1}	8.1×10^{-19}	3.3×10^{-5}	$\mathbf{3.1\times10^{7}}$	2.5×10^{6}	2.5×10^{2}

4-6. Charge-transporting Properties

Finally, the author evaluated the charge-transporting properties of naphthodiphospholes at short distance. The photoconductivity of **39**–**41** was measured by using the flash-photolysis time-resolved microwave conductivity (FP-TRMC) method.[68] The FP-TRMC profiles for powder samples of **39**–**41** upon irradiation at λ = 355 nm are shown in Figure 4-9. The maximum transient conductivities $(\phi\Sigma\mu)_{max}$ for **39-*trans*** (2.5×10^{-9} $m^2V^{-1}s^{-1}$), **40-*trans*** (2.4×10^{-9} $m^2V^{-1}s^{-1}$), and **41-*trans*** (2.9×10^{-9} $m^2V^{-1}s^{-1}$) are almost the same; ϕ and $\Sigma\mu$ represent the charge-carrier generation efficiency and sum of the charge-carrier mobility, respectively. For *trans* isomers, the position of fused heterole rings does not affect the charge-transport ability. On the other hand, the $(\phi\Sigma\mu)_{max}$ value for **40-*cis*** (5.4×10^{-9} $m^2V^{-1}s^{-1}$) is significantly higher than those for **39-*cis*** (3.5×10^{-9} $m^2V^{-1}s^{-1}$) and **41-*cis*** (3.2×10^{-9} $m^2V^{-1}s^{-1}$). The highest $(\phi\Sigma\mu)_{max}$ value for **40-*cis*** can be rationalized by effective electronic communication in the solid state derived from the unique 2D herringbone structure. Although the author has not succeeded to obtain the crystal structure of **39-*cis***, the position of fused heterole rings for *cis* isomers can influence their packing structures and resultant intermolecular electronic communications in the solid state. Accordingly, such 2D herringbone structure may become a potential platform to realize efficient charge-transporting properties by introducing suitable substituents into **40-*cis***.

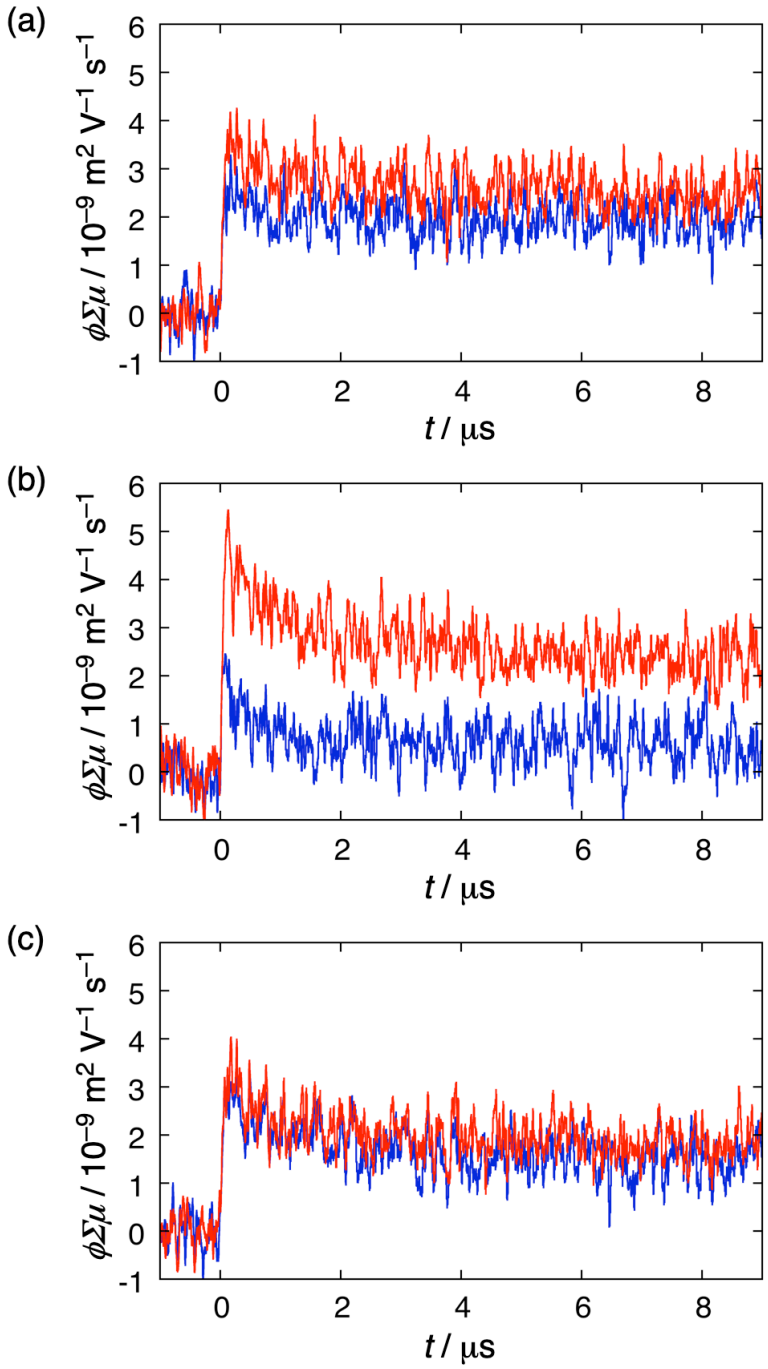

Figure 4-6. FP-TRMC profiles for powder samples of (a) **39-*trans*** (blue) and **39-*cis*** (red), (b) **40-*trans*** (blue) and **40-*cis*** (red), and (c) **41-*trans*** (blue) and **41-*cis*** (red) upon λ = 355 nm photoexcitation at 4.6 × 10^{15} photons cm^{-2} pulse^{-1} under air.

4-7. Summary

The author established the synthesis of a series of thiophene-fused naphthodiphospholes and evaluated their physicochemical properties comprehensively. The isomer **39** possessed larger HOMO–LUMO gaps than those of the isomers **40** and **41**. The DFT calculations showed that the LUMO of **39** has almost no distributions on the phosphorus atom, indicating that the σ*-π* interaction is hampered and in turn the phosphole-like character of **39** is limited. On the other hand, the isomers **40** and **41** achieved effective π-expansion and high electron-accepting ability owing to stronger σ*-π* interactions of **40** and **41** than **39**. Strikingly, the isomer **39** showed phosphorescence at 77 K, whereas the isomers **40** and **41** displayed no phosphorescence. The calculated ISC rate constants of **39** are larger by one order of magnitude than those of **40** and **42**, supporting the unique optical properties of **39**. Meanwhile, the X-ray crystal structures unveiled the effect of the orientations of fused phosphole rings and the *trans*/*cis* configurations of substituents on the phosphorus atoms in the solid state. The *trans* isomers **39-*trans*** and **40-*trans*** exhibited the 1D slip π-stacked arrangement. In contrast, the *cis* isomer **40-*cis*** displayed the 2D herringbone structure based on the multiple hydrogen bonds, while the packing structure of **41-*cis*** showed the columnar structure with a cavity. The isomer **40-*cis*** displayed the highest transient conductivity of 5.4×10^{-9} $m^2V^{-1}s^{-1}$ among **39**–**41**, which is associated with the 2D herringbone structure in the solid state of **40-*cis*.** Overall, the positions of fused heterole rings are utmost importance to tune their electronic structure and optical and electrochemical properties, while the orientations of fused heterole rings and substituents on the phosphorus atoms play critical roles in their molecular arrangements in the solid states. Therefore, the author accomplished the precise disposition of phosphorus and sulfur atoms in fused polycyclic aromatics where phospholes and thiophenes can be fused into a naphthalene core selectively. Considering that the α-positions of terminal thiophene rings can be easily functionalized, further functionalization of thiophene-fused naphthodiphospholes would open up for their new possibilities as organic functional materials.

Summary of This Thesis

In this thesis, synthesis and unique properties of phosphole and thiophene-fused π-conjugated molecules were described. The author elucidated the potential utilities of dithieno[3,4-*b*:3',4'-*d*]phosphole, doubly thiophene-fused benzodiphospholes, and naphthodiphospholes for functional materials.

In Chapter 1, the author mentioned the synthesis of dithieno[3,4-*b*:3',4'-*d*]phosphole as a new type of thiophene-fused phospholes. A series of diaryl-substituted derivatives were prepared in order to evaluate the fundamental properties of this platform. The dithienophosphole shows the hybrid character reflecting the nature of phosphole and thiophene, which means that the different types of intramolecular charge-transfer (ICT) interactions were observed by introducing electron-donating or electron-withdrawing aryl groups. Therefore, the author examined the modulation of dithieno[3,4-*b*:3',4'-*d*]phosphole by using donor-π-acceptor interaction in Chapter 2. The position of substituents is found to play an important role in the frontier molecular orbitals and the hybrid character. The introduction of electron-donating aryl group into 1,7-positions and electron-withdrawing group into 3,5-position can achieve more effective ICT interaction.

In Chapter 3, the author established the synthetic methodology of doubly thiophene-fused benzodiphosphole and their π-extended derivatives as a new class of π-conjugated molecules. Systematic investigations revealed their intriguing properties and potential utilities. The efficient fluorescence in red to NIR region with large Stokes shift is achieved by introducing electron-donating group at α-position of thiophene-ring and this character is useful in the field of biological imaging. Along with this, excellent two-photon absorption property of dimethylaminophenyl substituted derivative is also clarified. On the other hand, phenyl-substituted derivative shows excellent charge transporting ability derived from its 2D herringbone packing structure with intermolecular S–S interaction and hydrogen bondings.

In Chapter 4, doubly thiophene-fused naphthodiphospholes, which are π-expanded analogues of benzodiphospholes described in Chapter 4, were investigated. The author synthesized a series of six isomers depending on fused position and/or direction of phosphole rings, and the orientation of substituents on the phosphorus atoms (*trans/cis* configurations). The isomers with 2,3/6,7-fused structure display phosphorescence due to enhanced spin-orbit coupling whereas the isomers with 1,2/5,6-fused structure exhibit intense fluorescence. The *trans/cis* configurations affect the molecular arrangement in the slid state. Especially, *cis* isomers show unique packing structure, 2D herringbone structure of columnar structure with a cavity.

The author disclosed the intriguing properties of phosphole/thiophene-fused π-conjugated molecules and demonstrated their potential utilities. Therefore, this study will shed light to the chemistry of such class of compounds and be helpful for application as organic functional materials in various fields, for example, biological imaging, nonlinear optics, and organic transistors.

Experimental Section

Instrumentation and materials

Commercially available solvents and reagents were used without further purification unless otherwise mentioned. Silica-gel column chromatography was performed with UltraPure Silica Gel (230-400 mesh, SiliCycle) unless otherwise noted. Thin-layer chromatography (TLC) was performed with Silica gel 60 F_{254} (Merck). UV/Vis/NIR absorption spectra were measured with a Perkin-Elmer Lambda 900 UV/vis/NIR spectrometer. Steady-state fluorescence spectra were obtained by a HORIBA Nanolog spectrometer. Absolute fluorescence quantum yields were obtained by using a Hamamatsu Photonics Quantaurus-QY spectrometer. ^{1}H, ^{13}C, and ^{31}P NMR spectra were recorded with a JEOL EX-400 spectrometer (operating at 399.65 MHz for ^{1}H, 100.40 MHz for ^{13}C, and 161.7 MHz for ^{31}P) by using the residual solvent as the internal reference for ^{1}H ($CDCl_3$: δ = 7.26 ppm, CD_2Cl_2: δ = 5.32 ppm, $C_2D_2Cl_4$: δ = 6.00 ppm, $(CD_3)_2SO$: δ = 2.50 ppm, or $(CD_3)_2CO$: δ = 2.05 ppm), ^{13}C ($CDCl_3$: δ = 77.16 ppm, CD_2Cl_2: δ = 53.84 ppm, $(CD_3)_2SO$: δ = 39.52 ppm, or $(CD_3)_2CO$: δ = 206.26 ppm), and trimethylphosphite as the external reference for ^{31}P (δ = 140.0 ppm). High-resolution mass spectra (HRMS) were measured on a Thermo Fischer Scientific EXACTIVE Fourier-transform orbitrap mass spectrometer (APCI and ESI). Attenuated total reflectance-Fourier transform infrared (ATR-FTIR) spectra were taken with the golden gate diamond anvil ATR accessory (NICOLET 6700, Thermo scientific), using typically 64 scans at a resolution of 2 cm^{-1}. All samples were placed in contact with the diamond window using the same mechanical force. Single-crystal X-ray diffraction analysis data for the compounds **25** and ***trans*/*cis*-33** was collected at –150 ºC on a Rigaku Saturn70 CCD diffractometer with graphite monochromated $Mo_{K\alpha}$ radiation (0.71069 Å), **32b**, **32e**, **39-*trans***, **40-*trans*/*cis***, and **41-*cis*** were collected at –120 ºC on a Rigaku Saturn724+ CCD diffractometer with graphite monochromated $Mo_{K\alpha}$ radiation (0.71075 Å), and **34a** and **36a** were collected at –180 ºC on a Rigaku XtaLAB P200 apparatus by using a teo-dimensional PILATUS 100K/R detector with $Cu_{K\alpha}$ radiation (1.54187 Å). The structures were solved by direct method (SHELXS-2014). XRD measurements of powders on a quartz plate were performed on a Rigaku MiniFlex600 X-ray diffractometer equipped with an X-ray tube by using $Cu_{K\alpha}$ radiation beam with a wavelength of 1.54 Å. Diffraction intensities were recorded with 0.02º steps in θ at a scan rate of 0.1º min^{-1}. Redox potentials were measured by cyclic voltammetry and differential pulse voltammetry method on an ALS electrochemical analyzer model 660A.

Computational method

Density Functional Theory (DFT) Calculations

All calculations were carried out using the *Gaussian 09* program.[82] All structures were fully optimized without any symmetry restriction. The optimization were performed using the density functional theory (DFT) method with restricted B3LYP (Becke's three-parameter hybrid exchange functionals and the Lee-Yang-Parr correlation functional) level,[83,84] employing a basis set 6-31G(d,p) for C, H, N, O, F, P, and S. The optimized structures in solvents were obtained with COSMO solvation model.[85] Excitation energies and oscillator strengths on the optimized structures were calculated using the TD-SCF method at the B3LYP/6-31G(d,p) level.

Simulation of TPA spectrum

All DFT calculations were carried out also using the *Gaussian 09* program. The optimized geometry at the CAM-B3LYP/6-31+G(d) level was used for the calculations of the transition energies and transition dipole moments from the ground state to excited states by time-dependent CAM-B3LYP and the transition dipole moments between the excited sates by applying the Tamm-Dancoff approximation (TDA)[86] for CAM-B3LYP. The polarizable continuum model (PCM) for CH_2Cl_2 was applied for all DFT calculations. The homemade procedure based on the formalism reported elsewhere[87] was used to simulate TPA spectra. For the simulation, up to 15 excited states were considered and the relaxation constants of 0.1 eV were used.

Spin-orbit coupling matrix elemental values (SOCMEVs) and ISC rate constants (k_{ISC})

The SOCMEVs were calculated by TD-DFT in the Tamm-Dancoff approximation (TDA), where SOC was treated as a perturbation using ADF2019.302. PBE0 functional and all-electron Slater-type triple-zeta plus polarization basis set were used.

Considering that the photoexcitation corresponds to S_0–S_1 absorption, ISC can be expected between S_1 and T_n states. The k_{ISC} values were calculated by following equation. [88]

$$k_{\mathrm{ISC}}=\frac{2\pi}{\hbar}\cdot\frac{1}{\sqrt{4\pi\lambda_{\mathrm{M}}k_{\mathrm{B}}T}}\cdot e\left(-\frac{(\Delta E_{\mathrm{ST}}+\lambda_{\mathrm{M}})^2}{4\lambda_{\mathrm{M}}k_{\mathrm{B}}T}\right)\cdot\frac{1}{3}\left|\langle \mathrm{S}_1|\hat{H}_{\mathrm{SO}}|\mathrm{T}_{\mathrm{n}}\rangle\right|^2$$

$\hbar$: reduced Planck constant of 6.58×10^{-16} eV·s

k_{B} : Boltzmann constant of 8.62×10^{-5} eV·K^{-1}

T : temperature of 300 K

ΔE_{ST} : energy difference between S_1 and T_n states

For Marcus reorganization energy, λ_{M}, we reasonably set the value to 0.1 eV considering rigid molecular structure as demonstrated by small stokes shift.

Two-photon absorption cross-section ($\sigma^{(2)}$) measurements

TPA spectra of **36b** were measured in CH_2Cl_2 (spectroscopic grade) with a concentration of 0.3 mM by using the open-aperture Z-scan method.[89] A femtosecond optical parametric amplifier (Spectra-Physics *TOPAS Prime*) operating at 1 kHz was used as light source. The details of the setup and analytical procedure are described elsewhere.[90] The Rayleigh range was 6–8 mm, depending on the wavelength used, much longer then the path length of the sample (2 mm), satisfying the thin-sample condition. The average irradiation power was less than 0.7 mW, corresponding to the on-axis optical peak intensity at the focal point of ~300 GW/cm^2. The obtained open-aperture Z-scan traces were analyzed by curve fitting with the theoretical equation assuming the partial and temporal Gaussian pulses.[90] All values of the TPA cross section were corrected by referring to those of the in-house standard sample (MPPBT in dimethyl sulfoxide, 2.4 mM)[S6] measured at the same time.

Flash Photolysis Time-resolved Microwave Conductivity (FP-TRMC) Measurements

In Chapter 3, the charge carrier transport property was evaluated by FP-TRMC technique at room temperature under air. Transient charge carriers were generated through photoexcitation by laser pulses of third harmonic generation (λ_{ex}= 355 nm) from a Spectra Physics INDI-HG Nd:YAG laser with a pulse duration of 5–8 ns at the photon density of 4.6×10^{15} photon cm^{-2}. The frequency and power of probing microwave were set at around 9 GHz and 3 mW, respectively. Photoconductivity transients, demodulated through a GaAs crystal-diode with Schottky-barriers (rise time < 1 ns), were monitored by a Tektronix model TDS3032B digital oscilloscope. Time constant (τ) of the present TRMC system was then determined by the Q-value of microwave cavity (Q = 2000), leading to $\tau = Q/2f$ ~100 ns. The observed conductivities were normalized, given by a photocarrier generation yield (ϕ) multiplied by sum of the carrier mobilities of electron/hole ($\Sigma\mu$), according to the equation,

$$\phi\sum\mu=\frac{\mathrm{A}\Delta P_{\mathrm{r}}}{eI_0F_{\mathrm{L}}P_{\mathrm{r}}}$$

where, e, A, I_0, F_L, P_r, and ΔP_r are elementary charge, sensitivity factor (S cm^{-1}), incident photon density of the excitation laser (photon cm^{-2}), correction factor (cm^{-1}) for overlapping between special distribution of photo-generated charge carriers and electromagnetic field strength of probing microwave in the cavity, and reflected microwave power and its transient change, respectively. The samples for FP-TRMC were prepared by drop-casting a $CHCl_3$ solution onto a quartz plate (9 × 40 × 1 mm^3) or coating a poly(vinyl alcohol) (PVA) layer by using 2 wt% PVA/water over the powders on the quartz plate, and dried in vacuum for 2 h prior

to use. In Chapter 4, the measurements were carried out under same condition except for using Continuum Inc. Surelite II Nd:YAG laser and powder samples.

Chapter 1

4-Phenyldithieno[3,4-b:3′,4′-d]phosphole 4-Sulfide (23):

A solution of *t*-BuLi in pentane (1.64 M, 10.9 mL, 17.8 mmol) was added dropwise to a solution of 4,4′-dibromo-3,3′-bithiophene (**24**) (1.34 g, 4.14 mmol) in diethyl ether (100 mL) at –78 °C. After stirring for 2 h at –78 °C, dichlorophenylphosphine (0.673 mL, 4.97 mmol) was added slowly and stirred for 1 h at –78 °C. The mixture was allowed to warm to –55 °C for 2 h and then warmed to room temperature. S powder (159 mg, 4.96 mmol) was added and stirred for 1 h. The reaction mixture was quenched with water and extracted with dichloromethane (50 mL × 3). The organic layer was dried over Na_2SO_4 and concentrated in vacuo. The crude product was purified by reprecipitation from a 1:10 mixture of dichloromethane and *n*-hexane to give **23** as a pale-yellow solid (905 mg, 2.97 mmol, 72%).

^{1}H NMR (399.65 MHz, $CDCl_3$, 25 °C): δ = 7.77 (q, J = 6.8 Hz, 2H), 7.68 (dd, J = 6.4, 2.4 Hz, 2H), 7.48 (td, J = 7.2, 2.4 Hz, 1H), and 7.38−7.43 (m, 4H) ppm; ^{13}C NMR (100.40 MHz, $CDCl_3$, 25 °C): δ = 131.9, 131.8, 131.0 (d, J = 12.5 Hz), 130.3, 130.1, 128.6 (d, J = 13.5 Hz), 116.4, and 116.3 ppm; ^{31}P NMR (161.7 MHz, $CDCl_3$, 25 °C): δ = 16.8 ppm. UV/vis (CH_2Cl_2): λ (ε, M^{-1} cm^{-1}) = 260 (15000) and 302 (6500) nm. FT-IR (ATR): ν = 661 (P=S) cm^{-1}. HRMS (ESI, positive) calcd for $C_{14}H_{10}PS_3$ $[M+H]^+$ 304.9677; found 304.9679. Mp: 146−147 °C.

3,5-Diiodo-4-phenyldithieno[3,4-*b*:3',4'-*d*]phosphole 4-sulfide (25) and 1,5-diiodo-4-phenyldithieno[3,4-*b*:3',4'-*d*]phosphole 4-sulfide (26):

A solution of *n*-BuLi in hexane (1.55 M, 2.13 mL, 3.31 mmol) was added to a solution of dithienophosphole **23** (458 mg, 1.50 mmol) in THF (46 mL) at –70 ºC. After stirring for 1 h, perfluorohexyliodide (0.718 mL, 3.31 mmol) in THF (10 mL) was added dropwise and stirred for 30 min at –70 ºC. The mixture was allowed to warm to room temperature and stirred for 1 h. The reaction mixture was quenched with water and extracted with ethyl acetate (30 mL × 3). The organic layer was dried over Na_2SO_4 and concentrated in vacuo. Silica-gel column chromatography (hexane/THF = 5/1) provided **25** as a brown solid (214 mg, 0.385 mmol, 26%) along with **26** as a brown solid (332 mg, 0.597 mmol, 40%).

25: ^{1}H NMR (399.65 MHz, $CDCl_3$, 25 °C): δ = 7.85 (q, J = 7.2 Hz, 2H), 7.56 (td, J = 7.2 Hz, 2.4 Hz, 1H), 7.47 (m, 2H), and 7.39 (d, J = 2.4 Hz, 2H) ppm; ^{31}P NMR (161.7 MHz, $CDCl_3$,

25 °C): δ = 23.7 ppm. FT-IR (ATR): ν = 662 (P=S) cm^{-1}. HRMS (ESI, positive) calcd. for $C_{14}H_8PS_3I_2$ $[M+H]^+$ 556.7610; found 556.7618. m.p.: 230 ºC (decomp).

26: ^1H NMR (399.65 MHz, $CDCl_3$, 25 °C): δ = 7.99 (d, J = 1.6 Hz, 1H), 7.81 (q, J = 7.2 Hz, 2H), 7.74 (d, J = 7.2 Hz, 1H), 7.53 (m, 1H), and 7.45 (m, 2H) ppm; ^{31}P NMR (161.7 MHz, $CDCl_3$, 25 °C): δ = 19.3 ppm. FT-IR (ATR): ν = 657 (P=S) cm^{-1}. HRMS (ESI, positive) calcd. for $C_{14}H_8PS_3I_2$ $[M+H]^+$ 556.7610; found 556.7617. m.p.: 260 °C (decomp). **Due to the low solubility, we could not obtain the ^{13}C NMR spectra in a sufficient S/N ratio.**

General procedure for the cross-coupling of dithienophosphole 25 with aryl boronates.

A Schlenk flask containing dithienophosphole **25** (55 mg, 0.1 mmol), aryl boronate (0.25 mmol, 2.5 equiv), Na_2CO_3 (42 mg, 0.4 mmol, 4 equiv) and $Pd(PPh_3)_4$ (11 mg, 0.01 mmol, 10 mol%) was flushed argon and then THF (1.6 mL) and water (0.8 mL) were added. After stirring for 24 h at 70 ºC, the mixture was cooled to room temperature and extracted with AcOEt (10 mL × 3). The organic layer was washed with brine, dried over Na_2SO_4 and concentrated in vacuo. The crude product was purified by silica-gel column chromatography (hexane/CH_2Cl_2 = 1/3) to give aryldithienophospholes **27**.

3,5-Diphenyl-4-phenyldithieno[3,4-*b*:3',4'-*d*]phosphole 4-sulfide (27a):

A white solid (29.8 mg, 65.3 μmol, 66%).

^1H NMR (399.65 MHz, CD_2Cl_2, 25 °C): δ = 7.82 (q, J = 7.6 Hz, 2H), 7.64 (q, J = 4.0 Hz, 4H), 7.43 (m, 1H), 7.41 (d, J = 2.4 Hz, 2H), 7.35 (m, 2H), and 7.25–7.29 (m, 6H) ppm; ^{13}C NMR (100.40 MHz, $CDCl_3$, 25 °C): δ = 150.0, 141.5 (d, J = 18.3 Hz), 131.9, 131.4, 131.3, 128.8, 128.6, 128.5, 128.4, 128.3, 114.4, and 114.3 ppm; ^{31}P NMR (161.7 MHz, $CDCl_3$, 25 °C): δ = 23.3 ppm. UV/vis (CH_2Cl_2): λ (ε, $M^{-1}\,cm^{-1}$) = 270 (41000), 310 (14000), 355(sh) (2300) nm. Fluorescence (CH_2Cl_2, λ_{ex} = 323 nm): λ_{max} = 399 nm. FT-IR (ATR): ν = 652 (P=S) cm^{-1}. HRMS (ESI, positive) calcd. for $C_{26}H_{18}PS_3$ $[M+H]^+$ 457.0303; found 457.0305. m.p.: 267–269 °C.

3,5-Di(4-methoxyphenyl)-4-phenyldithieno[3,4-*b*:3',4'-*d*]phosphole 4-sulfide (27b):

A brown solid (32.2 mg, 62.3 μmol, 63%).

^1H NMR (399.65 MHz, $CDCl_3$, 25 °C): δ = 7.82 (q, J = 8.4 Hz, 2H), 7.64 (dt, J = 2.4, 9.2 Hz, 4H), 7.37-7.44 (m, 1H), 7.30–7.36 (m, 2H), 7.24 (d, J = 1.8 Hz, 2H), 6.78 (dt, J = 2.4, 9.2 Hz, 4H), and 3.78 (s, 6H) ppm; ^{13}C NMR (100.40 MHz, $CDCl_3$, 25 °C): δ = 160.1, 150.1 (d, J = 11.5 Hz), 138.8 (d, J = 622 Hz), 138.4 (d, J = 510 Hz), 131.8, 131.4, 131.3, 129.7, 128.5 (d, J =

13.5 Hz), 124.7, 113.8, 113.3 (d, J = 12.5 Hz), and 55.3 ppm; ^{31}P NMR (161.7 MHz, $CDCl_3$, 25 °C): δ = 21.2 ppm. UV/vis (CH_2Cl_2): λ (ε, $M^{-1}\,cm^{-1}$) = 279 (42000), 308 (21000), and 351 (8000) nm. Fluorescence (CH_2Cl_2, λ_{ex} = 323 nm): λ_{max} = 399 nm. FT-IR (ATR): ν = 1252 (C-O-C), 1026 (C-O-C), 673 (P=S) cm^{-1}. HRMS (ESI, positive) calcd. for $C_{28}H_{22}O_2PS_3$ $[M+H]^+$ 517.0514; found 517.0519. m.p.: 233–234 °C.

3,5-Bis(4-dimethylaminophenyl)-4-phenyldithieno[3,4-*b*:3',4'-*d*]phosphole 4-sulfide (27c):
A yellow solid (36.5 mg, 67.2 µmol, 68%).
^{1}H NMR (399.65 MHz, $CDCl_3$, 25 °C): δ = 7.89 (q, J = 7.6 Hz, 2H), 7.60 (d, J = 9.2 Hz, 4H), 7.30–7.40 (m, 3H), 7.13 (d, J = 1.8 Hz, 2H), 6.57 (d, J = 9.2 Hz, 4H), and 2.94 (s, 12H) ppm; ^{13}C NMR (100.40 MHz, $CDCl_3$, 25 °C): δ = 150.5, 141.6 (d, J = 19.3 Hz), 135.5 (d, J = 67.4 Hz), 134.4, 133.2 (d, J = 75 Hz), 131.5, 131.4, 129.3, 128.4 (d, J = 12.5 Hz), 120.2, 111.7 (d, J = 12.5 Hz), 111.6, and 40.2 ppm; ^{31}P NMR (161.7 MHz, $CDCl_3$, 25 °C): δ = 21.5 ppm. UV/vis (CH_2Cl_2): λ (ε, $M^{-1}\,cm^{-1}$) = 301 (35000) and 381 (25000) nm. Fluorescence (CH_2Cl_2, λ_{ex} = 323 nm): λ_{max} = 464 nm. FT-IR (ATR): ν = 1203 (C-N), 673 (P=S) cm^{-1}. HRMS (ESI, positive) calcd. for $C_{30}H_{28}N_2PS_3$ $[M+H]^+$ 543.1147; found 543.1155. m.p.: 240 °C (decomp).

3,5-Bis(4-trifluoromethylphenyl)-4-phenyldithieno[3,4-*b*:3',4'-*d*]phosphole 4-sulfide (27d):
A white solid (28.7 mg, 48.5 µmol, 49%).
^{1}H NMR (399.65 MHz, $CDCl_3$, 25 °C): δ = 7.78 (q, J = 7.2 Hz, 2H), 7.77 (d, J = 8.6 Hz, 4H), 7.52 (d, J = 8.6 Hz, 4H), 7.44 (m, 1H), 7.42 (d, J = 1.6 Hz, 2H), and 7.33–7.40 (m, 2H) ppm; ^{13}C NMR (100.40 MHz, $CDCl_3$, 25 °C): δ = 141.6, 141.5, 138.6 (d, J = 90.6 Hz), 135.1, 132.4, 131.3, 131.2, 130.5 (d, J = 32.8 Hz), 128.8, 128.7, 128.4, 125.5 (d, J = 3.9 Hz), and 115.8 (d, J = 12.5 Hz) ppm; ^{31}P NMR (161.7 MHz, $CDCl_3$, 25 °C): δ = 21.3 ppm. UV/vis (CH_2Cl_2): λ (ε, $M^{-1}\,cm^{-1}$) = 273 (33000), 314 (12000), and 350(sh) (2200) nm. Fluorescence (CH_2Cl_2, λ_{ex} = 323 nm): λ_{max} = 400 nm. FT-IR (ATR): ν = 1126 (C-F), 667 (P=S) cm^{-1}. HRMS (ESI, positive) calcd. for $C_{28}H_{16}F_6PS_3$ $[M+H]^+$ 593.0050; found 593.0057. m.p.: 276–277 °C.

3,5-Di(4-nitrophenyl)-4-phenyldithieno[3,4-*b*:3',4'-*d*]phosphole 4-sulfide (27e):
A yellow solid (22.2 mg, 40.5 µmol, 41%).
^{1}H NMR (399.65 MHz, $CDCl_3$, 25 °C): δ = 8.13 (dt, J = 9.2 Hz, 2.4 Hz, 4H), 7.85 (dt, J = 9.2 Hz, 2.4 Hz 4H), 7.80 (q, J = 8.4 Hz, 2H), 7.51 (d, J = 1.8 Hz, 2H), 7.43–7.49 (m, 1H), and 7.35–7.42 (m, 2H) ppm; ^{31}P NMR (161.7 MHz, $CDCl_3$, 25 °C): δ = 21.3 ppm. UV/vis (CH_2Cl_2): λ (ε, $M^{-1}\,cm^{-1}$) = 307 (24000), 336 (22000), and 385(sh) (12500) nm. Fluorescence (CH_2Cl_2, λ_{ex} =

323 nm): λ_{max} = 515 nm. FT-IR (ATR): ν = 1506 (NO_2), 1337 (NO_2), 669 (P=S) cm^{-1}. HRMS (ESI, negative) calcd. for $C_{26}H_{14}N_2O_4PS_3$ $[M–H]^-$ 544.9859; found 544.9868. m.p.: >280 °C. **Due to the low solubility, we could not obtain the ^{13}C NMR spectrum in a sufficient S/N ratio.**

3,5-Diphenyl-4-phenyldithieno[3,4-*b*:3',4'-*d*]phosphole (28):

A Schlenk tube equipped with magnetic stir bar was charged with dithienophosphole **27a** (3.4 mg, 7.5 μmol) and $P(NMe_2)_3$ (0.01 mL, 37.5 μmol), the mixture was dissolved in toluene (5 mL). The mixture was stirred for 5 h under Ar atmosphere at 90 ºC. After 5 h, water was added to the mixture and the product was extracted with CH_2Cl_2, and the combined organic layer was washed with water and brine, and dried over Na_2SO_4. After the solvent was removed under reduced pressure, the residue was purified by a silica gel column chromatography using a 5:6 mixture of CH_2Cl_2 and *n*-hexane to afford **28** as a white solid (2.2 mg, 5.6 μmol, 75 %).

^1H NMR (399.65 MHz, $CDCl_3$, 25 °C): δ = 7.63 (d, 4H, J = 8.0 Hz), 7.37 (s, 2H), 7.32 (m, 6H), 7.27 (m, 2H), and 7.16 (m, 3H) ppm; ^{13}C NMR (100.40 MHz, $CDCl_3$, 25 °C): δ = 144.0 (d, J = 15.4 Hz), 143.5, 143.3 (d, J = 14.5 Hz), 133.9, 133.1 (d, J = 20.2 Hz), 129.3, 128.7, 128.6 (d, J = 7.7 Hz), 127.8, 127.1, 127.0, and 113.5 ppm; ^{31}P NMR (161.7 MHz, $CDCl_3$, 25 °C): δ = –31.8 ppm. UV/vis (CH_2Cl_2): λ (ε, M^{-1} cm^{-1}) = 271 (40000), 291(sh) (25500), and 330(sh) (4000) nm. Fluorescence (CH_2Cl_2, λ_{ex} = 323 nm): λ_{max} = 429 nm. HRMS (ESI, positive) calcd. for $C_{26}H_{18}PS_2$ $[M+H]^+$ 425.0582; found 425.0581. m.p.: 148–149 °C.

Chapter 2

3,5-Di(4-methoxyphenyl)-4-phenyldithieno[3,4-*b*:3',4'-*d*]phosphole 4-oxide (30b):

To a solution of dithienophosphole **27b** (36.5 mg, 0.0706 mmol) in toluene (2.0 mL) was added $P(NMe_2)_3$ (65 μL, 0.35 mmol) and heated to 90 °C. After stirring for 3 h at 90 °C, the mixture was allowed to cool to ambient temperature and then an aqueous solution of hydrogen peroxide (30% in water, 1mL) was added. Stirring another 30 min, the reaction mixture was extracted with $CHCl_3$ (5 mL × 3). The organic layer was dried over with Na_2SO_4 and concentrated in vacuo. The residue was purified by silica-gel column chromatography (eluent: $CHCl_3$) to afford phosphole oxide **30b** (26.9 mg, 0.0537 mmol, 76%).

^1H NMR (395.88 MHz, $(CD_3)_2CO$, 25 °C): δ = 7.93 (d, 4H, J = 8.7 Hz), 7.67 (d, 2H, J = 2.3 Hz, 2H), 7.61–7.53 (m, 2H), 7.39–7.33 (m, 1H), 7.31–7.24 (m, 2H), 6.93 (d, 4H, J = 8.7 Hz), and 3.81 (s, 6H) ppm; ^{13}C NMR (100.40 MHz, $(CD_3)_2CO$, 25 °C): δ = 162.2, 152.6 (d, J = 11.6 Hz),

143.4 (d, J = 22.2 Hz), 136.9 (d, J = 113 Hz), 133.6, 133.5 (d, J = 110 Hz), 132.6 (d, J = 10.6 Hz), 130.6, 130.0 (d, J = 12.5 Hz), 126.9, 116.3 (d, J = 12.5 Hz), 115.9 and 56.4 ppm; ^{31}P NMR (161.7 MHz, $CDCl_3$, 25 °C): δ = 14.8 ppm. FT-IR (ATR): ν = 1030 (C–O–C) and 1180 (P=O) cm^{-1}. HRMS (ESI, positive) calcd. for $C_{28}H_{21}O_3PS_2Na$ $[M+Na]^+$ 523.0562; found 523.0559. m.p.: 249–250 °C.

3,5-Di(4-nitrophenyl)-4-phenyldithieno[3,4-*b*:3',4'-*d*]phosphole 4-oxide (30e):

To a solution of dithienophosphole **27e** (27.6 mg, 0.0505 mmol) in toluene (2.0 mL) was added $P(NMe_2)_3$ (92 μL, 0.50 mmol) and heated to 90 °C. After stirring for 3 h at 90 °C, the mixture was allowed to cool to ambient temperature and then an aqueous solution of hydrogen peroxide (30% in water, 1mL) was added. Stirring another 30 min, the reaction mixture was extracted with $CHCl_3$ (5 mL × 3). The organic layer was dried over with Na_2SO_4 and concentrated in vacuo. The residue was purified by silica-gel column chromatography (eluent: $CHCl_3$) to afford phosphole oxide **30e** (16.5 mg, 0.0311 mmol, 62%).

^{1}H NMR (395.88 MHz, (CD_2Cl_2, 25 °C): δ = 8.20 (d, 4H, J = 9.2 Hz), 8.08 (d, 4H, J = 9.2 Hz, 2H), 7.57 (d, 2H, J = 1.8 Hz), 7.61–7.52 (m, 2H), 7.39–7.33 (m, 1H) and 7.28–7.21 (m, 2H) ppm; ^{13}C NMR (100.40 MHz, CD_2Cl_2, 25 °C): δ = 148.7 (d, J = 9.6 Hz), 148.0, 142.5 (d, J = 20.2 Hz), 138.8 (d, J = 108 Hz), 138.7, 133.0, 131.4 (d, J = 11.6 Hz), 130.1 (d, J = 111 Hz), 129.1 (d, J = 13.5 Hz), 128.7, 124.6 and 118.2 (d, J = 12.5 Hz) ppm; ^{31}P NMR (161.7 MHz, $CDCl_3$, 25 °C): δ = 14.2 ppm. FT-IR (ATR): ν = 1509 (NO_2) and 1171 (P=O) cm^{-1}. HRMS (ESI, positive) calcd. for $C_{26}H_{15}N_2O_5PS_2Na$ $[M+Na]^+$ 553.0052; found 553.0051. m.p.: >300 °C.

1,7-Diiodo-3,5-di(4-methoxyphenyl)-4-phenyldithieno[3,4-*b*:3',4'-*d*]phosphole 4-oxide (31b):

To a solution of dithienophosphole **30b** (10.7 mg, 0.0214 mmol) in $CHCl_3$/AcOH (2.2 mL, v/v = 10/1) was added *N*-iodosuccinimide (10.6 mg, 0.470 mmol) and heated to 50 °C. After stirring for 18 h at 50 °C, the mixture was allowed to cool to ambient temperature and then the reaction was quenched with saturated aqueous solution of $Na_2S_2O_3$. The mixture was extracted with $CHCl_3$ (5 mL × 3). The organic layer was washed with sat. $NaHCO_3$ aq., dried over with Na_2SO_4 and concentrated in vacuo. The residue was purified by silica-gel column chromatography (eluent: $CHCl_3$) to afford diiodophosphole oxide **31b** (15.0 mg, 0.0199 mmol, 91%).

^{1}H NMR (395.88 MHz, CD_2Cl_2, 25 °C): δ = 7.67 (d, 4H, J = 9.2 Hz), 7.51–7.43 (m, 2H), 7.34–7.29 (m, 1H), 7.23–7.16 (m, 2H), 6.82 (d, 4H, J = 8.7 Hz), and 3.76 (s, 6H) ppm; ^{13}C NMR

(100.40 MHz, CD_2Cl_2, 25 °C): δ = 161.2, 158.1 (d, J = 10.6 Hz), 145.4 (d, J = 20.2 Hz), 138.8, 136.7 (d, J = 217 Hz), 132.4, 131.5 (d, J = 11.6 Hz), 129.8, 128.7, 128.6, 124.3, 114.6 and 55.7 ppm; ^{31}P NMR (161.7 MHz, $CDCl_3$, 25 °C): δ = 4.17 ppm. FT-IR (ATR): ν = 1030 (C–O–C) and 1174 (P=O) cm^{-1}. HRMS (ESI, positive) calcd. for $C_{28}H_{19}I_2O_3PS_2Na$ $[M+Na]^+$ 774.8495; found 774.8489. m.p.: 280 °C (decomp.).

1,7-Diiodo-3,5-di(4-nitrophenyl)-4-phenyldithieno[3,4-*b*:3',4'-*d*]phosphole 4-oxide (31e):

To a solution of dithienophosphole **30e** (20.9 mg, 0.0394 mmol) in $CHCl_3$/AcOH (2.2 mL, v/v = 10/1) was added *N*-iodosuccinimide (19.5 mg, 0.867 mmol) and heated to 50 °C. After stirring for 18 h at 50 °C, the mixture was allowed to cool to ambient temperature and then the reaction was quenched with saturated aqueous solution of $Na_2S_2O_3$. The mixture was extracted with $CHCl_3$ (5 mL × 3). The organic layer was washed with sat. $NaHCO_3$ aq., dried over with Na_2SO_4 and concentrated in vacuo. The residue was purified by silica-gel column chromatography (eluent: $CHCl_3$) to afford diiodophosphole oxide **31e** (10.1 mg, 0.013 mmol, 33%).

^{1}H NMR (395.88 MHz, CD_2Cl_2, 25 °C): δ = 8.18–8.12 (m, 4H), 7.98–7.92 (m, 4H), 7.55–7.44 (m, 2H), 7.37–7.30 (m, 1H) and 7.25–7.17 (m, 2H) ppm; ^{13}C NMR (100.40 MHz, CD_2Cl_2, 25 °C): δ = 148.3, 146.5 (d, J = 9.6 Hz), 139.2 (d, J = 105 Hz), 137.6, 136.4 (d, J = 19.3 Hz), 133.3 (m), 131.5 (d, J = 11.6 Hz), 129.0 (m), 128.95 (d, J = 113 Hz), 128.90, 125.0 (d, J = 15.4 Hz) and 124.6 ppm; ^{31}P NMR (161.7 MHz, $CDCl_3$, 25 °C): δ = 10.4 ppm. FT-IR (ATR): ν = 1506 (NO_2) and 1190 (P=O) cm^{-1}. HRMS (APCI, positive) calcd. for $C_{26}H_{14}I_2N_2O_5PS_2$ $[M+H]^+$ 782.8160; found 782.8169. m.p.: >300 °C.

1,7-Di(4-nitrophenyl)-3,5-di(4-methoxyphenyl)-4-phenyldithieno[3,4-*b*:3',4'-*d*]phosphole 4-oxide (32b):

A Schlenk flask containing dithienophosphole **31b** (15 mg, 0.020 mmol), 4-nitrophenyl boronate (12.4 mg, 0.0498 mmol), Na_2CO_3 (8.5 mg, 0.080 mmol) and $Pd(PPh_3)_4$ (2.3 mg, 2.0 μmol) was flushed argon and then THF (1.6 mL) and water (0.8 mL) were added. After stirring for 16 h at 70 °C, the mixture was cooled to room temperature and diluted with $CHCl_3$, dried over Na_2SO_4 and concentrated in vacuo. The crude product was purified by silica-gel column chromatography (eluent: $CHCl_3$) to give dithienophospholes **32b** (11.2 mg, 0.015 mmol, 76%).

^{1}H NMR (395.88 MHz, CD_2Cl_2, 25 °C): δ = 7.87 (d, J = 8.7 Hz, 4H), 7.73 (d, J = 8.7 Hz, 4H), 7.69–7.61 (m, 2H), 7.42–7.36 (m, 1H), 7.31–7.22 (m, 6H), 6.90 (d, J = 8.7 Hz, 4H) and 3.81 (s, 6H) ppm; ^{13}C NMR (100.40 MHz, CD_2Cl_2, 25 °C): δ = 161.3, 153.1 (d, J = 9.6 Hz), 147.4,

140.5, 138.0 (d, J = 107 Hz), 137.5 (d, J = 20.2 Hz), 132.5, 132.3 (d, J = 12.5 Hz), 131.6 (d, J = 10.6 Hz), 130.0 (d, J = 91.5 Hz), 129.8, 129.2, 128.8 (d, J = 13.5 Hz), 124.7, 123.4, 114.7 and 55.8 ppm; ^{31}P NMR (161.7 MHz, $CDCl_3$, 25 °C): δ = 11.0 ppm. UV/vis (CH_2Cl_2): λ (ε, M^{-1} cm^{-1}) = 280 (35000), 323 (30000), and 358 (28000) nm. Fluorescence (CH_2Cl_2, λ_{ex} = 400 nm): λ_{max} = 606 nm. FT-IR (ATR): ν = 1512 (NO_2), 1178 (P=O), and 1020 (C–O–C) cm^{-1}. HRMS (ESI, positive) calcd. for $C_{40}H_{28}N_2O_7PS_2$ [M+H]$^+$ 743.1070; found743.1074. m.p.: >300 °C.

1,7-Di(4-methoxyphenyl)-3,5-di(4-nitrophenyl)-4-phenyldithieno[3,4-*b*:3',4'-*d*]phosphole 4-oxide (32e):

A Schlenk flask containing dithienophosphole **31e** (10.0 mg, 0.013 mmol), 4-methoxyphenyl boronate (7.5 mg, 0.032 mmol), Na_2CO_3 (5.4 mg, 0.051 mmol) and $Pd(PPh_3)_4$ (1.5 mg, 1.3 µmol) was flushed argon and then THF (1.6 mL) and water (0.8 mL) were added. After stirring for 16 h at 70 °C, the mixture was cooled to room temperature and diluted with $CHCl_3$, dried over Na_2SO_4 and concentrated in vacuo. The crude product was purified by silica-gel column chromatography (eluent: $CHCl_3$) to give dithienophospholes **32e** (8.1 mg, 0.011 mmol, 85%).
^{1}H NMR (395.88 MHz, CD_2Cl_2, 25 °C): δ = 8.19 (d, J = 8.7 Hz, 4H), 8.11 (d, J = 8.7 Hz, 4H), 7.69–7.60 (m, 2H), 7.40–7.32 (m, 1H), 7.30–7.23 (m, 2H), 6.98 (d, J = 8.7 Hz, 4H), 6.44 (d, J = 8.7 Hz, 4H) and 3.76 (s, 6H) ppm; ^{13}C NMR (100.40 MHz, CD_2Cl_2, 25 °C): δ = 160.6, 147.9, 146.8 (d, J = 9.6 Hz), 140.9 (d, J = 105 Hz), 139.1 (d, J = 12.5 Hz), 138.8, 136.3 (d, J = 20.2 Hz), 132.8, 131.6 (d, J = 10.6 Hz), 130.3 (d, J = 111 Hz), 129.9, 129.0 (d, J = 13.5 Hz), 128.8, 125.2, 124.5, 113.6 and 55.4 ppm; ^{31}P NMR (161.7 MHz, $CDCl_3$, 25 °C): δ = 10.6 ppm. UV/vis (CH_2Cl_2): λ (ε, M^{-1} cm^{-1}) = 259 (35600), 294 (32700), 320 (31000), and 376 (26800) nm. Fluorescence (CH_2Cl_2, λ_{ex} = 400 nm): λ_{max} = 629 nm. FT-IR (ATR): ν = 1501 (NO_2), 1177 (P=O), and 1024 (C–O–C) cm^{-1}. HRMS (ESI, positive) calcd. for $C_{40}H_{28}N_2O_7PS_2$ [M+H]$^+$ 743.1070; found 743.1069. m.p.: >300 °C.

Chapter 3

1,4-Diboromo-2,5-bis(pinacolatoboryl)benzene: [91]

To a solution of 1,4-dibromobenzene (3.00 g, 12.7 mmol) in degassed cyclohexane (63.6 mL) was added $(Bpin)_2$ (8.06 g, 31.7 mmol) and $[Ir(cod)OMe]_2$ (84.2 mg, 0.127 mmol). After stirring for 4 h at 85 ºC, the mixture was cooled to ambient temperature and filtered. The residue was washed with hexane to afford 1,4-dibromo-2,5-bis(pinacolatoboryl)benzene as a white powder (4.94 g, 10.1 mmol, 80 % yield).

^{1}H NMR (395.88 MHz, $CDCl_3$, 25 °C): δ = 7.74 (s, 2H) and 1.37 (s, 24H) ppm.

1,4-Dibromo-2,5-bis(3-bromothiophen-2-yl)benzene (37): [92]

A 300 mL round flask containing 1,4-dibromo-2,5-bis(pinacolatoboryl)benzene (5.00 g, 10.2 mmol) Na_2CO_3 (5.43 g, 51.2 mmol) and $Pd(PPh_3)_4$ (1.18 g, 1.02 mmol) was flushed argon and then THF (125 mL), water (62.5 mL) and 2,3-dibromothiophene (2.55 mL, 22.5 mmol) were added. After stirring for 24 h at 70 ºC, the mixture was cooled to room temperature and extracted with $CHCl_3$ (50 mL × 2). The organic layer was washed with brine, dried over Na_2SO_4 and concentrated in vacuo. The crude product was added chloroform (5 mL) and filtered. The residue was washed with cooled chloroform to afford thienylbenzene **37** as a white solid (2.67 g, 4.79mmol, 49% yield).

^{1}H NMR (395.88 MHz, $CDCl_3$, 25 °C): δ = 7.71 (s, 2H), 7.42 (d, J = 5.2 Hz, 2H) and 7.09 (d, J = 5.2 Hz, 2H) ppm.

Doubly thiophene-fused benzodiphospholes (*trans*-33 and *cis*-33):

A solution of thienylbenzene **37** (50.0 mg, 0.0896 mmol) in THF (2 mL) was added dropwisely to a solution of *n*-BuLi (1.55 M in hexane, 0.243 mL, 0.376 mmol) in THF (1.8 mL) at –78 ºC. After stirring for 1 h at –78 ºC, dichlorophenylphosphine (26.7 µL, 0.197 mmol) was added slowly and stirred for 1 h at –78 ºC. The mixture was allowed to warm to ambient temperature and then aqueous solution of hydrogen peroxide (30% in water, 1 mL) was added. After stirring for 30 min, the reaction was quenched with water and extracted with chloroform (10 mL × 3). The combined organic layer was dried over Na_2SO_4 and concentrated in vacuo. The crude product was purified by column chromatography (eluent: chloroform) to give ***trans*-33** as a light yellow solid (7.2 mg, 14.8 µmol, 17% yield) and ***cis*-33** as a light yellow solid (7.7 mg, 15.8 µmol, 18% yield). Single crystals suitable for X-ray crystallographic analysis were obtained by vapor diffusion of *n*-hexane into $CHCl_3$ solutions of ***trans*-33** or ***cis*-33**.

***trans*-33:** ^{1}H NMR (395.88 MHz, $CDCl_3$, 25 °C): δ = 7.77 (q, J = 7.2 Hz, 4H), 7.68 (dd, J = 2.8, 11.2 Hz, 2H), 7.54 (m, 2H), 7.44 (m, 6H) and 7.20 (q, J = 2.8 Hz, 2H) ppm; ^{13}C NMR (100.40 MHz, $CDCl_3$, 25 °C): δ = 152.8 (d, J = 26.0 Hz), 142.1 (d, J = 107 Hz), 137.8 (t, J = 15.5 Hz), 136.8, 133.0, 132.0 (d, J = 742 Hz), 131.2 (d, J = 12.4 Hz), 131.0 (d, J = 15.5 Hz), 129.3 (d, J = 15.4 Hz), 126.2 (d, J = 15.4 Hz), and 121.9 (t, J = 9.6 Hz) ppm; ^{31}P NMR (161.7 MHz, $CDCl_3$, 25 °C): δ = 22.9 ppm. UV/Vis (CH_2Cl_2): λ (ε, $M^{-1}cm^{-1}$) = 271 (26300), 331 (12700), 346 (17600), and 404 (8000) nm. Fluorescence (CH_2Cl_2, λ_{ex} = 415 nm): λ_{max} = 481 nm; Φ_F = 0.92.

FT-IR (ATR): ν = 1242 cm^{-1} (P=O). HRMS (APCI, positive) calcd. for $C_{26}H_{16}O_2P_2S_2$ $[M+H]^+$ 487.0140; found 487.0131. m.p.: >280 °C.

***cis*-33:** ^{1}H NMR (395.88 MHz, $CDCl_3$, 25 °C): δ = 7.70 (m, 6H), 7.56 (t, J = 7.2 Hz, 2H), 7.45 (m, 6H) and 7.22 (dd, J = 2.4, 4.8 Hz, 2H) ppm; ^{13}C NMR (100.40 MHz, $CDCl_3$, 25 °C): δ = 153.0 (d, J = 27.9 Hz), 142.1 (d, J = 105 Hz), 137.4 (m), 135.7 (d, J = 110 Hz), 133.0, 131.2 (d, J = 11.6 Hz), 131.0 (d, J = 15.4 Hz), 129.2 (d, J = 107 Hz), 129.2 (d, J = 12.5 Hz), 126.3 (d, J = 14.5 Hz), and 121.8 (t, J = 9.6 Hz) ppm; ^{31}P NMR (161.7 MHz, $CDCl_3$, 25 °C): δ = 22.7 ppm. UV/Vis (CH_2Cl_2): λ (ε, $M^{-1}cm^{-1}$) = 273 (25000), 331 (12000), 346 (17000) and 404 (7600) nm. Fluorescence (CH_2Cl_2, λ_{ex} = 415 nm): λ_{max} = 478 nm; Φ_F = 0.91. FT-IR (ATR): ν = 1172 (P=O) cm^{-1}. HRMS (APCI, positive) calcd. for $C_{26}H_{16}O_2P_2S_2$ $[M+H]^+$ 487.0140; found 487.0141. m.p.: 191–192 °C.

Dibrominated benzodiphosphole 38:

To a solution of ***trans*-33** (100 mg, 0.206 mmol) in $CHCl_3$/AcOH (v/v = 3/2, 3.43 mL) was added *N*-bromosuccinimide (366 mg, 2.06 mmol) and stirred for 24 h at ambient temperature. Then, the reaction was quenched with acetone and extracted with chloroform (10 mL × 3). The organic layer was washed with sat. Na_2CO_3 aq., dried over Na_2SO_4 and concentrated in vacuo. The crude was purified by column chromatography (eluent: chloroform) to give benzodiphosphole **38** as a yellow solid quantitatively.

^{1}H NMR (395.88 MHz, $CDCl_3$, 25 °C): δ = 7.70 (q, J = 6.9 Hz, 4H), 7.61 (t, J = 7.6 Hz, 2H), 7.55 (dd, J = 2.8, 10.4 Hz, 2H), 7.50 (td, J = 3.2, 7.6 Hz, 4H), and 7.16 (d, J = 2.4 Hz, 2H) ppm; ^{13}C NMR (100.40 MHz, $CDCl_3$, 25 °C): δ = 152.4 (d, J = 25.1 Hz), 141.0 (d, J = 107 Hz), 136.5 (d, J = 107 Hz), 133.4, 131.2 (d, J = 11.6 Hz), 129.5 (d, J = 13.5 Hz), 128.6 (d, J = 13.5 Hz), 128.5, 127.1 (d, J = 67.4 Hz), 121.9 (t, J = 10.1 Hz), and 117.9 (d, J = 20.2 Hz) ppm; ^{31}P NMR (161.7 MHz, $CDCl_3$, 25 °C): δ = 24.6 ppm. FT-IR (ATR): ν = 1191 cm^{-1} (P=O). HRMS (ESI, positive) calcd. for $C_{26}H_{14}Br_2O_2P_2S_2$ $[M+H]^+$ 643.8343; found 643.8350. m.p.: >280 °C.

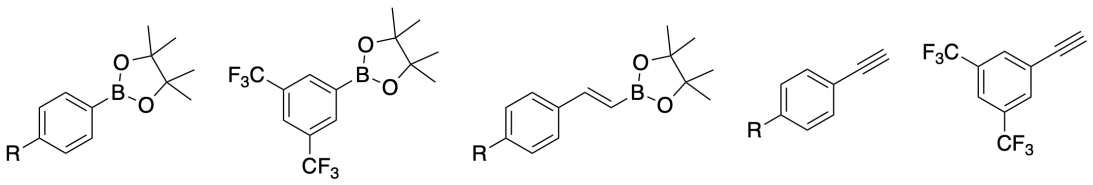

S1a (R = H) **S1b** (R = NMe_2) **S1c** **S2a** (R = H) **S2b** (R = NMe_2) **S3a** (R = H) **S3d** (R = NO_2) **S3c**

Figure 7-1. Structures of arylboronates and arylacetylenes.
Arylboronates **S1a, S1b**[93] and **S2a**[94] were synthesized according to the literatures.

4,4,5,5-Tetramethyl-2-(3,5-bis(trifluoromethyl)phenyl)-1,3,2-dioxaborolane (S1c):[95]

A 50 mL two-neck flask with 1-bromo-3,5-bis(trifluoromethyl)benzene (0.50 mL, 2.95 mmol), bis(pinacolato)diboron (900 mg, 3.54 mmol) and KOAc (869 mg, 8.86 mmol) was flushed with argon and then, DMSO (14.8 mL) and Pd(dppf)Cl_2·CH_2Cl_2 (72.3 mg, 0.0886 mmol) were added. After stirring 3 h at 80 ºC, the reaction mixture was allowed to cool to ambient temperature and added water (100 mL). The mixture was extracted with AcOEt/hexane (v/v =1/4, 30 mL × 3). The organic layer was washed with brine, dried over Na_2SO_4 and concentrated in vacuo. The crude product was purified by silica-gel column chromatography (eluent: AcOEt/hexane = 1/50) to give **S1c** as a white solid (684 mg, 2.01 mmol, 68%).
S1c: ^{1}H NMR (395.88 MHz, $CDCl_3$, 25 °C): δ = 8.23 (bs, 2H), 7.94 (bs, 1H) and 1.37 (s, 12H) ppm.

(*E*)-*N,N*-Dimethylamino-4-(2-(4,4,5,5-tetramethyl-1,3,2-dioxaborolan-2-yl)vinyl)aniline (S2b): [96]

A Schlenk flask containing 4-(dimethylamino)benzylacetylene (180 mg, 1.24 mmol), pinacolborane (0.234 mL, 1.61 mmol), and DIBAL-H (1 M in hexane, 0.124 mL, 0.124 mmol) was heated to 90 ºC. After stirring for 3 h, the mixture was cooled to room temperature and quenched with water. Then, the mixture was extracted with AcOEt (3 times). The organic layer was washed with brine, dried over Na_2SO_4 and concentrated in vacuo. The crude product was purified by silica-gel column chromatography (eluent: AcOEt/Hexane = 1/50) to give **S2b** as a pale yellow oil (131 mg, 0.483 mmol, 39% yield).
S2b: ^{1}H NMR (395.88 MHz, $CDCl_3$, 25 °C): δ = 7.41 (d, J = 8.4 Hz, 2H), 7.35 (d, J = 18.4 Hz, 1H), 6.67 (d, J = 8.4 Hz, 2H), 5.94 (d, J = 18.4 Hz, 1H), 2.96 (s, 6H) and 1.31 (s, 12H) ppm.

3,5-Bis(trifluoromethyl)phenylacetylene (S3c): [97,98]

A two-neck flask containing 3,5-bis(trifluoromethyl)-1-bromobenzene (0.578 mL, 3.41

mmol), $Pd(PPh_3)_2Cl_2$ (69.2 mg, 0.0986 mmol), and CuI (37.6 mg, 0.197 mmol) was flushed argon and then THF (8.5 mL), *N,N*-diisopropylethylamine (2.4 mL) and trimethylsilylacetylene (1.04 mL, 7.51 mmol) were added. After stirring for 15 h at 60 ºC, the mixture was cooled to room temperature and the solvent was removed under reduced pressure. The residue was purified by silica-gel column chromatography (Hexane) to give **TMS-S3c** as a colorless oil (560 mg, 2.35 mmol, 69%).

To a solution of **TMS-S3c** (400 mg, 1.29 mmol) in Et_2O (10 mL) was added KOH (50% in MeOH, 0.1 mL) and stirring for 10 min at ambient temperature. The reaction was quenched with water (100 mL) and extracted with Et_2O (10 mL × 3). The organic layer was washed with brine, dried over Na_2SO_4 and concentrated in vacuo. The crude product was used for next reaction without further purification due to low boiling point.

TMS-S3c: ^{1}H NMR (395.88 MHz, $CDCl_3$, 25 °C): δ = 7.79 (bs, 2H), 7.77 (bs, 1H) and 0.26 (s, 9H) ppm.

S3c: ^{1}H NMR (395.88 MHz, $CDCl_3$, 25 °C): δ = 7.91 (bs, 2H), 7.84 (bs, 1H), 3.26 (s, 1H) ppm.

4-Nitrophenylacetylene (S3d): [99]

A two-neck flask containing 4-iodonitrobenzene (651 mg, 2.61 mmol), $Pd(PPh_3)_2Cl_2$ (73.4 mg, 0.105 mmol) and CuI (10 mg, 0.0523 mmol) was flushed argon and then triethylamine (26 mL) and TMSA (0.542 mL, 3.92 mmol) were added. After stirring for 2 h at ambient temperature, TBAF (1M in THF, 3.92 mL, 3.92 mmol) was added. After stirring for 15 min, the solvent was removed under reduced pressure. The residue was purified by column chromatography (eluent: AcOEt/Hexane = 1/10) to give **S3d** (220 mg, 1.50 mmol, 57%).

S3d: ^{1}H NMR (395.88 MHz, $CDCl_3$, 25 °C): δ = 8.20 (d, J = 9.1 Hz, 2H), 7.64 (d, J = 9.1 Hz, 2H) and 3.36 (s, 1H) ppm.

Phenyl-substituted 34a:

A Schlenk flask containing benzodiphosphole **38** (18.9 mg, 0.0293 mmol), phenyl boronate **S1a** (15.0 mg, 0.0733 mmol), Na_2CO_3 (12.4 mg, 0.117 mmol) and $Pd(PPh_3)_4$ (3.4 mg, 2.93 μmol) was flushed argon and then THF (0.66 mL) and water (0.33 mL) were added. After stirring for 4 h at 70 ºC, the mixture was cooled to room temperature and extracted with $CHCl_3$ (5 mL × 3). The organic layer was washed with brine, dried over Na_2SO_4 and concentrated in vacuo. The crude product was purified by silica-gel column chromatography (eluent: $CHCl_3$) to give **34a** as an orange solid (17.3 mg, 27.1 μmol, 88%). Single crystals suitable for X-ray crystallographic analysis were obtained by vapor diffusion of acetonitrile into a $CHCl_3$ solution

of **34a**.

^{1}H NMR (395.88 MHz, $CDCl_3$, 25 °C): δ = 7.78 (q, J = 7.2 Hz, 4H), 7.66 (dd, J = 3.2, 10.0 Hz, 2H), 7.57 (m, 6H), 7.50 (td, J = 3.2, 8.0 Hz, 6H) and 7.38 (m, 6H) ppm; ^{13}C NMR (100.40 MHz, $CDCl_3$, 25 °C): δ = 151.1, 150.8, 137.8, 133.3, 133.1, 131.3, 131.2, 129.4, 129.35, 129.30, 129.0, 128.3, 126.1, and 121.6 (t, J = 14.4 Hz) ppm; ^{31}P NMR (161.7 MHz, $CDCl_3$, 25 °C): δ = 23.6 ppm. UV/Vis (CH_2Cl_2): λ (ε, $M^{-1}cm^{-1}$) = 286 (27000), 295 (29000), 360 (24500), 374 (27000) and 442 (19000) nm. Fluorescence (CH_2Cl_2, λ_{ex} = 415 nm): λ_{max} = 525 nm; Φ_F = 0.50. FT-IR (ATR): ν = 1207 cm^{-1} (P=O). HRMS (ESI, positive) calcd. for $C_{38}H_{24}O_2P_2S_2$ $[M+H]^+$ 639.0766; found 639.0762. m.p.: >280 °C.

4-Dimethylaminophenyl-substituted 34b:

A Schlenk flask containing benzodiphosphole **38** (30.8 mg, 0.0478 mmol), phenyl boronate **S1b** (29.5 mg, 0.119 mmol), Na_2CO_3 (20.2 mg, 0.191 mmol) and $Pd(PPh_3)_4$ (5.5 mg, 4.78 μmol) was flushed argon and then THF (1.2 mL) and water (0.60 mL) were added. After stirring for 23 h at 70 ºC, the mixture was cooled to room temperature and extracted with $CHCl_3$ (5 mL × 3). The organic layer was washed with brine, dried over Na_2SO_4 and concentrated in vacuo. The crude product was purified by silica-gel column chromatography (eluent: $CHCl_3$) to give **34b** as a dark red solid (23.1 mg, 31.9 μmol, 67%).

^{1}H NMR (395.88 MHz, $C_2D_2Cl_4$, 25 °C): δ = 7.76 (m, 4H), 7.62–7.57 (m, 4H), 7.52–7.48 (m, 4H), 7.45 (d, J = 8.6 Hz, 4H), 7.22 (d, J = 1.8 Hz, 2H), 6.70 (d, J = 9.1 Hz, 4H) and 3.00 (s, 12H) ppm; ^{13}C NMR (100.40 MHz, $C_2D_2Cl_4$, 25 °C): δ = 150.4, 140.7, 137.4, 130.9, 130.8, 129.1, 129.0, 128.2 (d, J = 29.6 Hz), 126.8, 120.7, 120.5, 120.2, 112.1, 99.4, and 40.1 ppm; ^{31}P NMR (161.7 MHz, $CDCl_3$, 25 °C): δ = 23.7 ppm. UV/Vis (CH_2Cl_2): λ (ε, $M^{-1}cm^{-1}$) = 264 (36000), 311 (37000), 401 (43000), and 505 (33000) nm. Fluorescence (CH_2Cl_2, λ_{ex} = 415 nm): λ_{max} = 650 nm; Φ_F = 0.51. FT-IR (ATR): ν = 1180 (P=O), 1113 (N–C) cm^{-1}. HRMS (ESI, positive) calcd. for $C_{42}H_{34}N_2O_2P_2S_2$ $[M+H]^+$ 725.1610; found 725.1603. m.p.: >300 °C.

3,5-Bis(trifluoromethyl)phenyl-substituted 34c:

A Schlenk flask containing benzodiphosphole **38** (19.0 mg, 0.0295 mmol), phenyl boronate **S1c** (25.0 mg, 0.0737 mmol), Na_2CO_3 (12.5 mg, 0.118 mmol) and $Pd(PPh_3)_4$ (3.4 mg, 2.95 μmol) was flushed argon and then THF (1.2 mL) and water (0.60 mL) were added. After stirring for 18 h at 70 ºC, the mixture was cooled to room temperature and extracted with $CHCl_3$ (5 mL × 3). The organic layer was washed with brine, dried over Na_2SO_4 and concentrated in vacuo. The crude product was purified by silica-gel column chromatography (eluent: $CHCl_3$) to

give **34c** as a dark red solid (18.6 mg, 20.4 μmol, 69%).

^{1}H NMR (395.88 MHz, $CDCl_3$, 25 °C): δ = 7.96 (bs, 4H), 7.83 (bs, 2H), 7.77 (m, 4H), 7.71 (m, 2H), 7.63 (m, 2H), and 7.55–7.49 (m, 6H) ppm; ^{31}P NMR (161.7 MHz, $CDCl_3$, 25 °C): δ = 23.1 ppm. UV/Vis (CH_2Cl_2): λ (ε, $M^{-1}cm^{-1}$) = 297 (35000), 361 (29000), 373 (34000), 434 (27000), and 456(sh) (22000) nm. Fluorescence (CH_2Cl_2, λ_{ex} = 415 nm): λ_{max} = 496, 514 nm; Φ_F = 0.28. FT-IR (ATR): ν = 1276 (P=O), 1135 (C–F) cm^{-1}. HRMS (ESI, positive) calcd. for $C_{42}H_{20}F_{12}O_2P_2S_2$ $[M+H]^+$ 911.0261; found 911.0248. m.p.: >300 °C. **Due to low solubility, we could not obtain the ^{13}C NMR spectrum with a sufficient S/N ratio.**

Styryl-substituted benzodiphosphole 35a:

Mizoroki-Heck Reaction: A Schlenk flask containing $Pd(OAc)_2$ (0.7 mg, 3.1 μmol) and XPhos (3.0 mg, 6.2 μmol) was flushed argon and DMF (1.0 mL) was added. After stirring 30 min at ambient temperature, benzodiphosphole **38** (20.0 mg, 0.031 mmol), styrene (14.2 μL, 0.124 mmol) and NEt_3 (10.8 μL, 0.0775 mmol) were added. After stirring for 20 h at 110 ºC, the mixture was cooled to room temperature. Water was added to the mixture and the mixture was extracted with $CHCl_3$ (5 mL × 3). The organic layer was washed with brine, dried over Na_2SO_4 and concentrated in vacuo. The crude product was purified by silica-gel column chromatography (eluent: $CHCl_3$) to give styryl-substituted **35a** as a red solid (5.7 mg, 8.25 μmol, 27%).

Suzuki-Miyaura coupling: A Schlenk flask containing benzodiphosphole **38** (21.2 mg, 0.0329 mmol), styryl boronate **S2a** (18.9 mg, 0.0823 mmol), Na_2CO_3 (13.9 mg, 0.132 mmol) and $Pd(PPh_3)_4$ (3.8 mg, 3.29 μmol) was flushed argon and then THF (0.66 mL) and water (0.33 mL) were added. After stirring for 3 h at 70 ºC, the mixture was cooled to room temperature and extracted with $CHCl_3$ (5 mL × 3). The organic layer was washed with brine, dried over Na_2SO_4 and concentrated in vacuo. The crude product was purified by silica-gel column chromatography (eluent: $CHCl_3$) to give styryl-substituted **35a** as a red solid (14.6 mg, 21.1 μmol, 65%).

^{1}H NMR (395.88 MHz, CD_2Cl_2, 25 °C): δ = 7.74 (q, J = 6.4 Hz, 4H), 7.65 (dd, J = 7.3, 2.7 Hz, 2H), 7.60 (t, J = 6.4 Hz, 2H), 7.5 (m, 8H), 7.3 (m, 6H), 7.21 (d, J = 16.0 Hz, 2H), 7.15 (d, J = 1.8 Hz, 2H) and 7.01 (d, J = 16.0 Hz, 2H) ppm; ^{31}P NMR (161.7 MHz, CD_2Cl_2, 25 °C): δ = 22.0 ppm. UV/Vis (CH_2Cl_2): λ (ε, $M^{-1}cm^{-1}$) = 295 (15000), 306 (19000), 380 (17600), 396 (18000) and 470 (15000) nm. Fluorescence (CH_2Cl_2, λ_{ex} = 415 nm): λ_{max} = 558 nm; Φ_F = 0.27. FT-IR (ATR): ν = 1169 (P=O) cm^{-1}. HRMS (ESI, positive) calcd. for $C_{42}H_{28}O_2P_2S_2$ $[M+H]^+$ 691.1079; found 691.1072. m.p.: >280 °C. **Due to low solubility, we could not obtain the ^{13}C NMR**

spectrum with a sufficient S/N ratio.

4-Dimethylaminostyryl-substituted benzodiphosphole 35b:

A Schlenk flask containing benzodiphosphole **38** (23.4 mg, 0.0363 mmol), 4-dimethylaminostyryl boronate **S2b** (24.8 mg, 0.0908 mmol), Na_2CO_3 (15.4 mg, 0.145 mmol) and $Pd(PPh_3)_4$ (4.2 mg, 3.63 μmol) was flushed argon and then THF (0.81 mL) and water (0.40 mL) were added. After stirring for 3 h at 70 ºC, the mixture was cooled to room temperature and extracted with $CHCl_3$ (5 mL × 3). The organic layer was washed with brine, dried over Na_2SO_4 and concentrated in vacuo. The crude product was purified by silica-gel column chromatography (eluent: $CHCl_3$) to give 4-dimethylaminostyryl-substituted **35b** as a dark red solid (22.0 mg, 28.3 μmol, 78%).

^{1}H NMR (395.88 MHz, $CDCl_3$, 25 °C): δ = 7.75 (m, 4H), 7.52 (m, 8H), 7.34 (d, J = 9.2 Hz, 4H), 7.01 (d, J = 2.4 Hz, 2H), 6.91 (d, J = 6.0 Hz, 4H) and 6.68 (d, J = 8.4 Hz, 4H) ppm; ^{31}P NMR (161.7 MHz, $CDCl_3$, 25 °C): δ = 23.5 ppm. UV/Vis (CH_2Cl_2): λ (ε, $M^{-1}cm^{-1}$) = 330 (24000), 420 (40000) and 520 (37000) nm. Fluorescence (CH_2Cl_2, λ_{ex} = 415 nm): λ_{max} = 699 nm; Φ_F = 0.22. FT-IR (ATR): ν = 1258 (P=O), 1165 (NMe_2) cm^{-1}. HRMS (APCI, positive) calcd. for $C_{46}H_{38}N_2O_2P_2S_2$ $[M+H]^+$ 777.1923; found 777.1922. m.p.: >280 °C. **Due to low solubility, we could not obtain the ^{13}C NMR spectrum with a sufficient S/N ratio.**

Typical procedure of Sonogashira coupling with arylacetylenes:

A Schlenk flask containing benzodiphosphole **38** (19.7 mg, 0.0306 mmol), CuI (0.3 mg, 1.5 μmol) and $Pd(PPh_3)_4$ (1.8 mg, 1.5 μmol) was flushed argon and then toluene (1.1 mL), triethylamine (0.5 mL) and arylacetylene **S3** (0.0673 mmol, 2.2 equiv.) were added. After stirring for 30 min at ambient temperature, the mixture was stirred for 4 h at 60 ºC. The mixture was cooled to room temperature, and water was added to the mixture. Then the mixture was extracted with $CHCl_3$ (10 mL × 3). The organic layer was washed with brine, dried over Na_2SO_4 and concentrated in vacuo. The crude product was purified by silica-gel column chromatography (eluent: $CHCl_3$) to give ethynyl-substituted **36**.

Phenylethynyl-substituted benzodiphosphole 36a:

A orange solid (18.9 mg, 26.3 μmol, 86%). Single crystals suitable for X-ray crystallographic analysis were obtained by vapor diffusion of acetonitrile into a $CHCl_3$ solution of **36a**.

^{1}H NMR (395.88 MHz, $CDCl_3$, 25 °C): δ = 7.73 (m, 4H), 7.62 (m, 4H), 7.5 (m, 8H), 7.36 (m, 6H) and 7.31 (d, J = 2.8 Hz, 2H) ppm; ^{13}C NMR (100.40 MHz, $CDCl_3$, 25 °C): δ = 152.1 (d, J =

25.1 Hz), 138.1, 137.0, 133.3, 131.7, 131.3, 131.1, 130.4, 130.3, 129.5, 129.4, 129.3, 128.7, 127.8, 122.1, 122.0, 99.6 ppm; ^{31}P NMR (161.7 MHz, $CDCl_3$, 25 °C): δ = 23.1 ppm. UV/Vis (CH_2Cl_2): λ (ε, $M^{-1}cm^{-1}$) = 292 (36500), 300 (39000), 365 (35000), 379 (39000) and 445 (30000) nm. Fluorescence (CH_2Cl_2, λ_{ex} = 415 nm): λ_{max} = 520 nm; Φ_F = 0.37. FT-IR (ATR): ν = 1197 (P=O) cm^{-1}. HRMS (ESI, positive) calcd. for $C_{42}H_{24}O_2P_2S_2$ $[M+Na]^+$ 709.0585; found 709.0577. m.p.: >280 °C.

3,5-Bis(trifluoromethyl)phenylethynyl-substituted benzodiphosphole 36c:

An orange solid (9.4 mg, 9.79 µmol, 32%).

^{1}H NMR (395.88 MHz, $CDCl_3$, 25 °C): δ = 7.94 (bs, 4H), 7.85 (bs, 2H), 7.74 (m, 4H), 7.68 (dd, J = 2.7, 10.0 Hz, 2H), 7.63 (m, 2H), 7.52 (m, 4H) and 7.40 (d, J = 2.7 Hz, 2H) ppm; ^{31}P NMR (161.7 MHz, $CDCl_3$, 25 °C): δ = 22.8 ppm. UV/Vis (CH_2Cl_2): λ (ε, $M^{-1}cm^{-1}$) = 291(sh) (26500), 302 (32000), 365(sh) (28500), 381 (36000), 439 (30000) and 460(sh) (27000) nm. Fluorescence (CH_2Cl_2, λ_{ex} = 415 nm): λ_{max} = 501, 520 nm; Φ_F = 0.34. FT-IR (ATR): ν = 1275 (P=O), 1080 (C–F) cm^{-1}. HRMS (APCI, positive) calcd. for $C_{46}H_{20}F_{12}O_2P_2S_2$ $[M+H]^+$ 959.0261; found 959.0269. m.p.: >280 °C. Due to low solubility, we could not obtain the ^{13}C NMR spectrum with a sufficient S/N ratio.

4-Nitrophenylethynyl-substituted benzodiphosphole 36d:

An orange solid (8.3 mg, 10.7 µmol, 35%).

^{1}H NMR (395.88 MHz, $CDCl_3$, 25 °C): δ = 8.22 (d, J = 9.2 Hz, 4H), 7.75-7.60 (m, 12H), 7.51 (m, 4H) and 7.39 (d, J = 2.3 Hz, 2H) ppm; ^{31}P NMR (161.7 MHz, $CDCl_3$, 25 °C): δ = 22.8 ppm. UV/Vis (CH_2Cl_2): λ (ε, $M^{-1}cm^{-1}$) = 296 (29500), 378(sh) (29500), 396 (34000), 447 (42000) and 469(sh) (36000) nm. Fluorescence (CH_2Cl_2, λ_{ex} = 415 nm): λ_{max} = 505, 532 nm; Φ_F = 0.30. FT-IR (ATR): ν = 1177 (P=O), 1515 (NO_2) cm^{-1}. HRMS (APCI, positive) calcd. for $C_{42}H_{22}N_2O_6P_2S_2$ $[M+H]^+$ 777.0467; found 777.0470. m.p.: >280 °C. **Due to low solubility, we could not obtain the ^{13}C NMR spectrum with a sufficient S/N ratio.**

Chapter 4

2,6-Dibromo-3,7-naphthalenedibronic acid (42):

To a solution of 2,2,6,6-tetramethylpiperidine (2.53 mL, 14.9 mmol) in THF (8.5 mL) was added dropwise *n*-BuLi (2.80 M in hexane, 5.31 mL, 14.9 mmol) at 0 ºC. After stirring for 30 min, the mixture was cooled to –78 ºC and triisopropylborate (4.09 mL, 17.8 mmol) was slowly

added to the mixture. After 10 min, a solution of 2,6-dibromonaphthalene (850 mg, 2.97 mmol) in THF (10 mL) was added dropwise to the reaction mixture. The mixture was stirred for 17 h while slowly warming to room temperature. The reaction was quenched with 1 M HCl aq. (65 mL) and stirred for 10 min. The mixture was extracted with NaOH aq. and then basic extracts were acidified with HCl aq. The precipitation was collected by filtration to afford the boronic acid **42** as a brown solid (528 mg, 1.41 mmol, 48%).

^{1}H NMR (395.88 MHz, $(CD_3)_2SO$, 25 °C): δ = 8.45 (bs, 4H), 8.16 (s, 2H) and 7.85 (s, 2H) ppm; ^{13}C NMR (100.40 MHz, $(CD_3)_2SO$, 25 °C): δ = 139.5, 132.1, 132.0, 129.2 and 123.0 ppm. FT-IR (ATR): ν = 3298 (br, OH) cm^{-1}. HRMS (ESI, negative) calcd. for $C_{10}H_8B_2Br_2O_4$ $[M–H]^-$ 372.9074; found 372.8882. m.p.: > 300 °C.

2,6-Dibromo-3,7-naphthalenediboronate 43:

To a solution of naphthaleneboronic acid **42** (424 mg, 1.13 mmol) in acetone (2.27 mL) was added pinacol (536 mg, 4.54 mmol) and the resultant mixture was stirred for 2 h. The solvent was removed *in vacuo* and the residue was washed with hexane to afford boronate **43** as a white solid (260 mg, 0.483 mmol, 43%).

^{1}H NMR (395.88 MHz, $CDCl_3$, 25 °C): δ = 8.02 (s, 2H) and 8.01 (s, 2H) ppm; ^{13}C NMR (100.40 MHz, $CDCl_3$, 25 °C): δ = 136.2, 133.2, 131.2, 128.3, 124.2, 84.7 and 25.0 ppm. FT-IR (ATR): ν = 1362 (B–O) cm^{-1}. HRMS (ESI, positive) calcd. for $C_{22}H_{28}B_2Br_2O_4$ $[M+Na]^+$ 561.0412; found 561.0413. m.p.: > 300 °C.

2,6-Dibromo-3,7-bis(3-bromothien-2-yl)naphthalene (44):

A Schlenk flask containing diboronate **43** (250 mg, 0.465 mmol), Na_2CO_3 (197 mg, 1.86 mmol), and $Pd(PPh_3)_4$ (53 mg, 0.0465 mmol) was flushed argon and then THF (3.0 mL), water (1.5 mL), and 2,3-dibromothiophene (0.131 mL, 1.16 mmol) were added. After stirring for 24 h at 70 ºC, the mixture was cooled to room temperature and extracted with $CHCl_3$ (10 mL × 2). The organic layer was washed with brine, dried over Na_2SO_4 and concentrated *in vacuo*. To the crude product was added chloroform (5 mL) and the product was filtered. The solid was washed with cold chloroform to afford bisthienylnaphthalene **44** as a white solid (96.5 mg, 0.159 mmol, 34% yield).

^{1}H NMR (395.88 MHz, $CDCl_3$, 25 °C): δ = 8.19 (s, 2H), 7.86 (s, 2H), 7.43 (d, J = 5.2 Hz, 2H) and 7.11 (d, J = 5.2 Hz, 2H) ppm; ^{13}C NMR (100.40 MHz, $CDCl_3$, 25 °C): δ = 136.5, 133.3, 132.7, 131.8, 131.2, 130.4, 126.6, 123.3 and 111.9 ppm. FT-IR (ATR): ν = 697, 714, 799, 859, 865, 888, 910, 1026, 1079, 1149, 1219, 1340, 1436, 1460, 1514, 1584 and 3108 cm^{-1}. HRMS

(APCI, positive) calcd. for $C_{18}H_8Br_4S_2$ $[M]^{\bullet+}$ 603.6795; found 603.6799. m.p.: 245–246 °C.

Naphthodiphosphole 39-*trans* and 39-*cis*:

A solution of bisthienylnaphthalene **45** (50 mg, 0.0822 mmol) in THF (0.50 mL) was added dropwise to a solution of *n*-BuLi (2.80 M in hexane, 0.123 mL, 0.345 mmol) in THF (1.0 mL) at –78 ºC. After stirring for 1 h at –78 ºC, dichlorophenylphosphine (24.5 µL, 0.181 mmol) was added slowly and stirred for 1 h at –78 ºC. The mixture was allowed to warm to room temperature and then 30% aqueous solution of hydrogen peroxide (1 mL) was added to the mixture. After stirring for 30 min, water was added and the mixture was extracted with chloroform (5 mL × 3). The combined organic layer was dried over Na_2SO_4 and concentrated *in vacuo*. The crude product was purified by column chromatography (eluent: chloroform/acetone = 5/1) to afford **39-*trans*** as a pale yellow solid (8.5 mg, 0.0158 mmol, 19%) and **39-*cis*** as pale yellow solid (9.1 mg, 0.0170 mmol, 21%). Single crystals suitable for X-ray crystallographic analysis were obtained by vapor diffusion of methanol into a $CHCl_3$ solution of **39-*trans***.

39-*trans*: ^{1}H NMR (395.88 MHz, CD_2Cl_2, 25 °C): δ = 8.05 (d, J = 11.9 Hz, 2H), 7.82 (d, J = 3.2 Hz, 2H), 7.72–7.64 (m, 4H), 7.56–7.47 (m, 4H), 7.46–7.39 (m, 4H) and 7.22 (dd, J = 2.7, 5.0 Hz, 2H) ppm; ^{31}P NMR (161.7 MHz, $CDCl_3$, 25 °C): δ = 22.8 ppm. UV/vis (CH_2Cl_2): λ (ε, M^{-1} cm^{-1}) = 294 (48000), 307 (19000), 350 (32000), 367 (42000), 393 (6200) and 413 (3000) nm. Fluorescence (CH_2Cl_2, λ_{ex} = 367 nm): λ_{max} = 431 and 452 nm; Φ_F = 0.06. FT-IR (ATR): ν = 1201 (P=O) cm^{-1}. HRMS (APCI, positive) calcd. for $C_{30}H_{18}O_2P_2S_2$ $[M+H]^+$ 537.0296; found 537.0297. m.p.: >300 °C.

Due to low solubility, we could not obtain the ^{13}C NMR spectrum with a sufficient S/N ratio.

39-*cis*: ^{1}H NMR (395.88 MHz, CD_2Cl_2, 25 °C): δ = 8.04 (d, J = 11.9 Hz, 2H), 7.80 (d, J = 3.2 Hz, 2H), 7.69–7.61 (m, 4H), 7.54–7.46 (m, 4H), 7.43–7.36 (m, 4H) and 7.24–7.20 (m, 2H) ppm; ^{31}P NMR (161.7 MHz, $CDCl_3$, 25 °C): δ = 22.5 ppm. UV/vis (CH_2Cl_2): λ (ε, M^{-1} cm^{-1}) = 294 (45000), 307 (17500), 350 (30800), 367 (40200), 393 (5900) and 413 (2800) nm. Fluorescence (CH_2Cl_2, λ_{ex} = 367 nm): λ_{max} = 431 and 452 nm; Φ_F = 0.04. FT-IR (ATR): ν = 1201 (P=O) cm^{-1}. HRMS (APCI, positive) calcd. for $C_{30}H_{18}O_2P_2S_2$ $[M+H]^+$ 537.0296; found 537.0299. m.p.: >230 °C (decomp.).

Due to low solubility, we could not obtain the ^{13}C NMR spectrum with a sufficient S/N ratio.

2,6-(pinB)$_2$naphthalene 45:[100]

A two-neck flask containing 2,6-dibromonaphthalene (605 mg, 2.12 mmol), bis(pinacolato)diborone (1.18 g, 4.65 mmol) and potassium acetate (910 mg, 9.27 mmol) was flushed argon, and then DMSO (10.4 mL) and Pd(dppf)Cl_2 (68.2 mg, 0.0932 mmol) were added. After stirring for 2 h at 80 ºC, the mixture was allowed to cool to room temperature and water (50 mL) was added to the mixture. The product was extracted with AcOEt/hexane (v/v = 1/4, 30 mL × 3), and the organic layer was dried over with Na_2SO_4 and concentrated *in vacuo*. The residue was washed with cold hexane to afford 2,6-(pinB)$_2$naphthalene **45** (578 mg, 1.52 mmol, 72%) as a white solid.

^{1}H NMR (395.88 MHz, $CDCl_3$, 25 °C): δ = 8.35 (s, 2H), 7.86 (d, J = 8.2 Hz, 2H), 7.82 (d, J = 8.2 Hz, 2H) and 1.39 (s, 24H) ppm.

2,6-Bis(3-bromothiophen-2-yl)naphthalene (46):

A two-neck flask containing 2,6-(pinB)$_2$naphthalene **45** (447 mg, 1.18 mmol) and K_3PO_4 (1.01 g, 4.70 mmol) was flushed argon, and then THF (12 mL), H_2O (3.0 mL) and 2,3-dibromothiophene (0.532 mL, 4.70 mmol) were added. After adding $Pd(PPh_3)_4$ (134 mg, 0.118 mmol), the mixture was stirred for 22 h at 70 ºC. The mixture was allowed to cool to room temperature and extracted with chloroform (10 mL × 2). The organic layer was washed with brine, dried over with Na_2SO_4 and concentrated *in vacuo*. To the crude product was added chloroform (3 mL) and the product was filtered. The solid was washed with small amount of cold chloroform to afford 2,6-bis(3-bromothiophen-2-yl)naphthalene (**46**) as a white solid (248 mg, 0.551 mmol, 47%).

^{1}H NMR (395.88 MHz, $CDCl_3$, 25 °C): δ = 8.15 (s, 2H), 7.94 (d, J = 8.4 Hz, 2H), 7.81 (d, J = 8.4 Hz, 2H), 7.35 (d, J = 5.4 Hz, 2H) and 7.11 (d, J = 5.4 Hz, 2H) ppm; ^{13}C NMR (100.40 MHz, $CDCl_3$, 25 °C): δ = 138.2, 132.7, 132.0, 131.1, 128.6, 128.2, 127.6, 125.6, and 108.2 ppm. FT-IR (ATR): ν = 604, 665, 678, 698, 806, 819, 839, 867, 895, 1082, 1129, 1146, 1171, 1272, 1329, 1343, 1360, 1440, 1484, 1520, 1600, 1743, 1787, 1917, 3049, 3081 and 3102 cm^{-1}. HRMS (APCI, positive) calcd. for $C_{18}H_{10}Br_2S_2$ $[M+H]^+$ 448.8663; found 448.8661. m.p.: 181–182 °C.

2,6-(3-Phenylphosphorylthiophen-2-yl)naphthalene (47):

To a solution of thienylnaphthalene **46** (150 mg, 0.333 mmol) in THF (15 mL) was slowly added *t*-BuLi (0.869 mL, 1.40 mmol, 1.61 M solution in pentane) at –78 ºC (dry ice/acetone bath). After stirring for 1 h, $PhPCl_2$ was added (99.3 μL, 0.733 mmol) and stirred for 30 min at –

78 ºC. The mixture was allowed to warm to room temperature and water (5 mL) was added to the mixture. After stirring for 30 min, the mixture was extracted with chloroform (10 mL × 3). The organic layer was washed with brine, dried over with Na_2SO_4 and concentrated *in vacuo*. The residue was purified by silica-gel column chromatography (eluent: chloroform/acetone = 10/1) and reprecipitated from chloroform/hexane to afford naphthalene **47** as a white solid (88.0 mg, 0.163 mmol, 49%).

^{1}H NMR (395.88 MHz, $(CD_3)_2CO$, 25 °C): δ = 8.30 (s, 2H), 8.05 (d, J = 490 Hz, 2H), 8.02 (d, J = 8.2 Hz, 2H), 7.87 (dd, J = 1.6, 8.2 Hz, 2H), 7.74 (dd, J = 1.8, 5.5 Hz, 2H) 7.69–7.60 (m, 4H), 7.56–7.49 (m, 2H), 7.48–7.41 (m, 4H) and 7.34 (td, J = 0.91, 5.5 Hz, 2H) ppm; ^{13}C NMR (100.40 MHz, $(CD_3)_2CO$, 25 °C): δ = 153.1 (d, J = 13.5 Hz), 133.8, 133.6, 133.1 (d, J = 1.9 Hz), 132.4 (d, J = 24.1 Hz), 132.3 (d, J = 16.4 Hz), 132.2, 132.1, 131.4 (d, J = 11.6 Hz), 129.8 (d, J = 36.6 Hz), 129.5 (d, J = 3.9 Hz), 128.9 and 128.0 (d, J = 15.4 Hz) ppm; ^{31}P NMR (161.7 MHz, $CDCl_3$, 25 °C): δ = 7.14 ppm. FT-IR (ATR): ν = 2330, 3057 and 3419 cm^{-1}. HRMS (APCI, positive) calcd. for $C_{30}H_{22}O_2P_2S_2$ $[M+H]^+$ 541.0609; found 541.0611. m.p.: 135–136 °C.

Naphthodiphosphole 40-*trans* and 40-*cis*:

To a solution of thienylnaphthalene **47** (24.7 mg, 0.0457 mmol) in toluene (1.0 mL) was added trifluoromethanesulfonic anhydride (18.5 mL, 0.109 mmol) and the reaction mixture was heated to 90 ºC. After stirring for 21 h, the reaction was quenched with sat. $NaHCO_3$ aq. and the mixture was extracted with chloroform (5 mL). The combined organic layer was dried over Na_2SO_4 and concentrated *in vacuo*. The crude product was purified by column chromatography (eluent: chloroform/acetone = 5/1) to afford **40-*trans*** as a pale yellow solid (4.4 mg, 0.00913 mmol, 18%) and **40-*cis*** as a pale yellow solid (2.1 mg, 0.00391 mmol, 17%). Single crystals suitable for X-ray crystallographic analysis were obtained by *n*-heptane into a $C_2H_2Cl_4$ solution of **40-*trans***, or vapor diffusion of acetonitrile into a $CHCl_3$ solution of **40-*cis***.

40-*trans*: ^{1}H NMR (395.88 MHz, CD_2Cl_2, 25 °C): δ = 8.22 (d, J = 8.2 Hz, 2H), 7.76–7.67 (m, 4H), 7.65 (dd, J = 2.7, 8.2 Hz, 2H), 7.56–7.49 (m, 2H), 7.47 (dd, J = 3.2, 4.6 Hz, 2H), 7.42 (td, J = 3.2, 7.3 Hz, 4H) and 7.23 (dd, J = 2.3, 4.6 Hz, 2H) ppm; ^{13}C NMR (100.40 MHz, CD_2Cl_2, 25 °C): δ = 153.2 (d, J = 29.9 Hz), 137.5 (d, J = 20.9 Hz), 137.2, 133.4,133.3 (d, J = 648 Hz) 132.9, 132.6, 131.3, 131.2 (d, J = 11.6 Hz), 130.9 (d, J = 14.5 Hz), 129.4 (d, J = 13.5 Hz), 126.2 (d, J = 15.4 Hz) and 122.1 (d, J = 9.6 Hz) ppm.; ^{31}P NMR (161.7 MHz, $CDCl_3$, 25 °C): δ = 24.6 ppm. UV/vis (CH_2Cl_2): λ (ε, M^{-1} cm^{-1}) = 295 (50000), 307 (89000), 358 (6300), 375 (8700), 420 (11000) and 438 (11000) nm. Fluorescence (CH_2Cl_2, λ_{ex} = 415 nm): λ_{max} = 462 and 486 nm; Φ_F = 0.26. FT-IR (ATR): ν = 1202 (P=O) cm^{-1}. HRMS (APCI, positive) calcd. for

$C_{30}H_{18}O_2P_2S_2$ $[M+H]^+$ 537.0296; found 537.0293. m.p.: >300 °C.

40-*cis*: ^{1}H NMR (395.88 MHz, CD_2Cl_2, 25 °C): δ = 8.25 (d, J = 8.7 Hz, 2H), 7.74–7.62 (m, 6H), 7.54–7.46 (m, 4H), 7.39 (td, J = 3.2, 7.5 Hz, 4H) and 7.24 (dd, J = 2.3, 4.6 Hz, 2H) ppm; ^{13}C NMR (100.40 MHz, CD_2Cl_2, 25 °C): δ = 153.4 (d, J = 29.9 Hz), 137.3 (d, J = 4.8 Hz), 133.6 (d, J = 704 Hz), 132.9, 132.5, 131.3 (d, J = 10.6 Hz), 131.0 (d, J = 15.4 Hz), 129.4 (d, J = 13.5 Hz), 126.3 (d, J = 15.4 Hz) and 122.1 (d, J = 10.6 Hz) ppm.; ^{31}P NMR (161.7 MHz, $CDCl_3$, 25 °C): δ = 24.3 ppm. UV/vis (CH_2Cl_2): λ (ε, $M^{-1}\,cm^{-1}$) = 295 (44600), 307 (77000), 358 (6100), 376 (8400), 419 (10000) and 439 (9600) nm. Fluorescence (CH_2Cl_2, λ_{ex} = 415 nm): λ_{max} = 462 and 485 nm; Φ_F = 0.24. FT-IR (ATR): ν = 1205 (P=O) cm^{-1}. HRMS (APCI, positive) calcd. for $C_{30}H_{18}O_2P_2S_2$ $[M+H]^+$ 537.0296; found 537.0295. m.p.: >300 °C.

1,5-(pinB)$_2$naphthalene 48:[101]

A two-neck flask containing 1,5-dibromonaphthalene (710 mg, 2.48 mmol), bis(pinacolato)diboron (1.39 g, 5.46 mmol) and potassium acetate (1.10 g, 11.2 mmol) was flushed argon, and then DMSO (12.4 mL) and Pd(dppf)Cl_2 (90.8 mg, 0.124 mmol) were added. After stirring for 24 h at 80 ºC, the mixture was allowed to cool to room temperature and water (50 mL) was added to the mixture. The product was extracted with AcOEt/hexane (v/v = 1/4, 30 mL × 3), and the organic layer was dried over with Na_2SO_4 and concentrated *in vacuo*. The residue was purified by silica-gel column chromatography (eluent: AcOEt/hexane = 1/5) to afford 1,5-(pinB)$_2$naphthalene **48** (534 mg, 1.40 mmol, 57%) as a white solid.

^{1}H NMR (395.88 MHz, $CDCl_3$, 25 °C): δ = 8.88 (dd, J = 1.4, 8.2 Hz, 2H), 8.06 (dd, J = 1.4, 6.9 Hz, 2H), 7.51 (dd, J = 6.9, 8.2 Hz, 2H) and 1.42 (s, 24H) ppm.

1,5-Bis(3-bromothiophen-2-yl)naphthalene (49):

A two-neck flask containing 1,5-(pinB)$_2$naphthalene **48** (506 mg, 1.33 mmol) and K_3PO_4 (1.18 g, 5.56 mmol) was flushed argon, and then THF (21.3 mL), H_2O (5.3 mL) and 2,3-dibromothiophene (0.603 mL, 5.32 mmol) were added. After adding $Pd(PPh_3)_4$ (154 mg, 0.133 mmol), the mixture was stirred for 16 h at 70 ºC. The mixture was allowed to cool to room temperature and extracted with chloroform (10 mL × 2). The organic layer was washed with brine, dried over with Na_2SO_4 and concentrated *in vacuo*. The residue was purified by silica-gel column chromatography (eluent: AcOEt/hexane = 1/15) to afford 1,5-bis(3-bromothiophen-2-yl)naphthalene (**49**) as a white solid (366 mg, 0.813 mmol, 61%).

^{1}H NMR (395.88 MHz, $CDCl_3$, 25 °C): δ = 7.85 (dd, J = 1.8, 7.3 Hz, 2H)7.58–7.51 (m, 4H),

7.45 (d, J = 5.2 Hz, 2H) and 7.17 (d, J = 5.2 Hz, 2H) ppm; ^{13}C NMR (100.40 MHz, $CDCl_3$, 25 °C): δ = 136.7, 132.4, 130.8, 130.6, 129.9, 127.7, 126.4, 125.8 and 111.3 ppm. FT-IR (ATR): ν = 540, 571, 623, 668, 712, 730, 753, 788, 860, 1009, 1067, 1087, 1146, 1210, 1338, 1392, 1443, 1497, 1528, 1591 and 3093 cm^{-1}. HRMS (APCI, positive) calcd. for $C_{18}H_{10}Br_2S_2$ $[M]^{\cdot+}$ 447.8585; found 447.8589. m.p.: 191–192 °C.

1,5-Bis(3-phenylphosphorylthiophen-2-yl)naphthalene (50):

To a solution of thienylnaphthalene **49** (75.9 mg, 0.169 mmol) in THF (8.0 mL) was slowly added *t*-BuLi (0.440 mL, 0.708 mmol, 1.61 M solution in pentane) at –78 ºC (dry ice/acetone bath). After stirring for 1 h, $PhPCl_2$ was added (50.3 µL, 0.371 mmol) and stirred for 30 min at –78 ºC. The mixture was allowed to warm to room temperature and water (5 mL) was added to the mixture. After stirring for 30 min, the mixture was extracted with chloroform (10 mL × 3). The organic layer was washed with brine, dried over with Na_2SO_4 and concentrated *in vacuo*. The residue was purified by silica-gel column chromatography (eluent: chloroform/acetone = 10/1) and reprecipitated from chloroform/hexane to afford 1,5-naphthalenylphosphine oxide **50** as a white solid (25.6 mg, 0.0474 mmol, 28%).

***NOTE*: NMR spectra provided two sets of peaks because of the mixture of atropisomers. However, we cannot completely distinguish two sets of peaks due to severe overlapping of peaks in ^{1}H and ^{13}C NMR spectra.**

^{1}H NMR (395.88 MHz, $C_2D_2Cl_4$, 50 °C): δ = 7.64 and 7.62 (P–H, J = 492 Hz, 2H), 7.73–7.62 (m, 4H), 7.55–7.48 (m, 4H), 7.44–7.24 (m, 12H) ppm; ^{13}C NMR (100.40 MHz, $CDCl_3$, 25 °C): δ = 132.7, 132.6, 131.5, 130.5, 130.3, 130.23, 130.19, 129.97, 129.94, 129.8, 129.6, 128.69, 128.65, 127.7, 127.5, 126.00, and 125.94 ppm; ^{31}P NMR (161.7 MHz, $CDCl_3$, 25 °C): δ = 7.41 and 7.33 ppm. FT-IR (ATR): ν = 2354, 3070 and 3409 cm^{-1}. HRMS (APCI, positive) calcd. for $C_{30}H_{22}O_2P_2S_2$ $[M+H]^+$ 541.0609; found 541.0609. m.p.: >220 °C (decomp.).

Naphthodiphosphole 41-*trans* and 41-*cis*:

To a solution of thienylnaphthalene **50** (9.6 mg, 0.0178 mmol) in toluene (1.0 mL) was added trifluoromethanesulfonic anhydride (7.2 µL, 0.0426 mmol) and the reaction mixture was heated to 90 ºC. After stirring for 23 h, the reaction was quenched with sat. $NaHCO_3$ aq. and the mixture was extracted with chloroform (5 mL). The combined organic layer was dried over Na_2SO_4 and concentrated *in vacuo*. The crude product was purified by column chromatography (eluent: chloroform/acetone = 5/1) to afford **41-*trans*** (2.2 mg, 0.00410 mmol, 23%) and **41-*cis*** (2.0 mg, 0.00373 mmol, 21%) as a yellow solid. Single crystals suitable for X-ray

crystallographic analysis were obtained by vapor diffusion of *n*-heptane into a $CHCl_3$ solution of **41-*cis***.

41-*trans*: ^{1}H NMR (395.88 MHz, $CDCl_3$, 25 °C): δ = 8.39 (dd, J = 3.2, 8.2 Hz, 2H), 7.88 (t, J = 8.6 Hz, 2H), 7.80–7.71 (m, 4H), 7.61–7.52 (m, 4H), 7.44 (td, J = 3.2, 7.3 Hz, 4H) and 7.36 (dd, J = 2.7, 5.0 Hz, 2H) ppm; ^{13}C NMR (100.40 MHz, $CDCl_3$, 25 °C): δ = 151.4 (d, J = 29.9 Hz), 137.4 (d, J = 41.4 Hz), 136.7, 136.1, 133.0, 132.2 (d, J = 788 Hz), 131.7 (d, J = 14.5 Hz), 131.2 (d, J = 10.6 Hz), 129.5 (J = 10.6 Hz), 129.2 (d, J = 12.5 Hz), 126.3 (d, J = 9.6 Hz), 126.0 and 125.7 ppm.; ^{31}P NMR (161.7 MHz, $CDCl_3$, 25 °C): δ = 23.0 ppm. UV/vis (CH_2Cl_2): λ (ε, M^{-1} cm^{-1}) = 286 (45800), 294 (43700), 353 (4500), 369 (7200), 424 (8600) and 441 (7900) nm. Fluorescence (CH_2Cl_2, λ_{ex} = 415 nm): λ_{max} = 467 and 488 nm; Φ_F = 0.23. FT-IR (ATR): ν = 1197 (P=O) cm^{-1}. HRMS (APCI, positive) calcd. for $C_{30}H_{18}O_2P_2S_2$ $[M+H]^+$ 537.0296; found 537.0298. m.p.: >300 °C.

41-*cis*: ^{1}H NMR (395.88 MHz, $CDCl_3$, 25 °C): δ = 8.39 (dd, J = 3.2, 8.2 Hz, 2H), 7.88 (t, J = 8.6 Hz, 2H), 7.72 (dd, J = 7.6, 12.8 Hz, 4H), 7.58 (dd, J = 2.7, 5.0 Hz, 2H), 7.53 (t, J = 7.3 Hz, 2H), 7.41 (td, J = 3.2, 7.7 Hz, 4H) and 7.35 (dd, J = 2.3, 5.0 Hz, 2H) ppm; ^{13}C NMR (100.40 MHz, $CDCl_3$, 25 °C): δ = 151.4 (d, J = 29.6 Hz), 137.3 (d, J = 40.1 Hz), 136.7, 136.5 (d, J = 2.9 Hz), 132.8, 132.3 (d, J = 753 Hz), 131.7 (d, J = 14.3 Hz), 131.2 (d, J = 10.5 Hz), 129.4 (d, J = 16.2 Hz), 129.2 (d, J = 13.4 Hz), 126.4 (d, J = 9.5 Hz), 126.0 and 125.9 (d, J = 3.8 Hz) ppm.; ^{31}P NMR (161.7 MHz, $CDCl_3$, 25 °C): δ = 22.7 ppm. UV/vis (CH_2Cl_2): λ (ε, M^{-1} cm^{-1}) = 285 (47600), 295 (45800), 353 (4700), 369 (7600), 424 (9000) and 441 (8300) nm. Fluorescence (CH_2Cl_2, λ_{ex} = 415 nm): λ_{max} = 467 and 487 nm; Φ_F = 0.20. FT-IR (ATR): ν = 1198 (P=O) cm^{-1}. HRMS (APCI, positive) calcd. for $C_{30}H_{18}O_2P_2S_2$ $[M+H]^+$ 537.0296; found 537.0297. m.p.: >300 °C.

Crystal Data

Table 7-1. Crystal data and structure refinement for compounds in Chapter 1 and 2.

	25	**32b**	**32e**
formula	$C_{14}H_7I_2PS_3$	$C_{40}H_{27}N_2O_7PS_2$	$C_{40}H_{27}N_2O_7PS_2 \cdot 0.5(CHCl_3)$
M_r	556.15	742.72	802.41
T [K]	123(2)	153(2)	153(2)
crystal system	monoclinic	monoclinic	triclinic
space group	$P2_1/n$ (No.14)	$P2_1/c$ (No.14)	P-1 (No.2)
a [Å]	8.1778(14)	6.3390(19)	6.440(2)
b [Å]	19.099(3)	27.942(8)	12.046(4)
c [Å]	11.0352(19)	19.134(6)	23.487(9)
a [°]	90	90	88.600(11)
b [°]	110.5706(19)	94.832(6)	88.639(9)
γ [°]	90	90	85.496(18)
V [Å^3]	1613.7(5)	3377.1(18)	1815.4(11)
Z	4	4	2
ρ_{calcd} [g cm^{-3}]	2.289	1.461	1.468
F [000]	1040	1536	826
crystal size [mm^3]	0.30×0.20×0.20	0.30×0.03×0.03	0.30×0.05×0.05
$2\theta_{max}$ [°]	55.00	54.92	51.02
reflections collected	12683	26589	14488
independent reflections	3683	7543	7862
parameters	181	471	507
R_1 [$I > 2s$ (I)]	0.0189	0.0766	0.0538
wR_2 [all data]	0.0400	0.1976	0.1426
GOF	1.016	1.074	1.019
CCDC number	1585540	1969127	1969128

Table 7-2. Crystal data and structure refinement for compounds in Chapter 3.

	***trans*-33**	***cis*-33**	**34a**	**36a**
formula	$C_{26}H_{16}O_2P_2S_2 \cdot 2(water)$	$2(C_{26}H_{16}O_2P_2S_2) \cdot CHCl_3 \cdot 3(water)$	$C_{38}H_{24}O_2P_2S_2$	$0.5(C_{42}H_{24}O_2P_2S_2) \cdot CHCl_3$
M_r	522.48	1140.26	638.63	462.70
T [K]	123(2)	123(2)	93(2)	93(2)
crystal system	orthorhombic	triclinic	monoclinic	triclinic
space group	$Pca2_1$ (No.29)	P-1 (No.2)	$P2_1/a$ (No.14)	P-1 (No.2)
a [Å]	26.069(5)	11.9560(19)	11.7657(15)	7.9275(2)
b [Å]	6.7969(14)	12.4019(18)	13.5469(16)	11.4092(3)
c [Å]	13.384(3)	19.522(4)	18.755(3)	11.9096(3)
α [°]	90	81.589(8)	90	100.993(2)
β [°]	90	87.982(9)	94.238(4)	93.983(2)
γ [°]	90	64.500(6)	90	102.168(2)
V [Å^3]	2371.4(8)	2583.3(8)	2981.2(7)	1026.89(5)
Z	4	2	4	2
ρ_{calcd} [g cm^{-3}]	1.463	1.466	1.423	1.496
F [000]	1080	1164	1312	470
crystal size [mm^3]	0.40×0.10×0.05	0.50×0.50×0.10	0.18×0.15×0.05	0.16×0.07×0.02
$2\theta_{max}$ [°]	54.97	55.00	133.99	133.98
reflections collected	18204	20963	19734	13264
independent reflections	5411	11330	5284	3582
parameters	323	677	397	253
R_1 [$I > 2\sigma(I)$]	0.0506	0.0538	0.0438	0.0498
wR_2 [all data]	0.1287	0.1651	0.1219	0.1375
GOF	1.019	1.015	1.037	1.051
CCDC number	1891464	1891463	1891461	1891462

Table 7-3. Crystal data and structure refinement for compounds in Chapter 4.

	39-*trans*	**40-*trans***	**40-*cis***	**41-*cis***
formula	$0.5(C_{30}H_{18}O_2P_2S_2)\cdot 2(water)$	$0.5(C_{30}H_{18}O_2P_2S_2)\cdot C_2H_2Cl_4$	$C_{30}H_{18}O_2P_2S_2$	$0.5(C_{30}H_{18}O_2P_2S_2)\cdot 0.5(water)$
M_r	268.25	436.09	536.50	277.26
T [K]	153(2)	153(2)	153(2)	153(2)
crystal system	monoclinic	triclinic	monoclinic	orthorhombic
space group	$P2_1/a$ (No.14)	P-1 (No.2)	$P2_1/n$ (No.14)	*Fddd* (No.70)
a [Å]	9.937(5)	7.0282(15)	12.839(5)	8.105(3)
b [Å]	12.080(6)	11.267(2)	8.355(3)	29.815(11)
c [Å]	10.521(5)	12.639(3)	23.324(10)	42.596(16)
α [°]	90	69.655(9)	90	90
β [°]	93.788(7)	78.810(10)	105.443(4)	90
γ [°]	90	77.246(11)	90	90
V [Å^3]	1260.2(11)	907.7(3)	2411.7(17)	10293(7)
Z	4	2	4	32
ρ_{calcd} [g cm^{-3}]	1.414	1.596	1.478	1.431
F [000]	552	440	1104	4576
crystal size [mm^3]	0.20×0.20×0.05	0.10×0.05×0.05	0.30×0.05×0.05	0.30×0.05×0.05
$2\theta_{max}$ [°]	54.93	54.99	55.52	54.96
reflections collected	9965	7402	19072	19770
independent reflections	2836	3974	5588	2947
parameters	163	272	325	172
R_1 [$I > 2\sigma(I)$]	0.0396	0.0432	0.0390	0.0548
wR_2 [all data]	0.0898	0.0976	0.1046	0.1508
GOF	1.018	1.030	1.051	1.029
CCDC number	2036180	2036178	2036181	2036179

References

[1] (a) Clar, E. *Polycyclic Hydrocarbons*; Academic Press: New York, **1964**; Vol. I/II; (b) Clar, E. *The Aromatic Sextet*; Wiley-VCH: London, **1972**; (c) Scholl, R.; Seer, C.; Weitzenbök, R. *Chem. Ber.* **1910**, *43*, 2202. (d) Scholl, R.; Seer, C. *Liebigs Ann. Chem.* **1912**, *394*, 111. (e) Scholl, R.; Seer, C. *Chem. Ber.* **1922**, *55*, 330. (f) Clar, E.; Stewart, D. G. *J. Am. Chem. Soc*. **1953**, *75*, 2667. (g) Clar, E.; Schmidt, W. *Tetrahedron* **1979**, *35*, 2673.

[2] Shirakawa, H.; Louis, E. J.; MacDiarmid, A. G.; Chiang, C. K.; Heeger, A. *J. Chem. Soc. Chem. Commun.* **1977**, *16*, 578.

[3] (a) Kroto, H. W.; Heath, J. R.; O'Brien, S. C.; Curl, R. F.; Smalley, R. E. *Nature* **1985**, *318*, 162; (b) Iijima, S. *Nature* **1991**, *354*, 56; (c) Novoselov, K. S.; Geim, A. K.; Morozov, S. V.; Jiang, D.; Zhang, Y.; Dubonos, S. V.; Grigorieva, I. V.; Firsov, A. A. *Science* **2004**, *306*, 666.

[4] (a) Müller, M.; Ahrens, L.; Brosius, V.; Freudenberg, J.; Bunz, U. H. F. *J. Mater. Chem.* **2019**, *7*, 14011; (b) Dorel, R.; Echavarren, A. M. *J. Org. Chem.* **2017**, 14; (c) Ye, Q.; Chi, C. *Chem. Mater.* **2014**, *26*, 4046; (d) Sun, Z.; Ye, Q.; Chi, C.; Wu, J. *Chem. Soc. Rev.* **2012**, *41*, 7857; (e) Wang, C.; Dong, H.; Hu, W.; Liu, Y.; Zhu, D. *Chem. Rev.* **2012**, *112*, 2208; (f) Anthony, J. E. *Angew. Chem. Int. Ed.* **2008**, *47*, 452; (g) Anthony, J. E. *Chem. Rev.* **2006**, *106* , 5028.

[5] Goldmann, C.; Haas, S.; Krellner, C.; Pernstich, K. P.; Gundlach, D. J.; Batlogg, B. *J. Appl. Phys.* **2004**, *96*, 2080.

[6] (a) de Boer, R. W. I.; Gershenson, M. E.; Morpurgo, A. F.; Podzorov, V. *Physica Status Solidi A Appl. Res.* **2004**, *201*, 1302; (b) Podzorov, V.; Menard, E.; Borissov, A.; Kiryukhin, V.; Rogers, J. A.; Gershenson, M. E. *Phys. Rev. Lett.* **2004**, *93*, 086602; (c) Menard, E.; Podzorov, V.; Hur, S.-H.; Gaur, A.; Gershenson, M. E.; Rogers, J. A. *Adv. Mater.* **2004**, *16*, 2097; (d) da Silva Filho, D. A.; Kim, E.-G.; Brédas, J.-L. *Adv. Mater.* **2005**, *17*, 1072; (e) Takeya, J.; Yamagishi, M.; Tominari, Y.; Hirahara, R.; Nakazawa, Y.; Nishikawa, T.; Kawase, T.; Shimoda, T.; Ogawa, S. *Appl. Phys. Lett.* **2007**, *90*, 102120.

[7] (a) Kelley, T. W.; Muyres, D. V.; Baude, P. F.; Smith, T. P.; Jones, T. D. *Mater. Res. Soc. Symp. Proc.* **2003**, *771*, L6.5.1; (b) Lin, Y.-Y.; Gundlach, D. I.; Nelson, S. F.; Jackson, T. N. *IEEE Trans. Electron Devices* **1997**, *44*, 1325.

[8] Chu, C.-W.; Shao, Y.; Shrotriya, V.; Yang, Y. *Appl. Phys. Lett.* **2005**, *86*, 243506.

[9] Yoo, S.; Domercq, B.; Kippelen, B. *Appl. Phys. Lett.* **2004**, *85*, 5427.

[10] Singh, S.; Jones, W. J.; Siebrand, W.; Stoicheff, B. P.; Schneider, W. G. *J. Chem. Phys.* **1965**, *42*, 330.

[11] Merrifield, R. E.; Avakian, P.; Groff, R. P. *Chem. Phys. Lett.* **1969**, *3*, 386.

[12] (a) Pope, M.; Kallmann, H. P.; Magnante, P. *J. Chem. Phys.* **1963**, *38*, 2042; (b) Helfrich, W.; Schneider, W. G. *Phys. Rev. Lett.* **1965**, *14*, 229; (c) Helfrich, W.; Schneider, W. G. *J. Chem. Phys.* **1966**, *44*, 2902.

[13] (a) Yamaguchi, S.; Tamao, K. *Chem. Lett.* **2005**, *34*, 2; (b) Parke, S. M.; Boone, M. P.; Rivard, E. *Chem. Commun.* **2016**, *52*, 9485; (c) Stępień, M.; Gońka, E.; Żyła, M.; Sprutta, N. *Chem. Rev.* **2017**, *117*, 3479; (d) Jiang, W.; Li, Y.; Wang, Z. *Chem. Soc. Rev.* **2013**, *42*, 6113.

[14] (a) Yuan, J.; Zhang, Y.; Zhou, L.; Zhang, G.; Yip, H.-L.; Lau, T.-K.; Lu, X.; Zhu, C.; Peng, H.; Johnson, P. A.; Leclerc, M.; Cao, Y.; Ulanski, J.; Li, Y.; Zou, Y. *Joule* **2019**, *3*, 1140; (b) Chen, W.; Zhang, Q. *J. Mater. Chem.* **2017**, *5*, 1275; (c) Wang, J.; Liu, K.; Ma, L.; Zhan, X. *Chem. Rev.* **2016**, *116*, 14675; (d) Wu, Y.; Zhu, W.-H.; Zakeeruddin, S. M.; Grätzel, M. *ACS Appl. Mater. Interfaces* **2015**, *7*, 9307; (e) Lu, L.; Zheng, T.; Wu, Q.; Schneider, A. M.; Zhao, D.; Yu, L. *Chem. Rev.* **2015**, *115*, 12666; (f) Umeyama, T.; Imahori, H. *J. Mater. Chem. A Mater. Energy Sustain.* **2014**, *2*, 11545. (g) Park, K. H.; Kim, Y. J.; Lee, G. B.; An, T. K.; Park, C. E.; Kwon, S.-K.; Kim, Y.-H. *Adv. Funct. Mater.* **2015**, *25*, 3991; (h) Kim, Y. J.; Kim, M.-J.; An, T. K.; Kim, Y.-H.; Park, C. E. *Chem. Commun.* **2015**, *51*, 11572.

[15] (a) Takimiya, K.; Shinamura, S.; Osaka, I.; Miyazaki, E. *Adv. Mater.* **2011**, *23*, 4347; (b) Endo, A.; Sato, K.; Yoshimura, K.; Kai, T.; Kawada, A.; Miyazaki, H.; Adachi, C. *Appl. Phys. Lett.* **2011**, *98*, 083302; (c) Kang, B.; Lee, W. H.; Cho, K. *ACS Appl. Mater. Interfaces* **2013**, *5*, 2302; (d) Yang, Z.; Mao, Z.; Xie, Z.; Zhang, Y.; Liu, S.; Zhao, J.; Xu, J.; Chi, Z.; Aldred, M. P. *Chem. Soc. Rev.* **2017**, *46*, 915; (e) Huang, T.; Jiang, W.; Duan, L. *J. Mater. Chem.* **2018**, *6*, 5577; (f) Yin, X.; He, Y.; Wang, X.; Wu, Z.; Pang, E.; Xu, J.; Wang, J.-A. *Front Chem* **2020**, *8*, 725.

[16] (a) Beija, M.; Afonso, C. A. M.; Martinho, J. M. G. *Chem. Soc. Rev.* **2009**, *38*, 2410; (b) Carter, K. P.; Young, A. M.; Palmer, A. E. *Chem. Rev.* **2014**, *114*, 4564; (c) Lavis, L. D.; Raines, R. T. *ACS Chem. Biol.* **2014**, *9*, 855; (d) Ni, Y.; Wu, J. *Org. Biomol. Chem.* **2014**, *12*, 3774; (e) Frath, D.; Massue, J.; Ulrich, G.; Ziessel, R. *Angew. Chem. Int. Ed.* **2014**, *53*, 2290; (f) Gorka, A. P.; Nani, R. R.; Schnermann, M. J. *Org. Biomol. Chem.* **2015**, *13*, 7584.

[17] (a) Andreu, R.; Blesa, M. J.; Carrasquer, L.; Garín, J.; Orduna, J.; Villacampa, B.; Alcalá,

R.; Casado, J.; Ruiz Delgado, M. C.; López Navarrete, J. T.; Allain, M. *J. Am. Chem. Soc.* **2005**, *127*, 8835.; (b) Meier, H. *Angew. Chem. Int. Ed.* **2005**, *44*, 2482; (c) Senge, M. O.; Fazekas, M.; Notaras, E. G. A.; Blau, W. J.; Zawadzka, M.; Locos, O. B.; Ni Mhuircheartaigh, E. M. *Adv. Mater.* **2007**, *19*, 2737; (d) Pawlicki, M.; Collins, H. A.; Denning, R. G.; Anderson, H. L. *Angew. Chem. Int. Ed.* **2009**, *48*, 3244.

[18] Tsumura, A.; Koezuka, H.; Ando, T. *Appl. Phys. Lett.* **1986**, *49*, 1210.

[19] (a) Bao, Z.; Dodabalapur, A.; Lovinger, A. J. *Appl. Phys. Lett.* **1996**, *69*, 4108; (b) Sirringhaus, H.; Tessler, N.; Friend, R. H. *Science* **1998**, *280*, 1741; (c) Dimitrakopoulos, C. D.; Furman, B. K.; Graham, T.; Hegde, S.; Purushothaman, S. *Synth. Met.* **1998**, *92*, 47; (d) Sirringhaus, H.; Brown, P. J.; Friend, R. H.; Nielsen, M. M.; Bechgaard, K.; Langeveld-Voss, B. M. W.; Spiering, A. J. H.; Janssen, R. A. J.; Meijer, E. W.; Herwig, P.; de Leeuw, D. M. *Nature* **1999**, *401*, 685; (e) Dimitrakopoulos, C. D.; Malenfant, P. R. L. *Adv. Mater.* **2002**, *14*, 99.

[20] (a) Gundlach, D. J.; Lin, Y. Y.; Jackson, T. N.; Nelson, S. F.; Schlom, D. G. *IEEE Electron Device Lett.* **1997**, *18*, 87; (b) Lin, Y.-Y.; Gundlach, D. J.; Nelson, S. F.; Jackson, T. N. *IEEE Electron Device Lett.* **1997**, *18*, 606;

[21] Horton, A. W. *J. Org. Chem.* **1949**, *14*, 761.

[22] (a) Košata, B.; Kozmík, V.; Svoboda, J. *Collect. Czechoslov. Chem. Commun.* **2002**, *67*, 645; (b) Košata, B.; Kozmik, V.; Svoboda, J.; Novotná, V.; Vaneˇk, P.; Glogarová, M. *Liq. Cryst.* **2003**, *30*, 603.

[23] (a) Kaszynski, P.; Dougherty, D. A. *J. Org. Chem.* **1993**, *58*, 5209; (b) Méry, S.; Haristoy, D.; Nicoud, J.-F.; Guillon, D.; Diele, S.; Monobe, H.; Shimizu, Y. Bipolar Carrier *J. Mater. Chem.* **2002**, *12*, 37.

[24] Takimiya, K.; Ebata, H.; Sakamoto, K.; Izawa, T.; Otsubo, T.; Kunugi, Y. *J. Am. Chem. Soc.* **2006**, *128*, 12604.

[25] (a) Ebata, H.; Izawa, T.; Miyazaki, E.; Takimiya, K.; Ikeda, M.; Kuwabara, H.; Yui, T. *J. Am. Chem. Soc.* **2007**, *129*, 15732; (b) Izawa, T.; Miyazaki, E.; Takimiya, K. *Adv. Mater.* **2008**, *20*, 3388; (c) Uemura, T.; Hirose, Y.; Uno, M.; Takimiya, K.; Takeya, J. *Appl. Phys. Express.* **2009**, *2*, 111501; (d) Takimiya, K.; Nakano, M.; Sugino, H.; Osaka, I. *Synth. Met.* **2016**, *217*, 68.

[26] Inokuchi, H.; Saitoh, G.; Wu, P.; Seki, K.; Tang, T. B.; Mori, T.; Imaeda, K.; Enoki, T. Higuchi, Y.; Inaka, K.; Yasuoka, N. *Chem. Lett.* **1986**, *15*, 1263.

[27] Yamamoto, T.; Takimiya, K. *J. Am. Chem. Soc.* **2007**, *129*, 2224.

[28] Kang, M. J.; Doi, I.; Mori, H.; Miyazaki, E.; Takimiya, K.; Ikeda, M.; Kuwabara, H. *Adv.*

Mater. **2011**, *23*, 1222.

[29] Nakayama, K.; Hirose, Y.; Soeda, J.; Yoshizumi, M.; Uemura, T.; Uno, M.; Li, W.; Kang, M. J.; Yamagishi, M.; Okada, Y.; Miyazaki, E.; Nakazawa, Y.; Nakao, A.; Takimiya, K.; Takeya, J. *Adv. Mater.* **2011**, *23*, 1626.

[30] (a) Braye, E. H.; Hübel, W. *Chem. Ind. (London)* **1959**, 1250; (b) Leavitt, F. C.; Manuel, T. A.; Johnson, F. *J. Am. Chem. Soc.* **1959**, *81*, 3163.

[31] Quin, L. D.; Bryson, J. G. *J. Am. Chem. Soc.* **1967**, *89*, 5984.

[32] Charrier, C.; Bonnard, H.; de Lauzon, G.; Mathey, F. *J. Am. Chem. Soc.* **1983**, *105*, 6871.

[33] Mathey, F. *Chem. Rev.* **1988**, *88*, 429.

[34] Hay, C.; Fischmeister, C.; Hissler, M.; Toupet, L.; Réau, R. *Angew. Chem. Int. Ed.* **2000**, *39*, 1812.

[35] (a) Baumgartner, T.; Neumann, T.; Wirges, B. *Angew. Chem. Int. Ed.* **2004**, *43*, 6197; (b)Baumgartner, T.; Bergmans, W.; Kárpáti, T.; Neumann, T.; Nieger, M.; Nyulászi, L. *Chem. –Eur. J.* **2005**, *11*, 4687; (c) Neumann, T.; Dienes, Y.; Baumgartner, T. *Org. Lett.* **2006**, *8*, 495; (d) Ren, Y.; Kan, W. H.; Henderson, M. A.; Bomben, P. G.; Berlinguette, C. P.; Thangadurai, V.; Baumgartner, T. *J. Am. Chem. Soc.* **2011**, *133*, 17014; (e) Ren, Y.; Kan, W. H.; Thangadurai, V.; Baumgartner, T. *Angew. Chem. Int. Ed.* **2012**, *51*, 3964; (f) Romero-Nieto, C.; Baumgartner, T. *Synlett* **2013**, *24*, 920; (g) Huynh, H. V.; He, X.; Baumgartner, T. *Chem. Commun.* **2013**, *49*, 4899; (h) Wang, Z.; Gelfand, B. S.; Baumgartner, T. *Angew. Chem. Int. Ed.* **2016**, *55*, 3481; (i) Demay-Drouhard, P.; Baumgartner, T. *J. Org. Chem.* **2020**, *85*, 14627.

[36] (a) Collins, D. J.; Rowley, L. E.; Swan, J. M. *Aust. J. Chem.* **1974**, *27*, 831; (b) Winter, W. *Tetrahedron Lett.* **1975**, *16*, 3913; (c) Chan, T. H.; Wong, L. T. L. *J. Org. Chem.* **1980**, *45*, 2519; (d) Nief, F.; Charrier, C.; Mathey, F.; Simalty, M. *Phosphorus Sulfur* **1982**, *13*, 259; (e) Butters, T.; Winter, W. Synthese von *Chem. Ber.* **1984**, *117*, 990; (f) Quin, L. D.; Rao, N. S.; Topping, R. J.; McPhail, A. T. *J. Am. Chem. Soc.* **1986**, *108*, 4519; (g) Märkl, G.; Jin, G. Y.; Berr, K.-P. *Tetrahedron Lett.* **1993**, *34*, 3103; (h) Kurita, J.; Ishii, M.; Yasuike, S.; Tsuchiya, T. A *J. Chem. Soc. Chem. Commun.* **1993**, *17*, 1309; (i) Decken, A.; Bottomley, F.; Wilkins, B. E.; Gill, E. D. *Organometallics* **2004**, *23*, 3683; (j) Cordaro, J. G.; Stein, D.; Grützmacher, H. *J. Am. Chem. Soc.* **2006**, *128*, 14962.

[37] (a) Tsuji, H.; Sato, K.; Ilies, L.; Itoh, Y.; Sato, Y.; Nakamura, E. *Org. Lett.* **2008**, *10*, 2263; (b) Sanji, T.; Shiraishi, K.; Kashiwabara, T.; Tanaka, M. *Org. Lett.* **2008**, *10*, 2689; (c) Fukazawa, A.; Ichihashi, Y.; Kosaka, Y.; Yamaguchi, S. *Chem. Asian J.* **2009**, *4*, 1729.

[38] (a) Hayashi, Y.; Matano, Y.; Suda, K.; Kimura, Y.; Nakao, Y.; Imahori, H. *Chem. –Eur. J.*

2012, *18*, 15972; (b) Matano, Y.; Hayashi, Y.; Suda, K.; Kimura, Y.; Imahori, H. *Org. Lett.* **2013**, *15*, 4458; (c) Fukazawa, A.; Osaki, H.; Yamaguchi, S. *Asian J. Org. Chem.* **2014**, *3*, 122; (d) Yamaguchi, E.; Wang, C.; Fukazawa, A.; Taki, M.; Sato, Y.; Sasaki, T.; Ueda, M.; Sasaki, N.; Higashiyama, T.; Yamaguchi, S. *Angew. Chem. Int. Ed.* **2015**, *54*, 4539; (e) Matano, Y.; Motegi, Y.; Kawatsu, S.; Kimura, Y. *J. Org. Chem.* **2015**, *80*, 5944; (f) Wang, C.; Fukazawa, A.; Taki, M.; Sato, Y.; Higashiyama, T.; Yamaguchi, S. *Angew. Chem. Int. Ed.* **2015**, *54*, 15213.

[39] (a) Tsuji, H.; Sato, K.; Sato, Y.; Nakamura, E. *J. Mater. Chem.* **2009**, *19*, 3364; (b) Tsuji, H.; Sato, K.; Sato, Y.; Nakamura, E. *Chem. Asian J.* **2010**, *5*, 1294.

[40] Hanifi, D.; Pun, A.; Liu, Y. *Chem. Asian J.* **2012**, *7*, 2615.

[41] (a) Furukawa, S.; Haga, S.; Kobayashi, J.; Kawashima, T. *Org. Lett.* **2014**, *16*, 3228; (b) Wu, B.; Yoshikai, N. *Angew. Chem. Int. Ed.* **2015**, *54*, 8736; (c) Onoda, M.; Koyanagi, Y.; Saito, H.; Bhanuchandra, M.; Matano, Y.; Yorimitsu, H. *Asian J. Org. Chem.* **2017**, *6*, 257.

[42] Fukazawa, A.; Hara, M.; Okamoto, T.; Son, E.-C.; Xu, C.; Tamao, K.; Yamaguchi, S. *Org. Lett.* **2008**, *10*, 913.

[43] Lampin, J.-P.; Mathey, F. *J. Organomet. Chem.* **1974**, *71*, 239.

[44] Cheng, Y.-H.; Wong, H.-L.; Hong, E. Y.-H.; Lai, S.-L.; Chan, M.-Y.; Yam, V. W.-W. *ACS Appl. Energy Mater.* **2020**, *3*, 3059.

[45] Ren, Y.; Baumgartner, T. *J. Am. Chem. Soc.* **2011**, *133*, 1328.

[46] (a) Hissler, M.; Dyer, P. W.; Réau, R. *Coord. Chem. Rev.* **2003**, *244*, 1; (b) Matano, Y.; Imahori, H. *Org. Biomol. Chem.* **2009**, *7*, 1258; (c) Ren, Y.; Baumgartner, T. *Dalton Trans.* **2012**, *41*, 7792; (d) Baumgartner, T. *Acc. Chem. Res.* **2014**, *47*, 1613; (e) Duffy, M. P.; Delaunay, W.; Bouit, P.-A.; Hissler, M. *Chem. Soc. Rev.* **2016**, *45*, 5296.

[47] (a) Durán, E.; Gordo, E.; Granell, J.; Velasco, D.; López-Calahorra, F. *Tetrahedron Lett.* **2001**, *42*, 7791; (b) Geramita, K.; McBee, J.; Tilley, T. D. *J. Org. Chem.* **2009**, *74*, 820; (c) Zhang, S.; Chen, R.; Yin, J.; Liu, F.; Jiang, H.; Shi, N.; An, Z.; Ma, C.; Liu, B.; Huang, W. *Org. Lett.* **2010**, *12*, 3438; (d) Kabe, R.; Lynch, V. M.; Anzenbacher, P., Jr. *CrystEngComm* **2011**, *13*, 5423; (e) Durben, S.; Baumgartner, T. *Inorg. Chem.* **2011**, *50*, 6823; (f) Bruch, A.; Fukazawa, A.; Yamaguchi, E.; Yamaguchi, S.; Studer, A. *Angew. Chem. Int. Ed.* **2011**, *50*, 12094; (g) Nakano, K.; Oyama, H.; Nishimura, Y.; Nakasako, S.; Nozaki, K. *Angew. Chem. Int. Ed.* **2012**, *51*, 695; (h) Lin, C.-H.; Hsu, C.-W.; Liao, J.-L.; Cheng, Y.-M.; Chi, Y.; Lin, T.-Y.; Chung, M.-W.; Chou, P.-T.; Lee, G.-H.; Chang, C.-H.; Shih, C.-Y.; Ho, C.-L. *J. Mater. Chem.* **2012**, *22*, 10684; (i) Hibner-Kulicka, P.; Joule, J.

A.; Skalik, J.; Bałczewski, P. *RSC Adv.* **2017**, *7*, 9194.

[48] (a) Kojima, T.; Furukawa, S.; Tsuji, H.; Nakamura, E. *Chem. Lett.* **2014**, *43*, 676; (b) Furukawa, S.; Suda, Y.; Kobayashi, J.; Kawashima, T.; Tada, T.; Fujii, S.; Kiguchi, M.; Saito, M. *J. Am. Chem. Soc.* **2017**, *139*, 5787; (c) Riobé, F.; Szűcs, R.; Lescop, C.; Réau, R.; Nyulászi, L.; Bouit, P.-A.; Hissler, M. *Organometallics* **2017**, *36*, 2502; (d) Riobé, F.; Szűcs, R.; Bouit, P.-A.; Tondelier, D.; Geffroy, B.; Aparicio, F.; Buendía, J.; Sánchez, L.; Réau, R.; Nyulászi, L.; Hissler, M. *Chem. –Eur. J.* **2015**, *21*, 6547; (e) Bouit, P.-A.; Escande, A.; Szűcs, R.; Szieberth, D.; Lescop, C.; Nyulászi, L.; Hissler, M.; Réau, R. *J. Am. Chem. Soc.* **2012**, *134*, 6524; (f) Matano, Y.; Saito, A.; Suzuki, Y.; Miyajima, T.; Akiyama, S.; Otsubo, S.; Nakamoto, E.; Aramaki, S.; Imahori, H. *Chem. Asian J.* **2012**, *7*, 2305; (g) Matano, Y.; Saito, A.; Fukushima, T.; Tokudome, Y.; Suzuki, F.; Sakamaki, D.; Kaji, H.; Ito, A.; Tanaka, K.; Imahori, H. *Angew. Chem. Int. Ed.* **2011**, *50*, 8016; (h) Saito, A.; Miyajima, T.; Nakashima, M.; Fukushima, T.; Kaji, H.; Matano, Y.; Imahori, H. *Chem. –Eur. J.* **2009**, *15*, 10000.

[49] (a) Dienes, Y.; Eggenstein, M.; Kárpáti, T.; Sutherland, T. C.; Nyulászi, L.; Baumgartner, T. *Chem. –Eur. J.* **2008**, *14*, 9878; (b) Durben, S.; Baumgartner, T. *Angew. Chem. Int. Ed.* **2011**, *50*, 7948; (c) He, X.; Woo, A. Y. Y.; Borau-Garcia, J.; Baumgartner, T. *Chem. –Eur. J.* **2013**, *19*, 7620; (d) Stolar, M.; Borau-Garcia, J.; Toonen, M.; Baumgartner, T. *J. Am. Chem. Soc.* **2015**, *137*, 3366; (e) Reus, C.; Stolar, M.; Vanderkley, J.; Nebauer, J.; Baumgartner, T. *J. Am. Chem. Soc.* **2015**, *137*, 11710; (f) Greulich, T. W.; Yamaguchi, E.; Doerenkamp, C.; Lübbesmeyer, M.; Daniliuc, C. G.; Fukazawa, A.; Eckert, H.; Yamaguchi, S.; Studer, A. *Chem. –Eur. J.* **2017**, *23*, 6029.

[50] (a) Vicente, V.; Fruchier, A.; Taillefer, M.; Combes-Chamalet, C.; Scowen, I. J.; Plénat, F.; Cristau, H.-J. *New J. Chem.* **2004**, *28*, 418; (b) Huy, N. H. T.; Donnadieu, B.; Mathey, F. *Organometallics* **2007**, *26*, 6497; (c) Kira, A.; Shibano, Y.; Kang, S.; Hayashi, H.; Umeyama, T.; Matano, Y.; Imahori, H. *Chem. Lett.* **2010**, *39*, 448.

[51] Given the IUPAC nomenclature, the correct name is phospholo[3,2-b:4,5-b′]dithiophene because a thiophene ring has a higher priority than a phosphole one. However, we use the conventional name for consistency with the previous literature.

[52] Rajca, A.; Miyasaka, M.; Pink, M.; Wang, H.; Rajca, S. *J. Am. Chem. Soc.* **2004**, *126*, 15211.

[53] (a) Matano, Y.; Kon, Y.; Saito, A.; Kimura, Y.; Murafuji, T.; Imahori, H. *Chem. Lett.* **2011**, *40*, 919; (b) Matano, Y.; Nakashima, M.; Imahori, H. *Angew. Chem. Int. Ed.* **2009**, *48*, 4002; (c) Wu, B.; Yoshikai, N. *Org. Biomol. Chem.* **2016**, *14*, 5402; (d) Yoshikai, N.;

Santra, M.; Wu, B. *Organometallics* **2017**, *36*, 2637.

[54] (a) Fukazawa, A.; Murai, T.-A.; Li, L.; Chen, Y.; Yamaguchi, S. *C. R. Chim.* **2010**, *13*, 1082; (b) Weymiens, W.; Hartl, F.; Lutz, M.; Slootweg, J. C.; Ehlers, A. W.; Mulder, J. R.; Lammertsma, K. *Eur. J. Org. Chem.* **2012**, *2012*, 6711; (c) Tran Huy, N. H.; Lu, Y.; Qune, L. F. N. A.; Mathey, F. *J. Organomet. Chem.* **2013**, *730*, 63.

[55] Lakowicz, J. R. *Principles of Fluorescence Spectroscopy*, 3rd Ed.; Springer: Berlin, 2006.

[56] (a) Fukazawa, A.; Yamada, H.; Yamaguchi, S. *Angew. Chem. Int. Ed.* **2008**, *47*, 5582; (b) Romero-Nieto, C.; Kamada, K.; Cramb, D. T.; Merino, S.; Rodríguez-López, J.; Baumgartner, T. *Eur. J. Org. Chem.* **2010**, 5225.

[57] Fadhel, O.; Benkö, Z.; Gras, M.; Deborde, V.; Joly, D.; Lescop, C.; Nyulászi, L.; Hissler, M.; Réau, R. *Chem. –Eur. J.* **2010**, *16*, 11340.

[58] Fukazawa, A.; Yamada, H.; Sasaki, Y.; Akiyama, S.; Yamaguchi, S. *Chem. Asian J.* **2010**, *5*, 466.

[59] Chua, C. J.; Ren, Y.; Stolar, M.; Xing, S.; Linder, T.; Baumgartner, T. *Eur. J. Inorg. Chem.* **2014**, 1767.

[60] (a) Mas-Torrent, M.; Rovira, C. *Chem. Rev.* **2011**, *111*, 4833; (b) Sun, Y.; Tan, L.; Jiang, S.; Qian, H.; Wang, Z.; Yan, D.; Di, C.; Wang, Y.; Wu, W.; Yu, G.; Yan, S.; Wang, C.; Hu, W.; Liu, Y.; Zhu, D. *J. Am. Chem. Soc.* **2007**, *129*, 1882; (c) Mas-Torrent, M.; Rovira, C. *J. Mater. Chem.* **2006**, *16*, 433; (d) Briseno, A. L.; Miao, Q.; Ling, M.-M.; Reese, C.; Meng, H.; Bao, Z.; Wudl, F. *J. Am. Chem. Soc.* **2006**, *128*, 15576; (e) Curtis, M. D.; Cao, J.; Kampf, J. W. *J. Am. Chem. Soc.* **2004**, *126*, 4318; (f) Mas-Torrent, M.; Hadley, P.; Bromley, S. T.; Ribas, X.; Tarrés, J.; Mas, M.; Molins, E.; Veciana, J.; Rovira, C. *J. Am. Chem. Soc.* **2004**, *126*, 8546; (g) Novoa, J. J.; Rovira, M. C.; Rovira, C.; Veciana, J.; Tarrés, J. *Adv. Mater.* **1995**, *7*, 233.

[61] Weymiens, W.; Zaal, M.; Slootweg, J. C.; Ehlers, A. W.; Lammertsma, K. *Inorg. Chem.* **2011**, *50*, 8516.

[62] (a) Kitamura, C.; Matsumoto, C.; Kawatsuki, N.; Yoneda, A.; Asada, K.; Kobayashi, T.; Naito, H. *Bull. Chem. Soc. Jpn.* **2008**, *81*, 754; (b) Sugino, M.; Araki, Y.; Hatanaka, K.; Hisaki, I.; Miyata, M.; Tohnai, N. *Cryst. Growth Des.* **2013**, *13*, 4986; (c) Liu, H.; Yao, L.; Li, B.; Chen, X.; Gao, Y.; Zhang, S.; Li, W.; Lu, P.; Yang, B.; Ma, Y. *Chem. Commun.* **2016**, *52*, 7356; (d) Sekiguchi, S.; Kondo, K.; Sei, Y.; Akita, M.; Yoshizawa, M. *Angew. Chem. Int. Ed.* **2016**, *55*, 6906; (e) Shen, Y.; Liu, H.; Zhang, S.; Gao, Y.; Li, B.; Yan, Y.; Hu, Y.; Zhao, L.; Yang, B. *J. Mater. Chem. C* **2017**, *5*, 10061.

[63] (a) Wrona-Piotrowicz, A.; Zakrzewski, J.; Métivier, R.; Brosseau, A.; Makal, A.; Woźniak,

K. *RSC Adv.* **2014**, *4*, 56003; (b) Piotrowicz, M.; Zakrzewski, J.; Métivier, R.; Brosseau, A.; Makal, A.; Woźniak, K. *J. Org. Chem.* **2015**, *80*, 2573; (c) Takaishi, K.; Takehana, R.; Ema, T. *Chem. Commun.* **2018**, *54*, 1449.

[64] Ren, Y.; Baumgartner, T. *Inorg. Chem.* **2012**, *51*, 2669.

[65] (a) Pansare, V. J.; Hejazi, S.; Faenza, W. J.; Prud'homme, R. K. *Chem. Mater.* **2012**, *24*, 812; (b) Ni, Y.; Zeng, L.; Kang, N.-Y.; Huang, K.-W.; Wang, L.; Zeng, Z.; Chang, Y.-T.; Wu, J. *Chem. Eur. J.* **2014**, *20*, 2301; (c) Ren, L.; Liu, F.; Shen, X.; Zhang, C.; Yi, Y.; Zhu, X. *J. Am. Chem. Soc.* **2015**, *137*, 11294.

[66] (a) Peng, X.; Song, F.; Lu, E.; Wang, Y.; Zhou, W.; Fan, J.; Gao, Y. *J. Am. Chem. Soc.* **2005**, *127*, 4170; (b) Jiang, M.; Gu, X.; Lam, J. W. Y.; Zhang, Y.; Kwok, R. T. K.; Wong, K. S.; Tang, B. Z. *Chem. Sci.* **2017**, *8*, 5440; (c) Gao, Z.; Hao, Y.; Zheng, M.; Chen, Y. *RSC Adv.* **2017**, *7*, 7604.

[67] Pommerehne, J.; Vestweber, H.; Guss, W.; Mahrt, R. F.; Bässler, H.; Porsch, M.; Daub, J. *Adv. Mater.* **1995**, *7*, 551.

[68] (a) Saeki, A.; Koizumi, Y.; Aida, T.; Seki, S. *Acc. Chem. Res.* **2012**, *45*, 1193; (b) Seki, S.; Saeki, A.; Sakurai, T.; Sakamaki, D. *Phys. Chem. Chem. Phys.* **2014**, *16*, 11093; (c) Prasanthkumar, S.; Ghosh, S.; Nair, V. C.; Saeki, A.; Seki, S.; Ajayaghosh, A. *Angew. Chem. Int. Ed.* **2015**, *54*, 946; (d) Basak, D.; Pal, D. S.; Sakurai, T.; Yoneda, S.; Seki, S.; Ghosh, S. *Phys. Chem. Chem. Phys.* **2017**, *19*, 31024.

[69] (a) Wu, W.; Liu, Y.; Zhu, D. *Chem. Soc. Rev.* **2010**, *39*, 1489; (b) Mei, J.; Diao, Y.; Appleton, A. L.; Fang, L.; Bao, Z. *J. Am. Chem. Soc.* **2013**, *135*, 6724; (c) Root, S. E.; Savagatrup, S.; Printz, A. D.; Rodriquez, D.; Lipomi, D. J. *Chem. Rev.* **2017**, *117*, 6467.

[70] (a) Endo, A.; Sato, K.; Yoshimura, K.; Kai, T.; Kawada, A.; Miyazaki, H.; Adachi, C. *Appl. Phys. Lett.* **2011**, *98*, 083302; (b) Uoyama, H.; Goushi, K.; Shizu, K.; Nomura, H.; Adachi, C. *Nature* **2012**, *492*, 234; (c) Yang, Z.; Mao, Z.; Xie, Z.; Zhang, Y.; Liu, S.; Zhao, J.; Xu, J.; Chi, Z.; Aldred, M. P. *Chem. Soc. Rev.* **2017**, *46*, 915; (d) Huang, T.; Jiang, W.; Duan, L. *J. Mater. Chem.* **2018**, *6*, 5577; (e) Wada, Y.; Nakagawa, H.; Matsumoto, S.; Wakisaka, Y.; Kaji, H. *Nat. Photonics* **2020**, *14*, 643.

[71] (a) Kumar, S. *Chem. Soc. Rev.* **2006**, *35*, 83; (b) Würthner, F.; Saha-Möller, C. R.; Fimmel, B.; Ogi, S.; Leowanawat, P.; Schmidt, D. *Chem. Rev.* **2016**, *116*, 962; (c) Das, A.; Ghosh, S. *Chem. Commun.* **2016**, *52*, 6860; (d) Hisaki, I.; Xin, C.; Takahashi, K.; Nakamura, T. *Angew. Chem. Int. Ed.* **2019**, *58*, 11160; (e) Little, M. A.; Cooper, A. I. *Adv. Funct. Mater.* **2020**, *30*, 1909842.

[72] (a) Watson, M. D.; Fechtenkötter, A.; Müllen, K. *Chem. Rev.* **2001**, *101*, 1267; (b) Wu, J.;

Pisula, W.; Müllen, K. *Chem. Rev.* **2007**, *107*, 718; (c) Rieger, R.; Müllen, K. *J. Phys. Org. Chem.* **2010**, *23*, 315; (d) Ball, M.; Zhong, Y.; Wu, Y.; Schenck, C.; Ng, F.; Steigerwald, M.; Xiao, S.; Nuckolls, C. *Acc. Chem. Res.* **2015**, *48*, 267; (e) Narita, A.; Wang, X.-Y.; Feng, X.; Müllen, K. *Chem. Soc. Rev.* **2015**, *44*, 6616.

[73] Takahashi, T.; Takenobu, T.; Takeya, J.; Iwasa, Y. *Adv. Funct. Mater.* **2007**, *17*, 1623.

[74] (a) Ionkin, A. S.; Marshall, W. J.; Fish, B. M.; Bryman, L. M.; Wang, Y. *Chem. Commun.* **2008**, 2319; (b) Wu, T.-L.; Chou, H.-H.; Huang, P.-Y.; Cheng, C.-H.; Liu, R.-S. *J. Org. Chem.* **2014**, *79*, 267; (c) Heard, K. W. J.; Morrison, J. J.; Weston, L.; Lo, C. H.; Pirvu, L.; Raftery, J.; Little, M. S.; McDouall, J. J. W.; Yeates, S. G.; Quayle, P. *Chem. Commun.* **2015**, *51*, 6115; (d) Sato, S.; Yoshii, A.; Takahashi, S.; Furumi, S.; Takeuchi, M.; Isobe, H. *Proc. Natl. Acad. Sci.* **2017**, *114*, 13097.

[75] (a) Umeyama, T.; Baek, J.; Sato, Y.; Suenaga, K.; Abou-Chahine, F.; Tkachenko, N. V.; Lemmetyinen, H.; Imahori, H. *Nat. Commun.* **2015**, *6*, 7732; (b) Gai, L.; Chen, H.; Zou, B.; Lu, H.; Lai, G.; Li, Z.; Shen, Z. *Chem. Commun.* **2012**, *48*, 10721; (c) Wu, K.-C.; Ku, P.-J.; Lin, C.-S.; Shih, H.-T.; Wu, F.-I.; Huang, M.-J.; Lin, J.-J.; Chen, I.-C.; Cheng, C.-H. *Adv. Funct. Mater.* **2008**, *18*, 67; (d) Winnik, F. M. *Chem. Rev.* **1993**, *93*, 587.

[76] (a) Tatum, L. A.; Johnson, C. J.; Fernando, A. A. P.; Ruch, B. C.; Barakoti, K. K.; Alpuche-Aviles, M. A.; King, B. T. *Chem. Sci.* **2012**, *3*, 3261; (b) Bisoyi, H. K.; Kumar, S. *Chem. Soc. Rev.* **2010**, *39*, 264; (c) Laschat, S.; Baro, A.; Steinke, N.; Giesselmann, F.; Hägele, C.; Scalia, G.; Judele, R.; Kapatsina, E.; Sauer, S.; Schreivogel, A.; Tosoni, M. *Angew. Chem. Int. Ed.* **2007**, *46*, 4832; (d) Osawa, T.; Kajitani, T.; Hashizume, D.; Ohsumi, H.; Sasaki, S.; Takata, M.; Koizumi, Y.; Saeki, A.; Seki, S.; Fukushima, T.; Aida, T. *Angew. Chem. Int. Ed.* **2012**, *51*, 7990.

[77] (a) Takimiya, K.; Konda, Y.; Ebata, H.; Otsubo, T.; Kunugi, Y. *Mol. Cryst. Liq. Cryst.* **2006**, *455*, 361; (b) Shinamura, S.; Osaka, I.; Miyazaki, E.; Nakao, A.; Yamagishi, M.; Takeya, J.; Takimiya, K. *J. Am. Chem. Soc.* **2011**, *133*, 5024.

[78] (a) Kuninobu, Y.; Yoshida, T.; Takai, K. *J. Org. Chem.* **2012**, *77*, 9436; (b) Kuninobu, Y.; Yoshida, T.; Takai, K. *J. Org. Chem.* **2011**, *76*, 7370.

[79] Nishimura, K.; Hirano, K.; Miura, M. *Org. Lett.* **2019**, *21*, 1467.

[80] Nishimura, K.; Hirano, K.; Miura, M. *Org. Lett.* **2020**, *22*, 3185.

[81] te Velde, G.; Bickelhaupt, F. M.; Baerends, E. J.; Fonseca Guerra, C.; van Gisbergen, S. J. A.; Snijders, J. G.; Ziegler, T. *J. Comput. Chem.* **2001**, *22*, 931.

[82] *Gaussian 09*, Revision D.01, Frisch, M. J.; Trucks, G. W.; Schlegel, H. B.; Scuseria, G. E.; Robb, M. A.; Cheeseman, J. R.; Scalmani, G.; Barone, V.; Mennucci, B.; Petersson, G. A.;

Nakatsuji, H.; Caricato, M.; Li, X.; Hratchian, H. P.; Izmaylov, A. F.; Bloino, J.; Zheng, G.; Sonnenberg, J. L.; Hada, M.; Ehara, M.; Toyota, K.; Fukuda, R.; Hasegawa, J.; Ishida, M.; Nakajima, T.; Honda, Y.; Kitao, O.; Nakai, H.; Vreven, T.; Montgomery, J. A. Jr.; Peralta, J. E.; Ogliaro, F.; Bearpark, M.; Heyd, J. J.; Brothers, E.; Kudin, K. N.; Staroverov, V. N.; Keith, T.; Kobayashi, R.; Normand, J.; Raghavachari, K.; Rendell, A.; Burant, J. C.; Iyengar, S. S.; Tomasi, J.; Cossi, M.; Rega, N.; Millam, J. M.; Klene, M.; Knox, J. E.; Cross, J. B.; Bakken, V.; Adamo, C.; Jaramillo, J.; Gomperts, R.; Stratmann, R. E.; Yazyev, O.; Austin, A. J.; Cammi, R.; Pomelli, C.; Ochterski, J. W.; Martin, R. L.; Morokuma, K.; Zakrzewski, V. G.; Voth, G. A.; Salvador, P.; Dannenberg, J. J.; Dapprich, S.; Daniels, A. D.; Farkas, O.; Foresman, J. B.; Ortiz, J. V.; Cioslowski, J.; Fox, D. J.; Gaussian, Inc.; Wallingford CT, **2013**.

[83] Becke, A. D. *J. Chem. Phys.* **1993**, *98*, 1372.

[84] Lee, C.; Yang, W.; Parr, R. G. *Phys. Rev. B* **1998**, *37*, 785.

[85] Klamt, A.; Schüürmann, G. *J. Chem. Soc. Perkin Trans. 2* **1993**, 799.

[86] Hirata, S.; Head-Gordon, M.; *Chem. Phys. Lett.* **1999**, *314*, 291.

[87] Ohta, K.; Yamada, S.; Kamada, K.; Slepkov, A. D.; Hegmann, F. A.; Tykwinski, R. R.; Shirtcliff, L. D.; Haley, M. M.; Sałek, P.; Gel'mukhanov, F.; Ågren, H. *J. Phys. Chem. A* **2011**, *115*, 105.

[88] Samanta, P. K.; Kim, D.; Coropceanu V.; Brédas, J.-L. *J. Am. Chem. Soc.* **2017**, *139*, 4042.

[89] Sheik-Bahae, M.; Said, A. A.; Wei, T. H.; Hagan, D. J. *IEEE J. Quantum Electron.* **1990**, *26*, 760.

[90] Kamada, K.; Matsunaga, K.; Yoshino, A.; Ohta, K. *J. Opt. Soc. Am. B* **2003**, *20*, 529.

[91] Akita, M.; Saito, M.; Osaka, I.; Koganezawa, V; Takimiya, K. *RSC Adv.* **2016**, *6*, 16437.

[92] Xiong, Y.; Wu, Q.; Li, J.; Wang, S.; Gao, X.; Li, H. *J. Org. Chem.* **2013**, *78*, 752.

[93] Ishiyama, T.; Murata, M.; Miyaura, N. *J. Org. Chem.* **1995**, *60*, 7508.

[94] Boelke, A.; Caspers, L. D.; Nachtsheim, B. J. *Org. Lett.* **2017**, *19*, 5344.

[95] Nguyen, T.-D.; Lin, C.-H.; Wu, C.-G *Inorg. Chem.* **2017**, *56*, 252.

[96] Wen, H.; Zhang, L.; Zhu, S.; Liu, G.; Huang, Z. *ACS Catal.* **2017**, *7*, 6419.

[97] Gallego, D.; Brück, A.; Irran, E.; Meier, F.; Kaupp, M.; Driess, M.; Hartwig, J. F. *J. Am. Chem. Soc.* **2013**, *135*, 15617.

[98] Beshai, M.; Dhudshia, B.; Mills, R.; Thadani, A. N. *Tetrahedron Lett.* **2008,** *49*, 6794.

[99] Ueda, H.; Yamaguchi, M.; Kameya, H.; Sugimoto, K.; Tokuyama, H. *Org. Lett.* **2014**, *16*, 4948.

[100] Meng, W.; League, A. B.; Ronson, T. K.; Clegg, J. K.; Isley, W. C.; Semrouni, D.; Gagliardi, L.; Cramer, C. J.; Nitschke, J. R. *J. Am. Chem. Soc.* **2014**, *136*, 3972.

[101] Xia, J.; Golder, M. R.; Foster, M. E.; Wong, B. M.; Jasti, R. *J. Am. Chem. Soc.* **2012**, *134*, 19709.

List of Publications

The content of this thesis is composed of the following papers.

Chapter 1

(1) "Phosphole-Thiophene Hybrid: A Dual Role of Dithieno[3,4-*b*:3',4'-*d*]phosphole as Electron Acceptor and Electron Donor"
Tomohiro Higashino, Keiichi Ishida, Takaharu Satoh, Yoshihiro Matano, Hiroshi Imahori, *Journal of Organic Chemistry*, **2018**, *83*, 3397-3402.
(Chapter 1 is the final version of a submitted work that was subsequently accepted for publication in *Journal of Organic Chemistry*, copyright © American Chemical Society after peer review. To access the final edited and published work, see the following website: https://pubs.acs.org/doi/abs/10.1021/acs.joc.8b00030)

Chapter 2

(2) "Modulation of Frontier Molecular Orbitals on Dithieno[3,4-*b*:3',4'-*d*]phosphole Derivatives by Donor-π-Acceptor Interaction"
Tomohiro Higashino, Keiichi Ishida, Hiroshi Imahori, *Chemistry Letters*, **2020**, *49*, 272-275.
(Chapter 2 is the final version of a submitted work that was subsequently accepted for publication in *Chemistry Letters*, copyright © Chemical Society of Japan after peer review. To access the final edited and published work, see the following website: https://www.journal.csj.jp/doi/full/10.1246/cl.190879)

Chapter 3

(3) "Pluripotent Features of Doubly Thiophene-Fused Benzodiphospholes as Organic Functional Materials"
Tomohiro Higashino, Keiichi Ishida, Tsuneaki Sakurai, Shu Seki, Tatsuki Konishi, Kenji Kamada, Hiroshi Imahori, *Chemistry – A European Journal,* **2019**, *25*, 6425–6438.
(Chapter 3 is the unedited author's version of a submitted work that was subsequently accepted for publication in *Chemistry – A European Journal*, copyright © John Wiley & Sons, Inc. after peer review. To access the final edited and published work, see the following website: https://chemistry-europe.onlinelibrary.wiley.com/doi/abs/10.1002/chem.201900661)

Chapter 4

(4) "Thiophene-Fused Naphthodiphospholes: Modulation of the Structural and Electronic Properties of Polycyclic Aromatics by Precise Fusion of Heteroles"
Keiichi Ishida, Tomohiro Higashino, Yoshimasa Wada, Hironori Kaji, Akinori Saeki, Hiroshi Imahori, *ChemPlusChem*, **2021**, *86*, 130–136.

Other Publications

(1) "Asymmetric Synthesis of Biaryl Atropisomers Using an Organocatalyst-Mediated Domino Reaction as the Key Step"
Yujiro Hayashi, Akira Takikawa, Seitaro Koshino, Keiichi Ishida, *Chemistry – A European Journal,* **2019**, *25*, 10319–10322.

(2) "Inversion of the Axial Information during Oxidative Aromatization in the Synthesis of Axially Chiral Biaryls with Organocatalysis as a Key Step"
Seitaro Koshino, Akira Takikawa, Keiichi Ishida, Tohru Taniguchi, Kenji Monde, Eunsang Kwon, Shigenobu Umemiya, Yujiro Hayashi, *Chemistry – A European Journal,* **2020**, *26*, 4524–4530.

(3) "Efficient light-harvesting, energy migration, and charge transfer by nanographene-based nonfullerene small-molecule acceptors exhibiting unusually long excited-state lifetime in the film state"
Tomokazu Umeyama, Kensho Igarashi, Daiki Sasada, Yasunari Tamai, Keiichi Ishida, Tomoyuki Koganezawa, Shunsuke Ohtani, Kazuo Tanaka, Hideo Ohlita, Hiroshi Imahori, *Chemical Science*, **2020**, *11*, 3250–3257.

(4) "Efficient Exciton Diffusion in Micrometer-Sized Domains of Nanographene-Based Nonfullerene Acceptors with Long Exciton Lifetimes in Blend Films with Conjugated Polymer"

Tomokazu Umeyama, Kensho Igarashi, Daiki Sasada, Keiichi Ishida, Tomoyuki Koganezawa, Shunsuke Ohtani, Kazuo Tanaka, Hiroshi Imahori, *ACS Applied Materials & Interfaces*, **2020**, *12*, 39236–39244.

(5) "Prolongation of the singlet exciton lifetime of nonfullerene acceptor films by the replacement of the central benzene core with naphthalene"

Tomokazu Umeyama, Kensho Igarashi, Yasunari Tamai, Tatsuho Wada, Taiki Takeyama, Daiki Sasada, Keiichi Ishida, Tomoyuki Koganezawa, Shunsuke Ohtani, Kazuo Tanaka, Hideo Ohkita, Hiroshi Imahori, *Sustainable Energy & Fuels*, **2021**, *5*, 2028–2035.

(6) "Effect of Terminal-Group Halogenation of Naphthalene-Based Nonfullerene Acceptors on Their Film Structure and Photophysical and Photovoltaic Properties"

Tomokazu Umeyama, Tatsuho Wada, Kensho Igarashi, Kosaku Kato, Akira Yamakata, Taiki Takeyama, Yuji Sakamoto, Yasunari Tamai, Hideo Ohkita, Keiichi Ishida, Tomoyuki Koganezawa, Shunsuke Ohtani, Kazuo Tanaka, Hiroshi Imahori, *ACS Applied Energy Materials*, **2021**, *in press*.

Acknowledgment

This thesis deals with the studies accomplished by the author under the direction of Professor Dr. Hiroshi Imahori in his laboratory at Kyoto University from April 2017 to March 2022.

First of all, the author would like to express his gratitude for Professor Dr. Hiroshi Imahori at Graduate School of Engineering, Kyoto University, for his supervision, precious advices, and encouragement throughout his study.

The author is deeply grateful to Professor Dr. Yosihiro Matano, Takaharu Satoh and Ayana Wakatsuki at Graduate School of Science, Niigata University, for the measurement of fluorescence quantum yield.

The author wishes to show his appreciation to Professor Dr. Akinori Saeki at Graduate School of Engineering, Osaka University, and Professor Dr. Shu Seki and Assistant Professor Dr. Tsuneaki Sakurai at Graduate School of Engineering, Kyoto University, for the TRMC measurement.

The author feels gratitude to Dr. Kenji Kamada and Tatsuki Konishi at Advanced Industrial Science and Technology, and School of Science and Technology, Kwansei Gakuin University, for the two-photon absorption measurement.

The author desires to express his appreciation to Professor Dr. Atsuhiro Osuka and Assistant Professor Dr. Takayuki Tanaka at Graduate School of Science, Kyoto University, for the single crystal X-ray analysis.

The author thanks to Professor Dr. Hironori Kaji and Dr. Yoshimasa Wada at Graduate School of Engineering, Kyoto University for the theoretical calculation.

The author is obliged to Professor Dr. Tomokazu Umeyama at University of Hyogo and Associate Professor Dr. Tomohiro Higashino at Kyoto University for their kind support and useful suggestion. The author is also deeply grateful to all members in the laboratory of Photoorganic Chemistry at Department of Molecular Engineering, Graduate School of Engineering, Kyoto University, for their valuable discussions and encouragements as well as delightful laboratory life. Especially, the author feels appreciate to Kensho Igarashi, Yuma Kurumisawa, Issei Nishimura, Hiroki Yamada, Hitomi Iiyama, Daiki Sasada, Tatsuho Wada and Rikiya Iizumi for their encouragements.

Finally, the author would like to thank his father, Hiroshi Ishida, and his mother, Kiyomi Ishida for their hearty encouragement and continuous assistant.

Keiichi Ishida